Physics 414/521 Lab Manual

2006 Spring Term Laboratory Staff

Dr. Jose Vithayathil
8-3173 (Office) or 610 520 2325 (home)
2N27, Lab rooms (2N23, 2N25, 2N44)
vithayat@dept.physics.upenn.edu

Prof. Joseph Kroll
215 573 6380 (office or 215 313 1615 (cell)
DRL 3N4A or DRL 1W1
kroll@hep.upenn.edu

The web page for the lab with is:

`http://surf.hep.upenn.edu/~kroll/p414_521_spring06/ijkroll_p414_521_spring06.html`

Contents

Chapter 1

Introduction

The goal of this course is to introduce you to the art and science of experimental physics, and to the tools physicists use to analyze, document and present results. We hope the experiments in this lab challenge you, give you a first look at modern instrumentation and techniques, and give you a taste of what "real experimental physics" is all about.

Some experiments are easier than others. You are can do an easy one first and perhaps second but at least one experiment should be challenging. It's a good idea to choose experiments that expose you to a wide range of physical systems (i.e., four experiments that concentrate on nuclear decay would not be a good idea). As you become familiar with experimental techniques, you will become more efficient, so do not be surprised if the first experiment takes longer than the rest. Do not feel limited by the experiments described in the manual or the equipment sitting by each bench. If you have an idea for another interesting measurement that could be done using the basic set-up, let your instructor know. The same is true if there is another experiment you think would be interesting to build and perform.

Report due dates for the labs and presentations are:

Assignment	Date
1st lab rough draft & homework	Fri Jan. 27
1st presentation	Tue., Wed. Jan31, Feb1
1st lab final version	Mon. Feb. 6
2nd lab rough draft	Fri. Feb. 24
2nd Presentation	Tue., Wed. Feb. 28, Mar. 1
2nd lab final version	Mon.Mar. 13

3rd lab rough draft	Fri. Apr. 7
3rd Presentation	Tue., Wed. Apr. 11,12
3rd lab final version	Mon. Apr. 17
Last Day of Classes	Apr. 21

You are expected to keep a laboratory notebook that you will use to record your data. Please purchase a 'computation notebook' or 'labbook' that is 11 $\frac{3}{4}$ inches by 9 $\frac{1}{4}$ inches with quadruled paper (the bookstore has these). You will hand in your lab book with your reports. Do not write data on loose pieces of paper and then transcribe these data into your lab book. This practice will be **actively discouraged by the instructors**. Your notebook will be reviewed at the discretion of the instructors. A lab notebook should contain enough data, like for example the relevant instrument settings, pulse widths observed, date and time, etc., so that you can tell someone later on how to duplicate the data. It is a good idea to estimate your final results or prepare a rough version of a plot **as you record the data** while doing the experiment, to be sure there are no obvious errors. This can save hours of recording meaningless data, along with the need to repeat the measurements.

A good estimate is that each lab will require 2 or 3 sessions in the lab, working 4 hours per session, plus the time to write the report.

You are encouraged to do the first lab with a partner. For the second lab, you may work alone, or with a partner. The third lab, however, must be a solo effort. For labs done with a partner, you will hand in a joint lab report, and you will make individual presentations on the laboratory.

Reports and Presentation

You will write a report on each experiment that you do, in a form that resembles a research manuscript. If you do an experiment with a partner, you will submit one lab report together, indicating which person was mostly responsible for writing each section . Your report should be held together with a staple or a binder: reports consisting of loose pages will not be accepted.

The lab reports should be aimed at your fellow students. After reading your report, your fellow students should understand the purpose of the experiment, the procedure, the data analysis, with an emphasis on error analysis, and the results. The reports should have 5 to 10 pages of text, maximum, plus additional pages as necessary for figures and tables.

Each report should contain

- a short introduction giving the history and motivation of the measurement,
- a discussion of the physics,
- a presentation of the data,
- an analysis of the data and the measurement of the relevant physics quantity,
- a discussion of statistical and systematic errors, and
- a conclusion that includes comparison with expectations.

We use your lab report for two purposes: first they help us understand what you did and to evaluate your results; second they are an exercise to help you learn how to describe clearly and concisely your work to your peers. The process of writing up your work often leads to reevaluating your procedure, your data analysis, and your results. We read the reports for content and clarity. We will correct poor diction and grammar errors. You should proofread your text carefully (e.g., you should check for spelling errors). Scientific journals expect carefully prepared articles: you should strive for the same standard.

Particular emphasis will be placed on the thoroughness of your evaluation of statistical and systematic errors. Techniques for doing this will be described in lecture.

Just like the lab reports, the presentations should be aimed at your fellow students. Structure the presentation to follow the same outline described above for the lab report. The ideal presentation would give a fellow student a clear idea of the physics, the experimental setup, the result, and the error analysis.

The length of the talk, uninterrupted by questions, should be 12 minutes. You should practice your presentation in advance so that you know what you want to say and you make sure that your presentation is within the time limit. Your slides should be prepared carefully, with the goal of providing a prop to explain what you did without writing out full sentences. Think instead of presenting the results using abbreviations similar to the abbreviations used in newspaper headlines, e.g., do not write

"The systematic error was dominated by two contributions: the measurement of the length and the measurement of the time,"

instead write

"Dominant systematics: length and time"

Your slides should not be too dense with text or too busy. Carefully prepared figures of the set up should be included. We expect you to listen to your colleagues presentations, and we encourage you to ask questions. At our "conferences," we expect all of the students to be available for the entire time allotted to the presentations.

Your oral presentation should be made available in electronic format to the instructors by the morning of the day of the presentation at the latest. Power point or pdf are acceptable format. We will display the presentations using a laptop or PC and a projector.

Preparation and Etiquette

You will need to prepare for the lab by reviewing the recommended reading, and searching out additional references in the library. This is an integral part of experimental (and theoretical) physics, and part of this course is to discover how to exploit the library. If you neglect this initial preparation, the lab itself will be extremely frustrating. Have an idea of what you'll be doing **before** you get started! Please do not remove any of the materials located with the apparatus. These contain much useful information, and you should consult them while working on the lab. If you have a good reason for taking the material home, please ask your laboratory instructor.

You **must** keep a lab notebook with a record of your activities in the lab, and the data and other information you need to write the report. It is a good idea to estimate your final results or prepare a rough version of a plot **as you record the data**, to be sure there are no obvious errors. This can save hours of recording meaningless data,

along with the need to repeat the measurements.

Please leave the lab equipment for the next group as you found it. If anything is lost or broken, please inform the lab staff.

Schedule

For each lab we will follow the following schedule:

(1) first Friday afternoon by 5pm

Hand in a rough draft of your lab report. This draft must be complete in terms of procedure, data, data analysis, error evaluation, and results. The text can be not polished and incomplete, as long as it is still possible to understand your results. Two of the three rough drafts handed in for the first lab did not meet this requirement.

We will read your rough draft before the oral presentations. This gives us the opportunity to be prepared for the talks and to give you feedback on your report. An incomplete rough draft will result in less useful feedback for the final report.

(2) Tuesday or Wednesday afternoon following this first Friday

We will hear the oral presentations and return the copies of your rough draft. Please bring two copies of your talk: one for each of us.

Again you are expected to be present for the entire set of presentations. We will solicit feedback from your fellow students on your presentation. There will be no passive involvement of the audience.

(3) the following Friday by 5pm

Hand in the final version of your lab report. We will both read it critically and if necessary we will meet with you to discuss it.

For the second report you will be asked to read one of your fellow students report and to comment on it.

Working with radioactive sources

Many advanced labs will include the use of radioactive sources. Part of your training in physics is to have an understanding of how to work with such substances **safely**. Everyone handling radioactive materials is is required to get certified by reviewing a web course on radioactive materials developed by the university environemntal health and safety department. All the sources in our lab are **sealed**, that is encapsulated in some way, making them significantly safer than unsealed sources. There is always the (remote) possibility that the seals can break, and there are two basic ways we stay alert to this problem. First, Penn radiation safety office “wipe tests” the lab every 6 months (they wipe the sources, and test the cloth for radioactive residue).

The second line of safety defense is you, the lab user. You should handle the sources carefully, check the level of radioactivity near your apparatus, and report any problems you discover promptly to the lab staff. You should do some reading on radiation safety before doing a lab that uses a source. The section in Melissinos provides a good introduction.

Procedures to follow while doing a lab involving a radioactive source.

These should be followed **every** lab session you work on the experiment, not simply the first one.

1. Do not eat or drink while working with radioactive sources. The most hazardous situation is when radioactive material is ingested.

2. Use a radiation monitor (e.g., a portable Geiger counter) to check the radiation levels in the vicinity of your experiment. Record the count rate in your log book, including the distance you are from the source. Check the radiation level where you plan to sit during the experiment. A level of 1 or 2 mrem/hr is acceptable, but if the level is above 5 mrem/hr, use lead bricks to provide additional shielding. Check the level again after you are done working. Notify the instructor in the event of a statistically significant discrepancy between the two results.

3. The stronger sources come with a handling rod that forces you to keep a good distance from the source. **Always** use such a rod, if the source comes with one.

4. Handle the sources carefully. Several of the sources have a thin window that allow the radiation to exit the enclosure. The windows are fragile and should not be touched.

5. Minimize your exposure to radiation by taking advantage of **shielding, distance, and time**.

6. When in doubt, ask your instructor for assistance.

7. **NEVER** remove a source from the laboratory!

Some Useful References for Experimenters

Experimental Methods and Apparatus

- W.D. Preston and E.R. Dietz, *The Art of Experimental Physics*, (Wiley, New York, 1991), Math/Phys/Astr QC33 .P74 1991.

- A.C. Melissinos, *Experiments in Modern Physics*, (Academic Press, New York, 1966), Math/Phys/Astr QC33 .M52 + others.

- J.H. Moore, C.C. Davis, and M.A Coplan, *Building Scientific Apparatus - A Practical Guide*, Second Edition (Addison-Wesley, Reading MA, 1989). Math/Phys/Astr Q185 M66 1983

- W. R. Leo, *Techiques for Nuclear and Particle Physics Experiments*, Second Edition, (Springer-Verlag, 1994), Math/Phys/Astr QC793.46 L44 1994

- Konrad Kleinknecht, *Detectors for Particle Radiation*, Second Edition, (Cambridge University Press, 1998), Math/Phys/Astr QC793.46 L44 1994

- G.F. Knoll, *Radiation Detection and Measurement*, John Wiley & Sons 1979 (The lab has a copy)

Good Basic Books on Optics, Atomic and Nuclear Physics

- Jurgen R. Meyer-Arendt, *Introduction to Classical and Modern Optics*, Second Edition, (Prentice-Hall, 1984), Math/Phys/Astr QC355.2 M49 1984 - Excellent development of basic optics with experimental details.

- Kenneth S. Krane, *Introductory Nuclear Physics*, (John Wiley & Sons, 1988), Math/Phys/Astr QC777 K73 1987

- Sune Svanberg *Atomic and Molecular Spectroscopy*, Second Edition (Springer-Verlag, 1992), Math/Phys/Astr QC454 A8 S85 1992 – Good concise description of basic theory, techniques and practical applications.

Electronics

- P. Horowitz and W. Hill, *The Art of Electronics*, Second Edition (Cambridge University Press, New York, 1989). Moore School TK7815 H67 1989

Statistics and Mathematical Analysis

Proper error analysis is extremely important for experimental measurements. Some references are given:

- Barford, *Experimental Measurements: Precision, Error, and Truth*, Math/Phys/Astr QA275 B27 1985.
- P.R. Bevington, *Data Reduction and Error Analysis for the Physical Sciences*, (McGraw Hill, New York, 1969). Math/Phys/Astr QA278 B48. The lab also has a copy.
- Glen Cowan, *Statistical Data Analysis*, Oxford Science Publications, 1998.
- Louis Lyons, *Statistics for nuclear and particle physicists*, Math/Phys/Astr Qc776 L96 1986.
- William H. Press, William T. Vetterling, Brian P. Flannery, Saul A. Teukolsky, *Numerical Recipes, The Art of Scientific Computing*, (Cambridge University Press, Cambridge, UK, 1992). Moore QA76.73.C15 N865 1992.
- John R. Taylor, *An Introduction to Error Analysis*, (University Science Books, Sausalito, 1982).

Handbooks

The books in this section are a good place to look for various data and to check experimental results.

- *A Physicist's Desk Reference - Second Edition of Physics Vade Mecum*, edited by H.L. Anderson (American Institute of Physics, New York, 1989), Math/Phys/Astr QC61 .P49.

- *CRC Handbook of Chemistry and Physics*, 75th Edition, CRC Press.
- *American Institute of Physics Handbook- Third Edition*, edited by Bruce H. Billings and others, New York,

  1972), Math/Phys/Astr QC61 .A5 1972.

Websites

The web page for the lab is:

`http://surf.hep.upenn.edu/~kroll/p414_521_spring04/`

Websites to advanced physics labs at other institutions are:

- `http://www.pma.caltech.edu/~ph77/`
- UC Berkeley

  `http://socrates.berkeley.edu/~phylabs/adv/index.html`
- Harvard

  `http://www.courses.fas.harvard.edu/~phys191r/`
- MIT

  `http://web.mit.edu/8.13`

  Websites for reference data are
- `http://nucleardata.nuclear.lu.se/nucleardata/toi/`
  Data on nuclear isotopes, half life, energies etc.
- `http://physics.nist.gov/cuu/Constants/index.html?/codata86.html`
  Physical reference data

  `http://www.ehrs.upenn.edu/`

  This website informs you about safety around radiation sources, lasers, etc.

The list of good references is "always under construction." Let Jose Vithayathil or Joe Kroll know if there is another reference that you find particularly helpful.

Chapter 2

Measurement of the Gravitational Constant

Introduction

Newton's law of universal gravitation states that any two (point) masses m_1 and m_2 separated by a distance r attract each other with a force

$$F = G\frac{m_1 m_2}{r^2}$$

where G is a universal constant. This constant may be measured with a torsional pendulum, or Cavendish balance. For more details, see Ref. 1. In our version the torsional pendulum consists of an aluminum beam of square cross-section (mass 31 gm) to which two lead spheres of mass 0.091 kgȧre attached at the ends. The center of each lead ball is 15.24 cm from the center of the beam. The beam is suspended inside an evacuated enclosure by a stainless-steel wire of 0.001 inch in diameter. Why is the chamber evacuated? The wire is just barely strong enough to support the beam, and is consequently very fragile. A mirror is attached to the center of the beam. A laser beam is reflected by the mirror onto a photodiode that is mounted on a printer carriage. The position of the photodiode is controlled by computer to track the position of the beam. Four large lead spheres can be arranged to exert either a positive or negative torque on the beam. To reduce the possibility of biased measurements , G, should be determined with the large mass as an unknown parameter. It will be supplied once you have completed the experiment.

Experimental Procedure

Evacuate the enclosure that surrounds the balance for several minutes to a pressure of approximately 50 millitorr. *Open the valve gradually.* If it is opened rapidly the balance can go into large amplitude oscillations and it will be a few hours before one can start taking data. Then close the valve between the vacuum enclosure and the pump and turn the pump off. The air flow from the evacuation usually generates an oscillation of the torsion balance.

Determine the period of the full oscillation of the torsion pendulum. From the period you can determine the spring constant of the wire. The data is recorded by computer using Labview[1]. The program to track and record the position of the beam is called 'Cavendish.vi'. It records the position of the beam every few seconds.

If the amplitude of the oscillation is inadequate for this purpose, it can be increased by "pumping" energy into the torsion balance through repeated repositioning of the large spheres in proper phase with the motion of the balance arm.

Observe the motion of the balance first with one pair of the large spheres in place and then for the other pair.

The position is determined in plotter units. To convert the plotter units to length run the program 'Cavendish-cal.vi'. It enables one to move the plotter by a certain number of plotter points. The displacement is measured with a vernier caliper.

From the net deflection of the equilibrium position, calculate G. (Remember to record all the distances that are required for the calculation.) For an accurate result numerous effects have to be considered such as damping, back attraction (reverse torque executed by the large sphere on the remote small one), torque on aluminum beam, non-harmonic terms in the oscillation, other masses in the room, etc. Consider these effects carefully and calculate corrections where necessary. Do the masses near the cavendish balance be taken into account? Do the effect of large masses like the moon and the sun be accounted for? From your value for 'G' determine the mass of the earth.

[1] Labview is a commercial programming environment used for data acquisition.

PRECAUTIONS

The laser is dangerous. Never look into the beam, or a specular reflection of it. Follow the operating instructions provided. The wire suspension of the balance if very delicate. Pump down slowly and carefully.

References

1. D. Halliday and R. Resnick, .*Fundamentals of Physics*, John Wiley and Sons, 1970.

2. E. M. Purcell, American Journal of Physics **25**, 393 (1957).

3. G. G. Luther and W. R. Towler, Phys. Rev. Letters . **48**, 121 (1982).

Chapter 3

Speed of Light

In this experiment we send a light pulse over a sufficiently long path, reflect it back and measure the travel time for the round trip. Then we measure the length of the flight path and determine the speed of light in air.

Apparatus

A block diagram of our setup is shown in figure 3.1.

Our light source is a Ga-As injection type laser, a device of the size of a common transistor. The Ga-As laser beam is near-infrared ($10500\mathring{A}$). Using the circuit shown in Fig 3.2, we can obtain repetitive pulses with a rise time of about 20 ns. The Ga-As laser acts like a diode with a very low forward resistance ($\approx 1\Omega$). Large current pulses of very short duration are "injected" into it to produce lasing. In our laser the threshold current is about 12A and the peak current about 30A. Rated peak output is 2W. In the circuit the 3300 pF capacitor is charged to 500V until the silicon controlled rectifier (SCR) is fired by an external trigger pulse. The capacitor then discharges through the laser. The requirements for the trigger pulse are not critical. We are using square shaped pulses from a pulse generator about 5V in height, a few microseconds long with a repetition rate around 200 s^{-1}.[1]

The photo detector is a silicon photo diode. A diagram of the circuit is shown in Fig. 3.3. The circuit can be powered either from the external 500V power supply that powers the laser or from a built-in 120V battery. Because

[1]Avoid looking directly at the laser while it is pulsing even though the average power is small $\approx$ 1 microwatt.

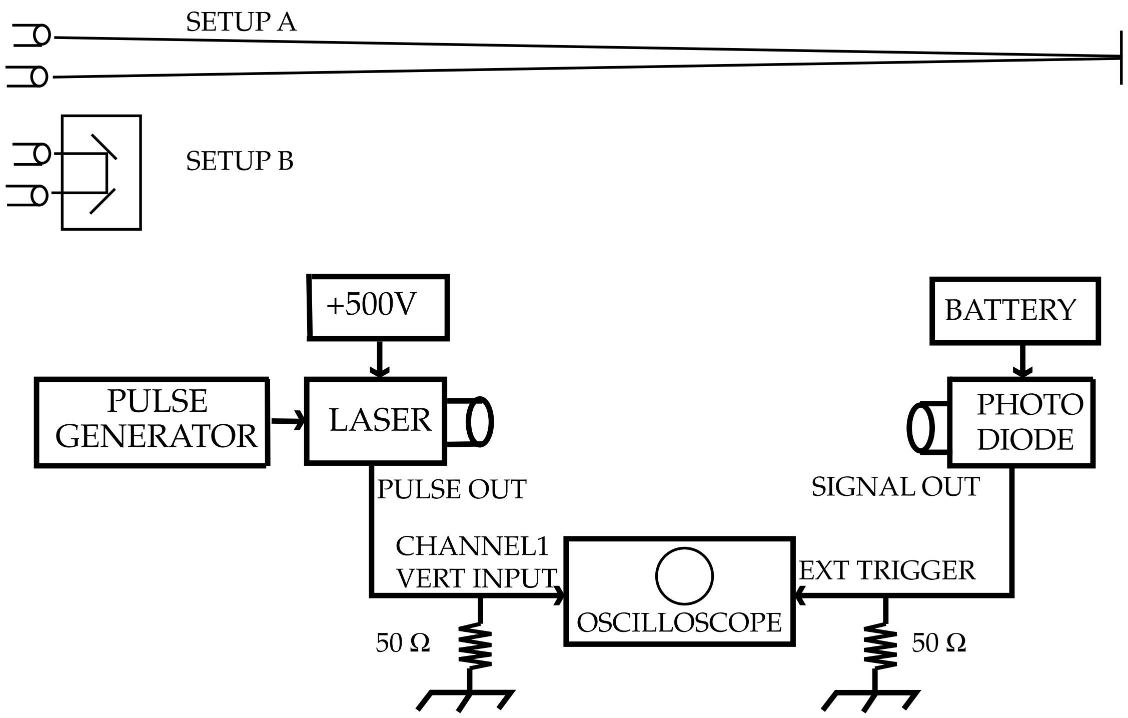

Figure 3.1: Setup and Block diagram of the apparatus

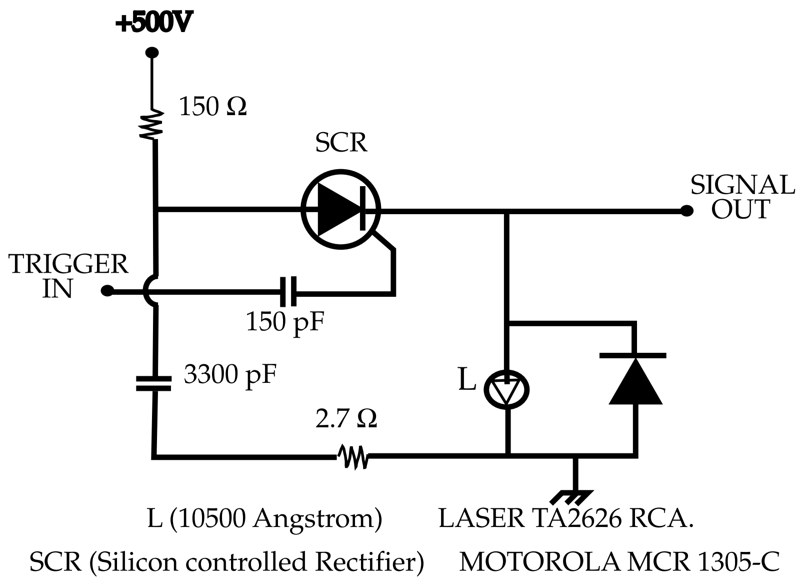

Figure 3.2: Trigger circuit for the laser

of the high signal strength from the laser pulse, the guard ring, which can help to reduce noise does not need to be biased. The RC filter at the output eliminates low frequency signals, such as 60 Hertz variations due to room lighting.

Both the laser and the detector are housed in aluminum enclosures which are equipped with camera lenses for good light transmission.

Flight time measurement with an oscilloscope

We choose the total length of the two rooms 2N23 and 2N25 as our flight path. The far mirror is already aligned. Do not change the alignment. The digital oscilloscope used has many features including averaging capability. Before taking real data one should be spend some time learning some of the features. The flight time is then measured with an oscilloscope which is triggered by the output signal from the laser circuit. The output pulse from the photo diode circuit is displayed on the oscilloscope screen. The delay between the trigger and the beginning of the pulse rise represents the flight time of the laser pulse plus some delay time that is built into the vertical amplifier of

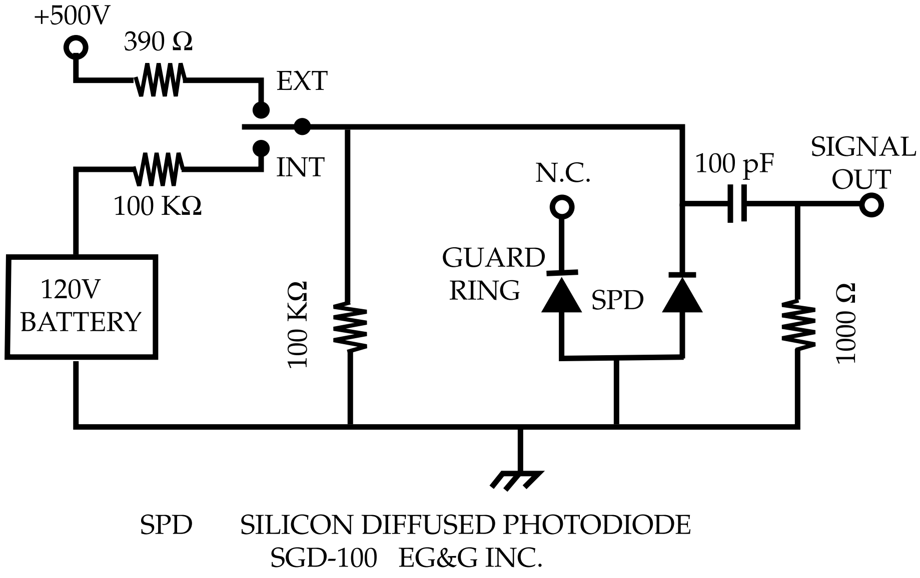

Figure 3.3: Detector Circuit

the oscilloscope. To eliminate this unknown oscilloscope delay we make a second measurement with the receiver placed directly in front of the laser (receiver position B) and determine the flight time from the time difference between the pulse rises for the two configurations. In position B the receiver is exposed to a much higher light intensity from the laser than in position A. To avoid a systematic error linked to the change in the pulse height of the receiver output, we slightly shift or rotate the receiver in position B until the pulse height assumes the same value as in the first measurement. Finally we have to measure the length of the flight path with a precision 100 ft. tape measure.

Flight time measurement with electronic circuitry

The accuracy of the result obtained using the oscilloscope is almost entirely limited by the precision of the time difference measurement with the oscilloscope. Two factors that cause the most error in the time measurement are changes in amplitude and rise time of the detected signal and the precision to which one can time difference.

How can small changes in signal amplitude effect the time difference? Clue – the oscilloscope triggers at a fixed voltage level.

In this part a constant fraction discrimator (CFT) is used to reduce the error due to changes in signal amplitude and rise time and a multichannel analyzer is used to improve the time resolution. To learn how a constant fraction timing discriminator works see reference [1]. Basically a CFT has circuitry that sums the input signal that is attenuated by a fixed fraction and the input signal that is delayed by an amount less than the rise time of the signal. The CFT outputs a pulse at the zero crossing time. The delay is determined by an internal delay (0.7ns) and an external delay 4.8ns from about 1m of coaxial cable. Since the delay is less than the rise time, the pulse is unaffected by slope changes later on.

The block diagram of a setup that permits such a measurement is shown in Fig. 3.4.

The output of the CFT goes to a time to amplitude converter (TAC). The TAC outputs a voltage proportional to the time difference between the start and stop pulses. The TAC output is recorded on a multichannel analyzer (MCA). An analogy to a MCA would be a oscilloscope with the x (time axis) on the oscilloscope replaced by the voltage for the MCA and the y axis (voltage) for the oscilloscope replaced by the number of counts (events) at that voltage for the MCA.

The signal is recorded on the MCA for both the long distance and the short distance. The peaks can be interpolated to better than one channel width. The difference in the channel numbers is proportional to the time difference.

Finally the channel numbers which are proportional to the time have to be converted to the time increments. This is done by the setup shown in figure 3.5.

A time calibrator (Ortec 462) is adjusted to output pulses separated by multiples of the set interval. (One should read the manual for the instrument to figure out how to use it). From this measurement the MCA channel number is converted to time.

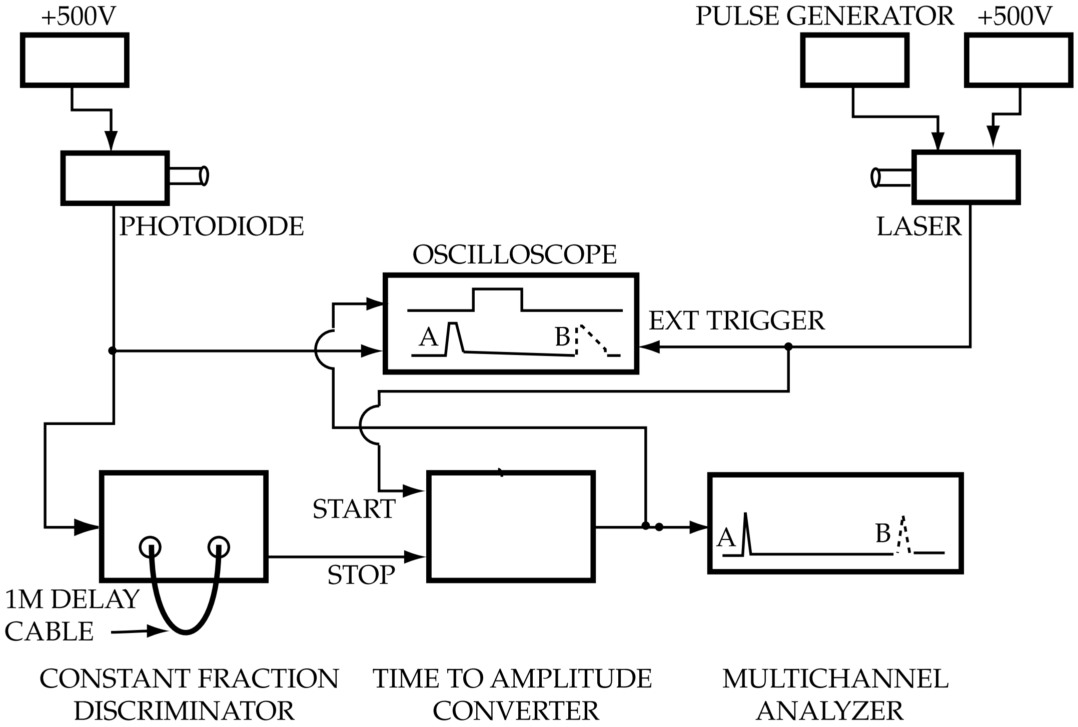

Figure 3.4: Constant Fraction Discriminator setup for the velocity of light

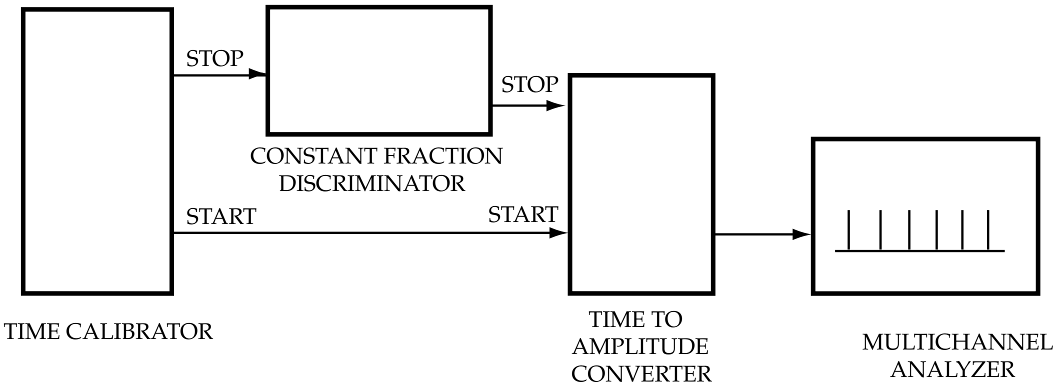

Figure 3.5: MCA calibration circuit

References

Radiation Detection and Measurement, G. F. Knoll, John Wiley & Sons 1979. (The lab has a copy)

Chapter 4

Stern-Gerlach Experiment

Introduction

In this experiment we employ the technique of measuring atomic magnetic moments by the deflection pattern of a beam on passing through an inhomogeneous magnetic field that was initiated by the classic experiment of Stern and Gerlach in 1921.

A schematic view of the apparatus is shown in the figure 4.1.

A beam of neutral atoms leaves the oven and passes through two sets of narrow defining slits and a shutter into the magnetic field region. Here the atoms are deflected by the magnetic field gradient. The intensity distribution formed by the deflected atoms is scanned by a surface ionization detector at some distance behind the magnet. The drawing is not to scale and the actual beam deflection is only a few millimeters. In our experiment we are using a beam of potassium atoms, a convenient choice for several reasons. From an atomic structure point of view, we know that potassium, an alkali metal, has one electron in an $S_{\frac{1}{2}}$ state outside the closed shell of argon. Therefore there is no orbital contribution to the angular momentum and the magnetic moment is equal to the intrinsic magnetic moment of the electron. From the experimental point of view potassium has the advantage of a low melting point and a sufficiently high vapor pressure to produce beams of adequate intensity at temperatures between 120^0C and 180^0C.

The potassium is ionized with close to 100% probability when it strikes a hot tungsten filament maintained at around 1800K. The ionization potential for potassium (I) is 4.34 eV ($\approx$ 50000K). The work function of tungsten (ϕ)

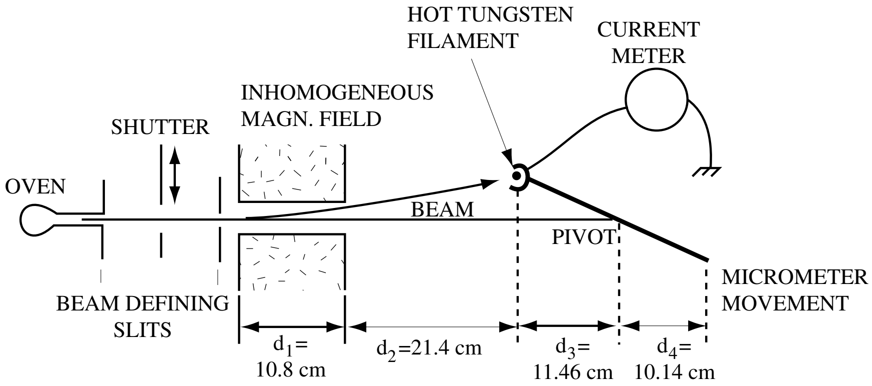

Figure 4.1: Block diagram of the apparatus

is 4.5 eV. Near a tungsten surface the energy to ionize the potassium atom is reduced by the work function (see for example Solid State Physics by Ashcroft and Mermin for an explanation of work function) . For n potassium atoms striking the tungsten surface, the number of ionized atoms, n^+, is given by

$$\frac{n^+}{n} = e^{-e(I-\phi)/kT}$$

The potassium ions are collected by the collector which is $\approx$ -20V with respect to the tungsten filament. The current is proportional to the number of potassium atoms striking the tungsten filament.

The entire apparatus is enclosed in a high vacuum chamber. It is essential to keep the pressure low (better than 10^{-6} Torr) because poor vacuum can lead to serious side effects. Inside the oven it can oxidize the potassium and thereby greatly reduce the beam intensity. The beam itself can be broadened in poor vacuum because of the large cross section for small angle scattering. The detector also requires excellent vacuum because it shows a background current roughly proportional to the residual pressure. In addition, any contamination of the detector region with potassium (other than the very small amount present in the beam) can lead to a very large increase in the background current and can render the detector unusable. For these reasons a considerable effort has been made to equip our setup with two small, but effective, oil diffusion pumps. Also, the vacuum systems on the two opposite sides of the magnet are almost completely separated. They are only joined by a very narrow stainless steel tubing. Excellent vacuum can be maintained in the detector region even during startup, when the oven outgases heavily. Therefore, good results can routinely be obtained.

The Magnetic Moment of Potassium

The precision of our measurement of the magnetic moment of potassium is determined by the accuracy of our knowledge of the magnetic field gradient and of the broadening of the deflected beams by the velocity distribution of the atoms in the beam. In the derivation below we assume a Maxwell-Boltzmann distribution for the atoms in the oven, despite uncertainties in the understanding of the emission process from the oven wall and the collision process between potassium atoms (e.g., the formation of clusters). The velocity distribution of the beam is then given by:

$$\frac{dI}{dV} = 2I_0 \frac{\nu^3}{\alpha^4} e^{-\frac{\nu^2}{\alpha^2}}$$

with $\alpha^2 = \frac{2kT}{M}$ where,

I_0	total intensity of the beam
v	velocity of an atom
α	most probable velocity of atoms in the oven (not the beam)
k	Boltzmann constant
M	mass of the atom

If we neglect transverse velocity components resulting from the finite slit geometry and from small angle scattering, we find for the beam deflection s(v) at the detector

$$s(v) = \mu_z \frac{\partial B_z}{\partial z} [d_1^2 + 2d_1 d_2] \frac{1}{2Mv^2}$$

where

μ_z	magnetic moment of the atom
$\frac{\partial B_z}{\partial z}$	magnetic field gradient
d_1, d_2	distances indicated in Figure 4.1

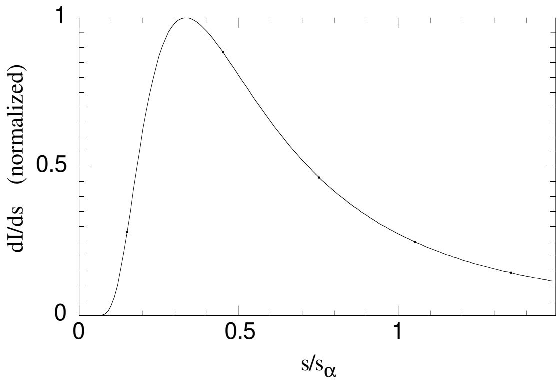

Figure 4.2: See text for definition of axis

The deflection pattern for atoms at the detector is given by

$$\begin{aligned} \frac{dI}{ds} &= \frac{dI}{dv}\left(\frac{ds}{dv}\right)^{-1} \\ &= -I_0 \frac{s_\alpha^2}{s^3}\exp\left(-\frac{s_\alpha}{s}\right) \end{aligned}$$

where $s_\alpha = s(\alpha)$

It peaks at $s = \frac{1}{3}s_\alpha$ (see Fig. 4.2

We find for the magnetic moment

$$\mu_z = \frac{12kTs_{peak}}{[d_1^2 + 2d_1 d_2]}\left(\frac{\partial B}{\partial z}\right)^{-1}$$

Experimental Procedure

Take measurements at two different temperatures between 120 and 170C. At each temperature make measurements for atleast 4 field gradients including 0. The oven should be set for a given temperature. It takes 90 minutes for the temperature to equilibrate. The data is recorded on a chart recorder. It can also be optionally acquired on a computer so that the line shapes can be fitted to the predicted shapes to determine the peaks more accurately. For each temperature the steps are as follows:

1. Measure the beam intensity as a function of detector position with the magnet off and a stable furnace temperature of about 130^0 (between 120^0 and 170^0 C). Use the automatic drive and X-Y recorder. Take curves in both positive and negative directions (different color pens are useful). Calibrate the X-axis of the recorder in terms of micrometer reading.

2. Repeat the measurement for different magnetic field gradients.

3. Measure the distances d_1, d_2, d_3, and d_4 on the apparatus as carefully as possible and convince yourself that your results are consistent with the data given in the figure. Determine the magnetic field gradient from the data displayed on the wall charts.

4. Use the data to determine the g-factor of potassium and compare with the theoretical value.

Do not leave the oven on overnight. If the furnace stays hot too long, all the potassium boils off and plates the inside of the apparatus. This is to be avoided.

References

1. O. Stern, Zeitschrift fr Physik **7**, 249 (1921); W. Gerlach and O. Stern, Zeitschrift fr Physik **8**, 110 (1922).

2. F. Smith, *Molecular Beams*, John Wiley & Sons, New York (1955).

Chapter 5

DC Magnetic Susceptibility of Materials

Aim of the Experiment

The aim of the experiment is to measure the DC magnetic susceptibility of several substances.

Before you start

1. Review what causes a substance to be a diamagnet, a paramagnet or a ferromagnet [2].

2. How does the susceptibility of a diamagnet or a paramagnet vary with temperature? What is the Curie-Weiss relation for susceptibility?

3. How does a magnetic field gradient produce a force on a material in the direction of the field gradient? Would a diamagnetic substance be attracted or repelled from the region of increasing magnetic field?

4. What is the Guoy method [3] to measure magnetic susceptibility? Why is it not necessary to know the magnetic field gradient? Would the Guoy method applicable for a ferromagnetic material?

Measurement

In this experiment you will measure the DC magnetic susceptibility for three substances — a diamagnet, a paramagnet and a paramagnet that becomes a ferromagnet when cold. The materials are bismuth, $NiCl_2.6H_2O$ and an amorphous metal alloy. The amorphous metal alloy is commercially known as metglas 2826A. It's composition is $Fe_{.32}Ni_{.36}Cr_{.14}P_{.12}B_{.06}$. The substances are in a glass tube. An empty glass tube is provided to compensate for the susceptibility of the glass.

The susceptibility of all the materials are to be measured at room temperature. In addition the temperature dependence of the susceptibility of $NiCl_2.6H_2O$ and metglas has to be measured from around 130K to room temperature to determine the magnetic moment on a molecule of $NiCl_2.6H_2O$ and to determine the ferromagnetic transition temperature of metglas.

As usual errors in the measurement should be determined. The result for bismuth and $NiCl_2.6H_2O$ should be compared with published values.

Introduction

A sample an applied magnetic field 'H' has a magnetic flux density 'B' given by,

$$B = \mu_0(H + M)$$

'M' the net magnetic moment due to microscopic magnetic dipoles per unit volume. The magnetic susceptibility 'χ' and the magnetic permeability 'K' are obtained from the relation as

$$1 + \chi = K = \frac{B}{\mu_0 H} \tag{5.1}$$

'μ_0' is the permeability of vacuum[1].

The molar susceptibility, 'χ_{mol}', can be obtained from the volume susceptibility using $\chi_{mol} = \chi\frac{A}{D}$. D is the density and A the atomic weight.

A diamagnetic sample reduces the magnetic flux through it and χ is negative. Diamagnetism occurs because shielding currents are set up in atoms and molecules opposing the magnetic field. It turns out that even closed 'S' orbital electrons develop a magnetic moment opposed to the magnetic field.

[1]SI units are used

A paramagnetic sample or a ferromagnet increases the magnetic flux through it and χ is positive. Paramagnetism can occur for a variety of reasons. If there are closely spaced energy levels in an atom or molecule Van Vleck paramagnetism occurs. In a metal one has Pauli paramagnetism. Paramagnetism also occurs in a solid because an atom or ion has a magnetic moment. The magnetic moment arises because the free atom or ion has a magnetic moment or because of an interaction between atoms or ions in a solid called the 'exchange' interaction. Both diamagnets and paramagnets have no macroscopic magnetic moment in the absence of a field. Van Vleck and Pauli paramagnetism are usually temperature independent. The temperature dependent macroscopic paramagnetism due to permanent microscopic moments is given by the well known Curie-Weiss relation —

$$\chi = \frac{Nm^2}{3Vk(T - \Theta)} \tag{5.2}$$

where 'N' is the total number of molecules in a volume 'V', 'm' the magnetic moment per molecule, 'k' the Boltzmann constant and 'T' is the temperature. The magnetic moment of $NiCl_2.6H_2O$ should be determined and checked with the magnetic moment expected due to the magnetic moment of a nickel atom.

A ferromagnet has groups of magnetic moments aligned in regions called domains in zero field[2]. Neighboring domains are aligned in different directions [5]. In a small applied field the magnetic domain walls move reversibily so that there is a net magnetic moment aligned in the direction of the magnetic field. As the field is increased the domain walls move through imperfections like dislocations in the crystal. This results in hysteresis. A typical hysteresis curve is shown in figure 5.1. The susceptibility of ferromagnetic materials is generally a few orders of magnitude greater than the susceptibility of paramagnetic and diamagnetic substances[3]. The susceptibility is also field dependent. In our experiment there is always a residual field of ≈ 35 Oe. Even at this relatively high field the susceptibility of ferromagnets is large and of the order of 100. This property will be used to determine the ferromagnetic transition temperature. Table 5.1 shows the susceptibilities of

[2]This occurs because the interactions between magnetic moments is short ranged and goes as 'n' — the number of molecules while the magnetic energy is $\int \frac{B^2 V dV}{2\mu_0}$ varies as n^2.

[3]For ferromagnets, it is customary to give the permeability K, which is $1 + \chi$. In a ferromagnet the internal field due the magnetic moments is much greater than the applied field. Since the the applied field is responsible for domain wall motion and not the response of individual magnetic moments the concept of susceptibility has little meaning.

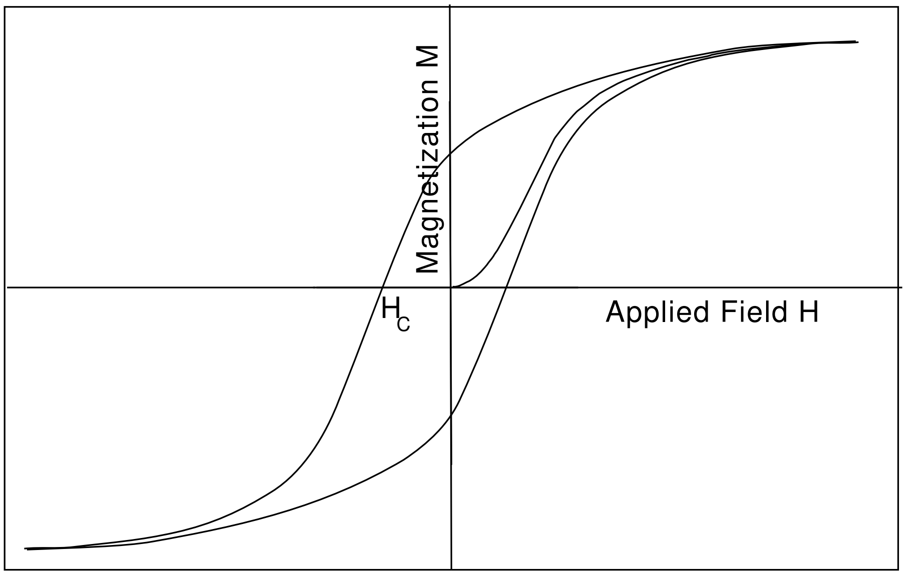

Figure 5.1: Hysteresis curve for a ferromagnetic substance

Material		Susceptibility χ_{mol}		Coercivity H$_c$ (Oe)
		Initial	Maximum	
Diamagnet	Copper	-5.4610^{-5}		
	Diamond	-5.910^{-5}		
Paramagnet	Aluminium	16.510^{-6}		
	Oxygen (1 atm at 273K)	344910^{-6}		
Ferromagnet	Pure Iron (annealed)	25000	350000	0.05
	Mumetal	20000	100000	0.05

Table 5.1: Room temperature molar susceptibilities of some materials in cgs units. To convert to SI units use 1 A/m = $4\pi 10^{-3}$ Oe. To convert the molar susceptibility from the cgs value to SI the cgs value has to be multiplied by 4π. Data taken from [1], [4] .

some materials. A paramagnetic substance when cooled sufficiently will become a ferromagnetic below a critical temperature. One might naively expect a glass like behavior for the magnetization of metglas. However amorphous magnets are seen to exhibit standard critical behavior with a well defined critical temperature and exponents[4],[5].

The Guoy method to determine susceptibility

The setup for the Guoy method is shown in figure 5.2. The expression for the force can be determined from simple energy considerations[6]. Assume a long sample of cross sectional area 'a'. One end of it is in zero applied field and the other end is in an applied field 'H'. Turn off the field move the sample an infinitesimal distance 'dx' into the previous magnetic field and then ramp back the magnetic field to the original value. The change in energy is[7]

$$\Delta E = -\int_H \mu_0 (H+M) dHadx + \int_H \mu_0 HdHadx \tag{5.3}$$

$$= -\frac{\mu_0 \chi H^2 adx}{2} \tag{5.4}$$

The force is 'F' is $\frac{-dE}{dx}$. This gives the volume susceptibility. If the medium is not vacuum the '$\chi - \chi(medium)'$ must be substituted for 'χ'.

Because of the cylindrical geometry with the field perpendicular to the axis, there is a correction due to shielding by the surface magnetic moments. The demagnetization factor is $\frac{1}{2}$ for a long cylinder with a magnetic field perpendicular to the axis is $\frac{1}{2}M$. Estimate if this correction needs to be applied to obtain the actual susceptibility.

If the magnetization is not linear with applied field as is the case with a ferromagnet then one would expect a deviation from the force varying as H^2.

[4]This is because critical behavior occurs when there are correlations on ever larger length scales and the microscopic structure is not relevant.

[5]Amorphous magnets are important technologically because they have high permeability and low hysteresis losses compared to the same crystalline materials. Hysteresis is thought to occur in amorphous magnets mainly due to variation in the coupling between local moments rather than imperfections in the structure.

[6]See [3] for an alternate derivation.

[7]This is the total energy, including the energy required to create the magnetic field by say sending current to a coil

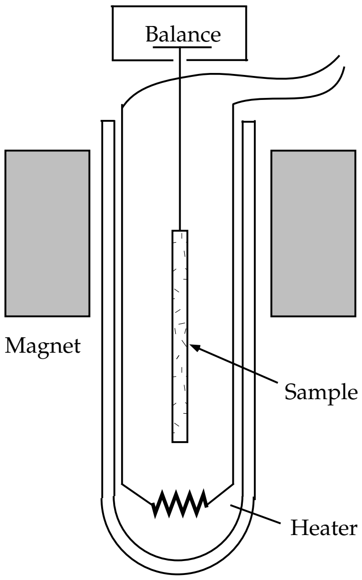

Figure 5.2: Apparatus

Procedure

A schematic of the apparatus is shown in figure 5.2

The sample is hung from a balance between the pole pieces of a magnet. The force is determined by weighing the sample as the magnetic field is varied. The field is measured by a Hall probe permanently installed on one of the magnet pole faces.

Room temperature measurements

For the first part the susceptibility is measured at room temperature. The sample should be gently hung from the balance. Care should be taken to make sure that the frayed ends of teflon do not touch the sides of the dewar or the insert. Looking with a flashlight may be helpful. *Turn on* the cooling water to the magnet before turning on the magnet. The tap is by the sink. Check that the magnet current knob is turned all the way to zero and then turn on the magnet. Turn just the current knob. Make measurements of the force as a function of field up to a maximum field of 8000 gauss. large *Make sure the field does not exceed 9000 gauss.* The balance can be tared so that the weight of the sample is zeroed out. When making measurements check for drifts in the balance.

Temperature dependence of susceptibility

Pour some liquid nitrogen into the dewar. Once the bubbling stops pour more liquid up to the mark on the masking tape. Suspend one of the samples – either the $NiCl_2.6H_2$ or the intermetallic compound as in the first part. Make sure the sample does not touch the sides of the insert. If it does touch it will give wrong readings. One can check for this by ramping the field up and down. If there is static friction due to contact hysteresis in the force should be observed.

Put 10 volts into the heater resistance (22 Ω at room temperature). The vapor from the liquid nitrogen will cool the sample. The temperature is measured by the thermocouple. The temperature should fall to around 130K and then start rising. Why does it start rising? At this point reduce the heater supply voltage to 7 volts to reduce the warmup rate.

Measure the force as a function of field. Since the temperature is rising it should also be recorded. It might also be good to measure the time. One would have to determine the rate at which moisture is condensing on the sample. How would one do this? If it is significant it has to be corrected. When the rise in temperature becomes low the heater power supply can be increased to 10 volts.

Metglas becomes ferromagnetic when cold. There is an appreciable sideways force on the sample at large field and this causes the sample to touch the insert. So measurements have to be made at a field lower than this. The maximum field can be determined visually be checking when the sample moves towards the pole faces and also by checking for hysteresis in the force. The force is of the order of 1 gram weight. Measurements should be made so that the force is less than this. Since the susceptibility is temperature dependent the field for this force would vary with temperature.

The calibration of the thermocouple should be checked by inserting it in liquid nitrogen and ice. If there is an offset, a linear approximation must be made to correct for the temperature.

Material	Mass (gms)
Bismuth	40.03
$NiCl_2.6H_2O$	7.56
Metglas	0.2235
Reference glass tube	13

Table 5.2: Mass of the samples

Miscellaneous Data

The masses of the samples are given in table 5.2

The inner diameter of the reference glass tube should be measured and used as the inner diameter of the the bismuth and $NiCl_2.6H_2O$ glass tubes.

The metglass is in a glass tube that is of a different mass than the reference glass tube. Since the susceptibility of metglass is large ignore the small correction due to the glass.

Bibliography

[1] Herbert L. Anderson, editor. *Physics Vade Mecum.* American Institute of Physics, 1981. (In Mat/Phys/Astr library Call Number QC61 .A37)

[2] Neil W. Ashcroft and N. David Mermin. *Solid State Physics.* Saunders College, 1976. (In Mat/Phys/Astr library Call Number QC176 .A83)

[3] B. D. Cullity. *Introduction to Magnetic Materials.* Addison-Wesley Publishing Company, 1972. (In Mat/Phys/Astr library Call Number QC753.3 .C84 and also in Moore library)

[4] david R. Linde, editor. *Handbook of Chemistry and Physics 73rd edition.* CRC Press, 1992. (In Mat/Phys/Astr library reserve)

[5] Rita G. Lerner and George L. Trigg, editors. *Encylopedia of Physics.* VCH Publisher, 1990.

Chapter 6

Nuclear Magnetic Resonance

Nuclear magnetic resonance is a very useful technique to study condensed matter. The tiny nuclear magnets are excellent probes to study phenomena without disturbance because they interact weakly with their environment.

This experiment uses pulsed nuclear magnetic resonance. The sample used is water. The aim of the experiment is to determine nuclear spin relaxation times (T_1 and T_2 and to study spin echoes. You will also measure the coefficient of self diffusion of water molecules. A background on NMR and the experiment is available as a written handout. More details will be added later.

Reference

D. Slichter C.P., .*Principles of magnetic resonance*, John Wiley and Sons, 1990.

Chapter 7

Optical Tweezer

(Lab Manual incomplete)

Optical tweezers allow one to manipulate mesoscopic matter in various environments especially in aqueous solutions. It is particularly used to study biological and other dielectric media.

This experiment optically traps polystyrene and silica beads with a laser at 780nm. The aim is to calibrate the trapping force on various micron size beads with varying laser power.

A background on the optical tweezer setup and the experiment would be described in more detail to the interested student.

Reference

Mara Prentiss etal, *American Journal of Physics* **67**, 26 (1999).

Chapter 8

Atomic Spectroscopy – Fine Structure

Introduction

This lab is to determine fine structure splitting in sodium and the isotope splitting in atomic hydrogen and deuterium[1]. A Fabry Perot interferometer is the ideal instrument for determining small shifts in wavelength optically and it is used in this experiment. A Fabry Perot interferometer is typically able to resolve wavelength to a part in 10^5 or better[2]. The instrument is described in most optics texts[3]. It consists of two parallel highly reflecting surfaces separated by a distance which can be varied.[4]

Fine structure splittings are $\approx 10^{-3}$eV or less. Fine structure splittings for rubidium which is an alkali metal like sodium are discussed in the appendix to the Optical Pumping lab in the next chapter and it should be read. The isotope shift occurs because the deuterium nucleus has a larger mass than hydrogen. The two body system of the electron and the nucleus can be reduced to a single fictitious mass — $\frac{m_{el}+m_{nuc}}{m_{el}+m_{nuc}}$, in a central potential. It is

[1]Atomic hydrogen and deuterium is produced by electric discharge in a specially designed designed tube. Care is taken to absorb most of the molecular hydrogen and deuterium

[2]To resolve much smaller splittings (Hyperfine shifts) radio frequency techniques like nuclear magnetic resonance (see the optical pumping experiment) or the mossbauer effect are used.

[3]See for example reference 1 for a description and formulas.

[4]If the distance is fixed it is called a Fabry Perot etalon.

discussed in many quantum mechanics texts[5].

Experimental Procedure

Initally familiarize yourself with the Fabry Perot interferometer. It has two knobs (coarse and fine) to adjust the separation between the mirrors. The experiment consists of two parts.

In the first part the fine structure splitting of sodium is determined. It has two strong yellow lines at ≈5890 angstroms. Turn on the sodium lamp and observe the circular interference fringes. At an arbitrary separation between the mirrors there are two concentric sets of fringes due to the two lines. As the distance between the mirrors is increased the fringes appear to move outwards with new fringes created at the center. As the mirror separation is varied, at certain separations the fringes from the two lines merge. Record the various distances at which the fringes merge. and from this determine the splitting. Vary the separation from ≈1–6mm.

In the second part turn on the HD lamp. A lens is used to collimate the beam. A red filter is used to transmit just one of the many lines in the Balmer series at ≈6480 angstroms. The experiment is identical to the first part, however the splittings between the lines are smaller. Repeat the measurement as in the first part. Since the splitting is smaller than before only about two merges are observed while varying the separation between ≈1–6mm. From the splitting determine the ratio of the mass of the electron and the proton.

As an optional part a Michelson interfometer can be used to obtain another set of data and the results from the two instruments can be compared.

PRECAUTIONS

The Fabry Perot instrument is delicate. Be *very careful* when the plates are close together and do not let them run into each other. Only vary the separation between the plates using the rough and fine adjust knobs. There are a few other knobs that are for making the surfaces parallel. They are preadjusted and are difficult to set. The HD and sodium discharge lamps use

[5] See for example reference 2.

high voltages, be careful. Also do not leave the HD lamp on for an extended period. It has a limited lifetime.

References

1. Jurgen R. Meyer-Arendt, *Introduction to Classical and Modern Optics*, Second Edition, (Prentice-Hall, 1984), Math/Phys/Astr QC355.2 M49 1984 - Excellent development of basic optics with experimental details.

2. Claude Cohen-Tannoudji, Bernard Diu, Franck Laloe, .*Quantum Mechanics Vol 1 p800-804*, Wiley Interscience, 1977.

3. Sune Svanberg .*Atomic and Molecular Spectroscopy*, Second Edition (Springer-Verlag, 1992), Math/Phys/Astr QC454 A8 S85 1992 – Excellent concise description of basic theory, techniques and practical applications.

Chapter 9

Optical Pumping of Rubidium Vapor

Introduction

Optical pumping is a technique that was developed starting in the 1950's . Alfred Kastler received a Nobel prize in 1966 for his work in the field. It is a technique that has found use in physics, chemistry and medicine. In physics the technique is used in spectroscopy, laser cooling of atoms, preparation of spin polarized nuclei for particle physics and fusion experiments. In chemistry it is used i n the study of surfaces and similar techniques are used in NMR spectroscopy. In medicine it is used for MRI of lungs and biological surfaces.

By optical pumping, atoms can be created with significant changes in the thermal equilibrium population of the hyperfine[1] levels of atoms. In a $\approx$1 Tesla magnetic field at 300K equilibrium, the relative population difference in the hyperfine levels is $\approx 10^{-6}$, with optical pumping techniques it is possible to prepare atoms all of which are in essentially a particular hyperfine level.

For the lab experiment ^{85}Rb and ^{87}Rb are studied[2]. Rubidium has a single 5S electron outside it's closed shell. In addition ^{85}Rb has a nuclear spin of $\frac{5}{2}$ and ^{87}Rb has a nuclear spin of $\frac{3}{2}$. The nuclear magnetic moment splits the 5S and 5P levels to sub levels. In optical pumping the rubidium atoms are

[1] The term hyperfine explained in the appendix.

[2] Rubidium is used because inexpensive commercial lasers used for compact disks are in the right wavelength range and because little or no heating is required to obtain an adequate vapor pressure of rubidium.

excited to ($^2P_{3/2}$) levels in a magnetic field, by circularly polarized light (or photons selected to have angular momentum either $+\hbar$ or $-\hbar$). The selection rules for the decay cause particular sub levels of the 5S hyperfine levels to be populated. To see how this happens one has to know some background material which is developed in the appendix. An excellent source to learn about the material is [1].

Aims of the experiment

The aims of the experiment are as follows:

- Determine the hyperfine coupling constants for ^{85}Rb and ^{87}Rb.
- Determine the nuclear spin of ^{85}Rb and ^{87}Rb.
- Determine the line widths of magnetic resonance signals.

This experiment is fun and rich in phenomena one can observe and measure. For example signals vary in intensity, line width, light intensity and polarization, magnetic field and radio frequency and amplitude in a known way. It is important to vary parameters and to observe and record the observations.

Apparatus

A block diagram of the optical pumping arrangement is shown in figure 9.1. The individual components are described below.

Rubidium cells

There are four cells. Cell 'A' has ^{87}Rb with unknown buffer gas[3]. Cell 'B' has both isotopes of Rb at natural abundance with a buffer gas of 4 torr nitrogen. Cell 'C' has a mixture of ^{85}Rb and ^{87}Rb with ^{85}Rb and ^{87}Rb. unknown buffer gases. Cell 'D' also has a mixture of ^{85}Rb and ^{87}Rb. The line widths are quite broad for cell D.

[3] Buffer gas is used to reduce the collision rate with the walls of the cell. Paramagnetic impurities on the cell walls relax the atoms.

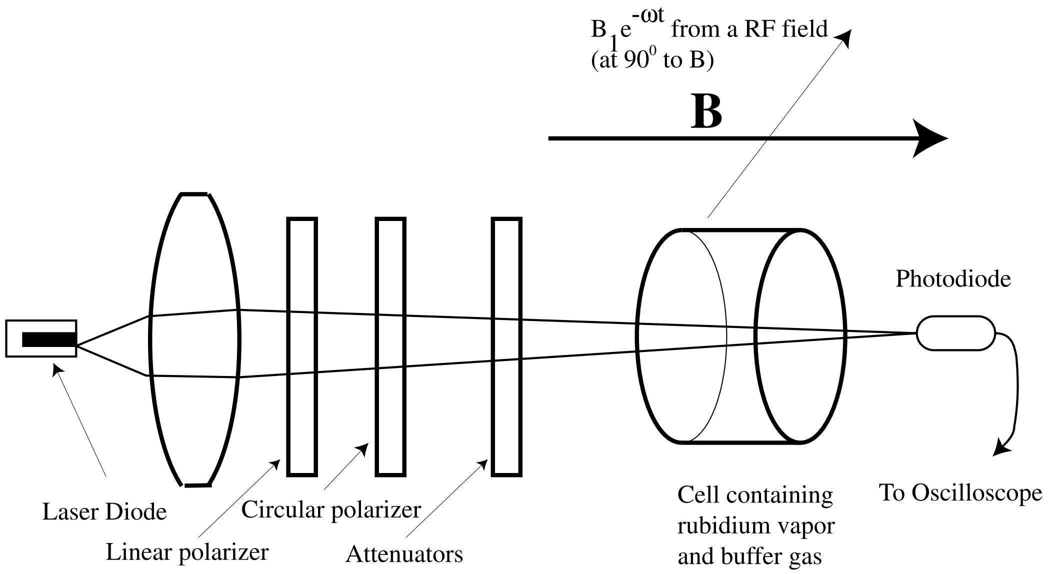

Figure 9.1: Schematic diagram of the apparatus

Laser and control

The laser diode is a 5 milliwatt laser diode[4]. It is mounted on a thermoelectrically temperature controlled block. A controller[5] is used to set the current to the laser diode to make it lase. The controller has an input to modulate the current. Modulating the current modulates the laser frequency (typically a few GHZ). A temperature controller[6] controls the temperature of the block to $\approx$ 1 millikelvin. The temperature changes the frequency of the laser diode much more than with a current sweep. Between 0 – 50C the wavelength changes from $\approx$775 – 790 nm. The frequency of the laser is stable to $\approx$50 MHZ.

Coils

The earth's magnetic field is cancelled out by applying current to two perpendicular Helmholtz coils. The optical bench is oriented to be parallel to

[4]ML4402 from Mitsubishi
[5]LD 2310 from Seastar Optics.
[6]TC5000 from Seastar Optics.

the horizontal component of the earth's field. A radio frequency Helmholtz coil perpendicular to the other coils is used to saturate the spin polarization.

Optical Components

The laser light which is linearly polarized is further polarized by a calcite prism[7]. A variable quarter wave plate circularly polarizes the light when set at $+/-45^0$.[8]. The detector is a 13 mm^2 silicon photodiode biased at 9V. The output goes directly to an oscilloscope without any amplification.

Precautions

The laser diode can be easily burned out by static electricity and surges in current caused by turning on and off equipment connected to it. It is **very important** that the laser current be set to 0, the laser input shorted and the external sweep disabled, before any connections to the laser diode controller are changed or the external current sweep instrument is turned on.

Procedure

Startup

Turn on the laser diode. To do this the following steps must be done in sequence.

- Check that the 'EXT' switch position is on 'DISABLE', 'MODE' switch on 'CURRENT' and 'LASER' switch on 'SHORT' on the laser con-

[7] This is mainly for pedagogic reasons.

[8] Calcite (calcium carbonate crystal) is a rhombohedral crystal. It is optically anisotropic like many non cubic crystals. In a anisotropic crystal there are two special axes called the optic axes (they are not necessarily along the crystallographic axes). In calcite the two axes coincide and the crystal is said to be uniaxial. If unpolarized or linearly (plane) polarized light in an arbitrary direction is incident along the optic axis, it is split into two orthogonal linear polarized components (called the normal and extraordinary ray) which travel with different velocities in the crystal. In a quarter wave plate the thickness is set so that the phase shift is $\frac{\pi}{2}$ For a particular orientation linearly polarized light is split into equal amplitudes of the orthogonal components to produce circularly polarized light. Left or right elliptically polarized light can be produced by rotating the quarter wave plate with respect to the fixed orientation of polarized light. See [2] for more details.

troller (LD-2300)[9]. Turn the 'BIAS CONTROL' on the controller to 0. This sets the laser diode current to 0.

- Turn on the temperature controller (TC-5000). It is preset for the correct temperature and it takes only about a minute to regulate at the set temperature.

- Turn on the current sweep oscillator connected to the laser controller and set the 'AC' knob around the middle of its range.

- Place the rubidium cell 'B' on the platform.

- Turn on the detector and the scope (The settings are: Input - DC coupled, xy display, 1 V/div).

- Next set the controller to 'EXT' switch position to 'ENABLE' and 'LASER' switch to 'NORMAL'.

- Slowly turn the 'BIAS CONTROL', above a threshold current of ≈36 mA the diode starts to lase and you should see a signal on the scope. At ≈49.4 mA the rubidium cell should absorb the light and dips should be observed on the scope because of absorption.

Measurement

The first measurement is the hyperfine constant 'A'. For this –

1. Adjust the current sweep so that the absorption signals are well separated on the scope. Measure in scope units the absorption amplitudes, line widths and signal separation. The photodiode output is linear with light intensity.

2. Insert cells 'B','C' and 'D' and repeat the step 1. You will have to adjust the height using wooden blocks labelled '1' and '2'. Cell 'B' has to be heated for ≈10 minutes to ≈ 50C to get a good signal. Cell 'C' and 'D' are spherical and act as weak lenses. You may have to adjust the focus a tiny bit.

[9]Note the 'up' and 'down' position of the switches are hard to distinguish as they are only slightly different.

3. Next the measurements should be converted to actual frequency. For this we use the Fabry-Perot interferometer formed by the glass faces of cell 'A' or 'B'. Slowly orient the cell, when the faces of the cell are perpendicular to the beam because of interference the photodiode output on the scope becomes periodic[10]. Measure the separation of the beat pattern on the oscilloscope and use the separation of the inner walls of the cells to be 5.12 ($\pm$ 0.01) cm for cell 'A' and 7.71 ($\pm$ 0.01) cm for cell 'B'. **Do not** try to measure the separation with a set of calipers.[11].

Next measure the Zeeman coupling. For this use cell 'A' first.

1. First cancel the earth's field by applying current to the vertical and 'Z' coils. The current setting are: vertical coil –180 mA and to the 'Z' coil at – 4.2 mA. The 'Z' field is modulated at 60HZ with a 12V transformer. Apply a 'Z' field of $\approx$1 Gauss[12].

2. Set quarter wave plate to 45^0 to circularly polarize the light.

3. Turn current sweep amplitude all the way to 0 while staying on one of the absorption lines. Turn off the laser controller sweep oscillator.

4. Connect a rf source (HP 651B) to the third coil. The oscilloscope settings should be changed to 'Input coupling': AC and Y sensitivity to 1mV/div (5mV/div with the X5 MAG knob pulled). Set the frequency to 700 KHZ and an amplitude of $\approx$0.5V peak to peak.

5. Slowly vary the 'BIAS CURRENT' to the laser using the 'DC' knob on the external sweep oscillator connected to the laser controller. You should see sharp dips at the resonances.

6. Measure the absorption amplitudes, rf frequency and the linewidths. Observe how they change with rf amplitude.

7. Reverse the 'Z' field and measure the the rf frequency. *Reduce* the 'Z' field to 0 before reversing the switch since sudden switching effects the temperature controller.

[10] You may have to slightly tilt up the cell.

[11] The separation is the separation of the inner glass faces plus the optical thickness of one glass plate. This gives 4 times the intensity of reflection from any of the other surfaces. 1.5 was used for the refractive index of the glass to get the effective path length quoted.

[12] The Z coil sensitivity is $\approx$36.5mA/G

8. Measure the rf frequency for magnetic fields 0.5 – 5 G.

9. Change the polarization from left circularly polarized to linear polarized to right circularly polarized light. Observe the change in signal. Does it agree with what you expect?

10. Set the 'Z' field at 0 gauss. You should see an absorption signal (the rf is not needed for this). Why do you see this? Is the linewidth related to the magnetic resonance linewidth?

11. Determine the rf frequencies and linewidths for cells 'B', 'C' and 'D'. Since cells 'C' and 'D' have both ^{85}Rb and ^{87}Rb, you can see magnetic resonance signal from both isotopes[13].

12. You should calibrate the 'Z' magnetic field either using a gauss meter and/or calculating the axial field produced by the Helmholtz coil. The formula is given by eqn **??** in appendix2.

Shutdown

- Set the BIAS CONTROL to 0 on the laser controller and the switch 'LASER' to 'SHORT' and switch 'EXT' to 'DIASBLE'.

- Turn off the temperature controller.

- Turn off the detector. It runs on a special battery.

- Make sure that cell 'B' is not being heated.

- Now turn of all the other equipment.

Appendix1

The following is a brief exposition of the physics necessary to understand optical pumping. For a more in depth and clear description see [1].

[13]The signals from cell 'C' are difficult to see.

Interactions

The energy level diagrams for the 5S electron in ^{85}Rb and ^{87}Rb are shown in figure 9.2 It is seen that there are successively smaller perturbations that perturb and split the energy levels. The major interaction is the coulomb potential of the nucleus and all the closed shell electrons. This results in the hydrogenic levels. The noncentral coulomb forces and the spin-orbit interaction between the outer electron and all the other electron gives the splitting of states with a given orbital angular momentum but different total angular momentum. The energy eigenstates are of the total angular momentum - $J = \vec{L} + \vec{S}$[14]. This is the the fine structure. The next significant interaction is the interaction between the nuclear magnetic moment and the electron spin. This is the hyperfine interaction. Like in the case for the fine structure the energy eigenstates are states of the total angular momentum, $f = \vec{J} + \vec{I}$, obtained from the electronic angular momentum, J and the nuclear angular momentum, I[15]. Finally in an external magnetic field the magnetic moment of the atom (combined electronic and nuclear magnetic moment) is split into zeeman levels.

Selection rules and transition rates

The selection rules for absorption of light incident from an arbitrary direction with respect to the atom in the dipole approximation are[16]:

$$\Delta f = \pm 1, 0 \quad (F = 0 <\not> F = 0) \tag{9.1}$$

$$\Delta m_f = \pm 1, 0 \tag{9.2}$$

[14]The orbital angular momentum - L, and the spin angular momentum - S, couple together to form the total angular momentum - J. The energy eigenstates are states of definite J. This is called the L-S coupling and gives the Hund's rules in atomic physics.

[15]The total electronic momentum - J, and the nuclear spin angular momentum - I, couple together to form the total angular momentum - f. The energy eigenstates are states of definite f. This is is in exact analogy to the L-S coupling. At magnetic fields above 0.1T this breaks down and the energy eigenstates are defined by J and I separately. Our experiment is in the weak field region.

[16]For electric dipole transition which is the dominant relaxation mode there should also be a change in parity between the transition states. For magnetic dipole transitions which occurs when one applies radio frequency to induce transitions between the Zeeman magnetic sub levels there is no change in parity between the transition states.

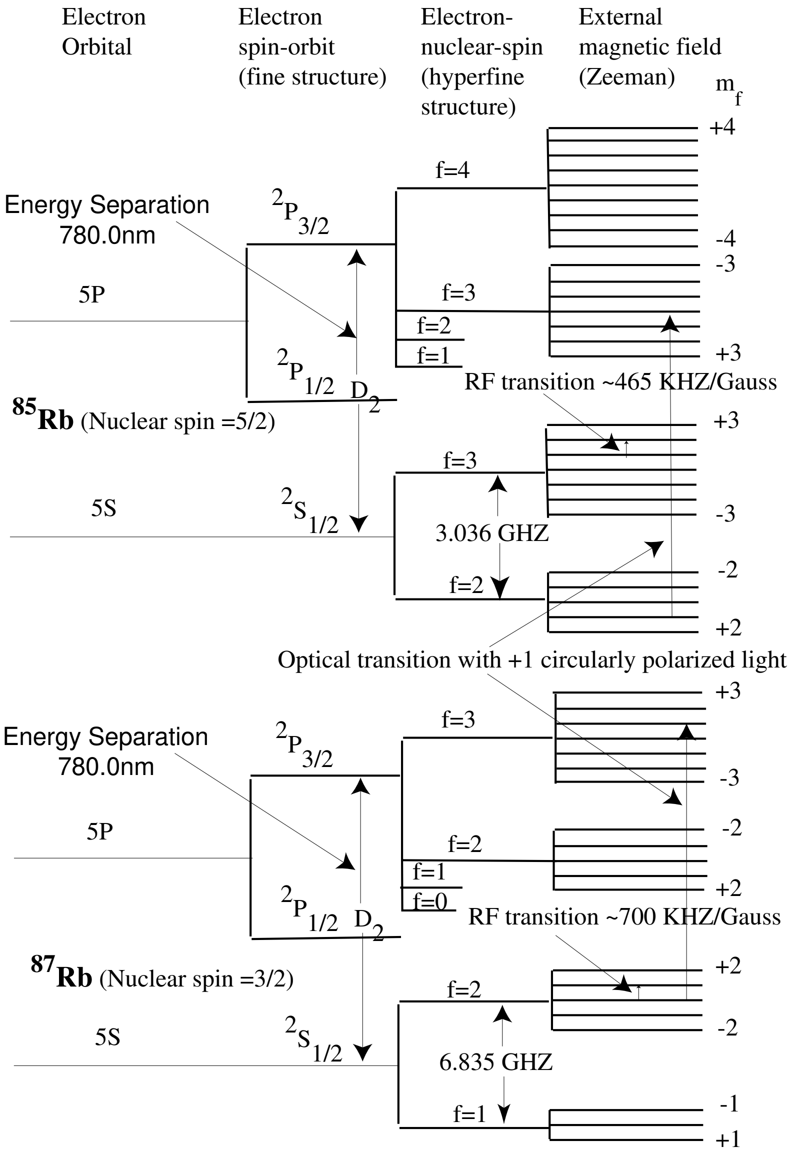

Figure 9.2: Energy levels (not to scale) of ^{85}Rb (top) and ^{87}Rb (bottom) as successively weaker interactions are turned on. The splitting due to each interaction is of the order of a 10^3 times less than the preceding interaction. (Modified from the MIT Lab manual for the $5P_{3/2}$ transition)

'f' and 'm_f' are the angular momentum and its projection along an arbitrary direction. In our experiment defining 'm_f' along the laser light propagation direction (which is also magnetic field direction) simplifies things. Consider left circularly polarized light (which has $+1\hbar$ angular momentum along the propagation direction) absorbed by an atom. To conserve angular momentum 'm_f' and 'f' has to increase by +1. The excited atom can emit the radiation in any direction. In this case using the selection rules for dipole radiation 9.2, 'm_f' however can now change by 0, ± 1 ie., there are more paths for decay.

The transition rates can be readily calculated from perturbation theory. The lifetime of a excited state varies as ω^3. Typically an atom with an energy separation of the order of rubidium – 780nm or 1.5eV, decays by electric dipole radiation in $\approx 10^{-8} - 10^{-7}$s. The lifetime for the hyperfine excited ground state – 3GHZ or 1.2×10^{-5}eV, is of the order of 10 years[17]

Optical pumping of levels

To understand optical pumping of a level consider first the simple case where the nuclear spin of rubidium is ignored. Consider exciting from the $^2S_{1/2}$ to the $^2P_{3/2}$ levels with left circularly polarized light. This case is shown in figure 9.3. The transitions allowed by the selection rules for the pumping radiation and the de-excitation radiation are shown. The probabilities of the various de-excitation transitions from perturbation theory are also shown. If the rubidium atoms are excited from their ground state level and allowed to relax it is seen that 3/4 of the atoms fall to the $m_f = +1/2$ level. If the atoms are pumped repeatedly essentially all the atoms will be in that level.

The same thing happens when the nuclear spin is included. There are more sub levels, a particular set is shown in figure 9.4. The transition rates are different, however one can see that there is still selective occupation of the ground state hyperfine levels. It turns out that the hyperfine interaction reduces the efficiency of the pumping. This occurs regardless of whether one applies a zeeman field.

[17]One thing to note is that at room temperature the thermal energy kT is 25 meV. So for our experiment at thermal equilibrium the ground state levels are equally populated, while there are essentially no atoms in the excited state.

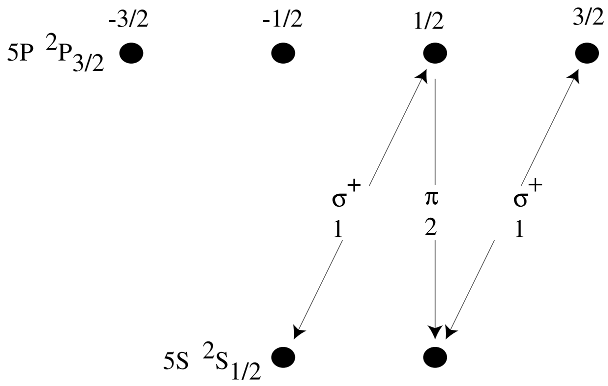

Figure 9.3: Spin polarization of ^{87}Rb by optical pumping. The Rb atoms are pumped by σ^+ radiation from the ground states to the levels shown. The excited atom can decay to either of two ground states. The numbers on the arrows are the probabilities of transitions from the excited state to the ground state sublevels. The fine structure due to the nuclear spin is ignored. Figure taken from [1]

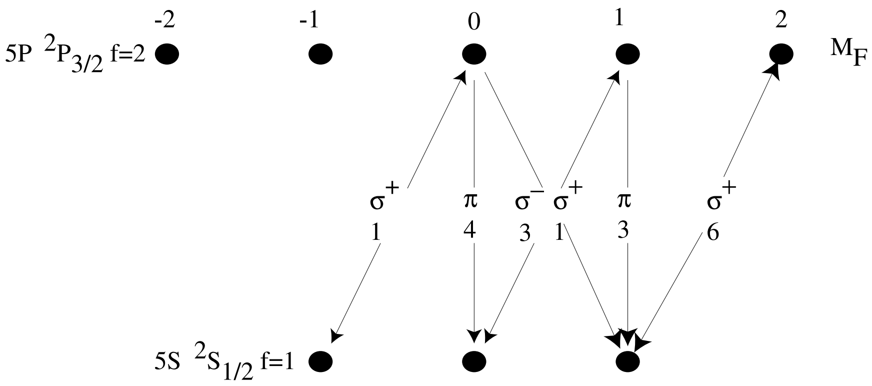

Figure 9.4: Spin polarization of ^{87}Rb by optical pumping including the effects of the nuclear spin. The Rb atoms are pumped by σ^+ radiation from the ground states to the levels shown. The excited atom has more ways to decay to the ground states. The numbers on the arrows are the probabilities of transitions for electric dipole radiation from the excited state. Figure taken from [1]

Magnetic Resonance

When a magnetic field is applied, the 'f' levels get split into the Zeeman sublevels defined by 'm_f'. If one applies a rf magnetic field, B_1, perpendicular to the zeeman field, at the frequency defined by the separation of the Zeeman levels, one can induce magnetic transitions between the zeeman levels, similar to what one does in nuclear magnetic resonance. The selection rules in this case turn out to be:

$$\begin{aligned} \Delta f &= 0, \pm 1 \\ \Delta m_f &= \pm 1 \end{aligned}$$

From the selection rules it follows that with enough rf field one can equalize the population of the Zeeman sub levels.

So when the rf is applied at the resonant frequency the levels get unsaturated and more light can be absorbed by the atoms. In our experiment we fix the frequency and modulate the zeeman magnetic field. At a particular magnetic field there is magnetic resonance and the detector sees less light due to absorption by the rubidium atoms.

At zero magnetic field one sees an absorption dip independent of the rf frequency. This is probably because there is a small inhomogeneous DC magnetic field transverse to the direction of propagation of the light. These spins precess about the inhomogeneous field. Can you think of a way to check this?

g factor

The Zeeman splitting of an atom is given by:

$$E_{f,m_f} = g_f \mu_B B m_f$$

g_f is called the 'g' factor. The calculation is analogous to the calculation of the Landé g factor where the spin - S and the orbital angular momentum - L are coupled to give a total angular momentum - J

$$g_f = g_J \frac{f(f+1) + J(J+1) - I(I+1)}{2f(f+1)} - g_I \frac{m}{M} \frac{f(f+1) + I(I+1) - J(J+1)}{2f(f+1)}$$

g_J is the electronic g factor which is just the spin g factor for the 5S state, m is the electron mass and M is the atomic mass. The second term is 10^{-3} less than the first term and can not be resolved in our experiment.

Hyperfine Coupling

The hyperfine coupling constant - A_J[18] gives the strength of the coupling between the electronic angular momentum and the nuclear spin. This coupling depends on the electron density at the nucleus. It is is large for the S electrons. A_J for the 5P electrons is $\approx 1/40$ of the value for the 5S electrons and can be ignored in our experiment.

$$\Delta E = E_f - E_{f-1} = A_J f$$

[18]We are ignoring the interaction B_J between the nuclear quadrupole moment and the electric field gradient at the nucleus due to electron. This is exactly 0 for the 5S state but of the same order as A_J for the 5P state. This is acceptable since we are ignoring A_J for the 5P state in our determination of the hyperfine coupling constant for the ground state.

Bibliography

[1] Alan Corney *Atomic and Laser Spectroscopy*, Oxford University Press, 1979 Chemistry Library – Call Number QC688 C67)

[2] R. W. Ditchburn *Light*, John Wiley and Sons Inc., 1963 (The lab has a copy)

Chapter 10

Moseley's Law – X-ray Fluorescence

Objective

Identify a number of unknown samples from their characteristic x-ray emission lines. Verify the validity of Moseley's law.

Introduction

In 1913 only a short time after Rutherford and Bohr had conceived their atomic model, Moseley investigated the systematics of energies of K x-rays and found the empirical dependence:

$$\nu\ (Z-1)^2$$

Where ν is the frequency of the radiation and Z is the atomic number. Before that time atomic weight and chemical properties had to be used to establish the periodic table of elements. But these two methods disagreed, for instance, in the ranking of Co and Ni as well as Te and I. Moseley's investigation allowed an unambiguous ranking of all elements. It also led to the discovery of a gap in the periodic table at Z=43. (Technetium is an element with no stable isotope but it is present as a fission product in uranium ore).

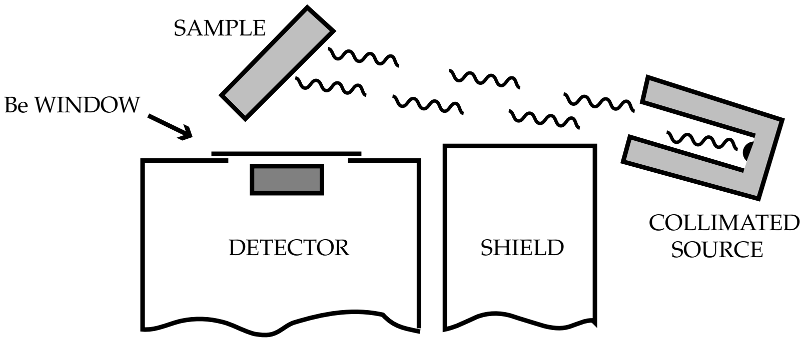

Figure 10.1: Layout of the source and detector to minimize direct γ-rays

Experimental Setup

Geometry

The geometrical arrangement for the experiment is shown in Figure 10.1.

A collimated ^{57}Co source is used to create K vacancies via photoelectric excitation in the sample materials which range from Cu(Z=29) to U(Z=92). The x-rays emitted by the sample are then detected in a high resolution Ge detector. The detector has to be kept at liquid nitrogen temperature and is isolated by a vacuum container. A .125 micrometer thick Be(Z=3) window in front of the detector serves to minimize absorption of x-rays before they can reach the detector. (Caution: This window is extremely fragile and very brittle.) The detector is completely shielded from direct radiation of the ^{57}Co by a massive shield of lead or iron.

The Source

We are using a ^{57}Co source (from the Mossbauer experiment) to irradiate the samples. The decay scheme is shown in figure 10.2.

The dominant γ-ray from this source is the 122.06 KeV transition between the second and first excited state. In addition there is a weaker γ-ray at 136.48 KeV. The 14.41 KeV is also relatively weak because of the strong competition from internal conversion. An energy of 122 KeV is ideal to produce K vacancies in heavy atoms and it works sufficiently well on medium weight atoms. But it is not well matched for light atoms and, therefore,

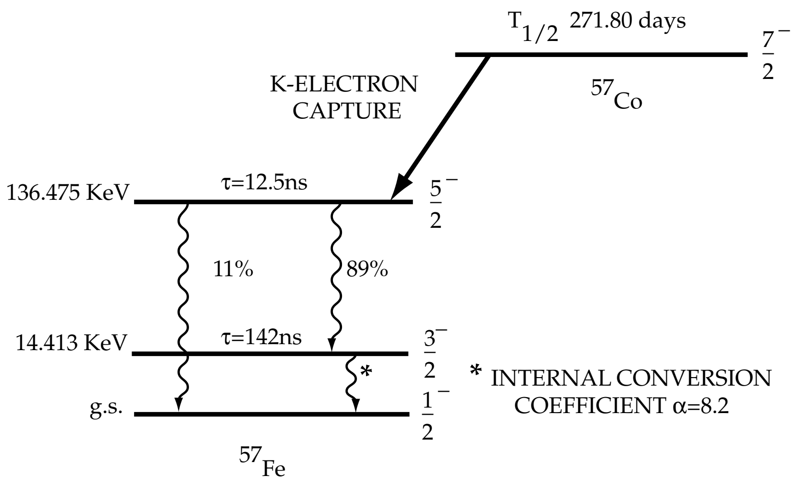

Figure 10.2: Decay scheme of ^{57}Co

copper is usually the lightest element where we still can observe K x-rays without difficulties.

The Samples

A large variety of samples is provided for these measurements. Most of the samples are labelled (lead, uranium, silver, tin, cadmium, copper, indium). Some just carry a number and these should be identified from their characteristic x-ray spectra.

The detector

The detector is a high resolution Ge detector manufactured by Princeton Gamma-Tech, Inc. You should carefully read the instruction manual and consult the instructor before you use the detector because improper operation can seriously damage this delicate device. Some of the important detector properties are given below.

Material:	High purity n-type Ge. Excess donor density less than 1 atom in 10 sup 13@ atoms of Ge.
Active area:	5 mm^2
Thickness:	5 mm

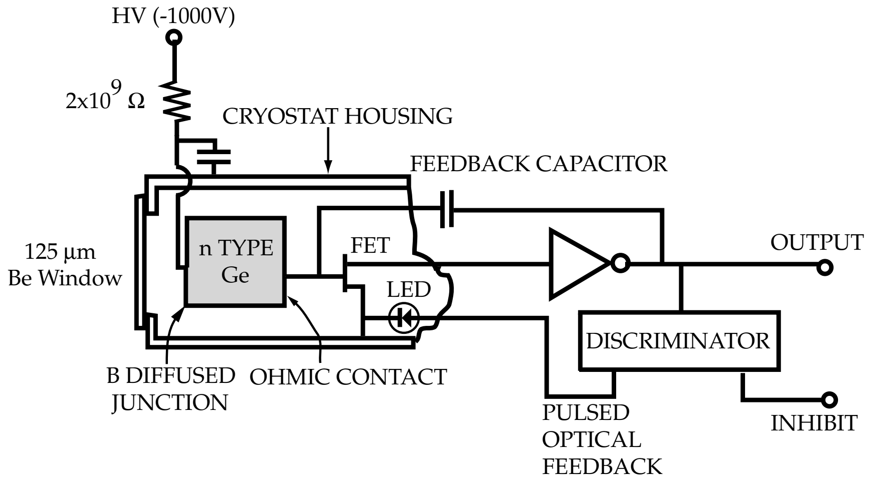

Figure 10.3: Block diagram of the charge integrating amplifier

Rectifying junction	B diffused layer
Bias for full depletion:	-1500 V
Optimum operating bias	-1000 V

Properties of Ge	
Atomic number	32
Density	5.33 gm/cm^3
	4.41 x 1022 atoms/cm^3
Crystal structure	diamond
Band gap	0.665 eV
Energy per hole-electron pair	2.96 eV

Electronics

A block diagram of the charge integrating preamplifier is shown in figure 10.3.

To satisfy the extreme requirements for low noise performance of the preamplifier, one has to operate the input FET at low temperature inside the cryostat. Also, the 1000 MΩ discharge resistor that is usually found in parallel to the feedback capacitor in such circuits had to be omitted because it would inject too much noise into the input FET. Instead, the feedback capacitor is periodically discharged through the junction FET with the aid

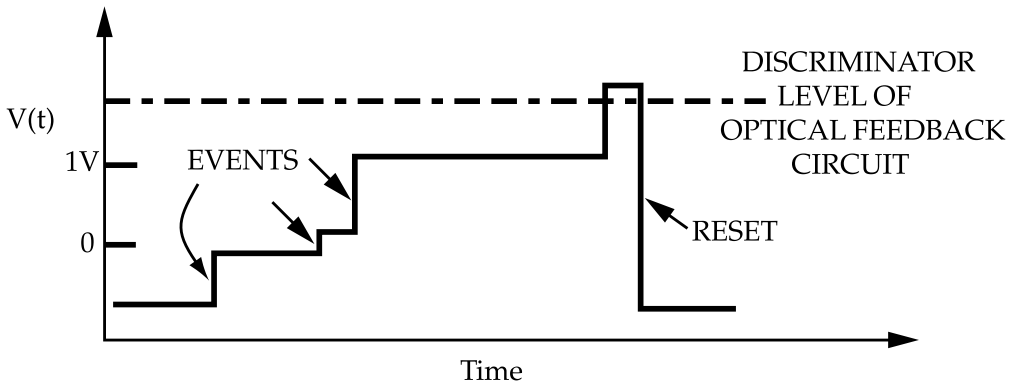

Figure 10.4: Buildup and flushing of the charge accumulated

of the pulsed optical feedback circuit. The preamplifier output voltage as a function of time is shown in figure 10.4.

The positive voltage steps represent charge collected in the feedback capacitor from events in the Ge detector. These steps are processed in a shaping amplifier (figure 10.5) and, after further amplification, they are presented to an ADC. The negative reset pulse is also processed in the shaping amplifier, but it is blocked in a linear gate before it can reach the ADC.

Measurements and Analysis

Calibration of amplifier-ADC Systems

Use the direct spectrum from the source to calibrate the multichannel analyzer. To avoid gain and baseline shifts the count rate should be limited to less than 3000 cps. Use the maximum available channel number. Adjust the amplifier gain to place the 136.48 KeV line near the highest channel. In addition to the three nuclear transitions shown in fig. 10.2, the spectrum contains several additional peaks. These correspond to the K_α and K_β lines in ^{57}Fe (a consequence of K electron capture and internal conversion) and the two K lines in the source backing (usually Pd). From the centroids of the three nuclear transitions, you can determine the energy calibration of the system. The 136.48 KeV line has only a small effect on the fit because it is very close to the much stronger 122.06 KeV line. But we still want to include

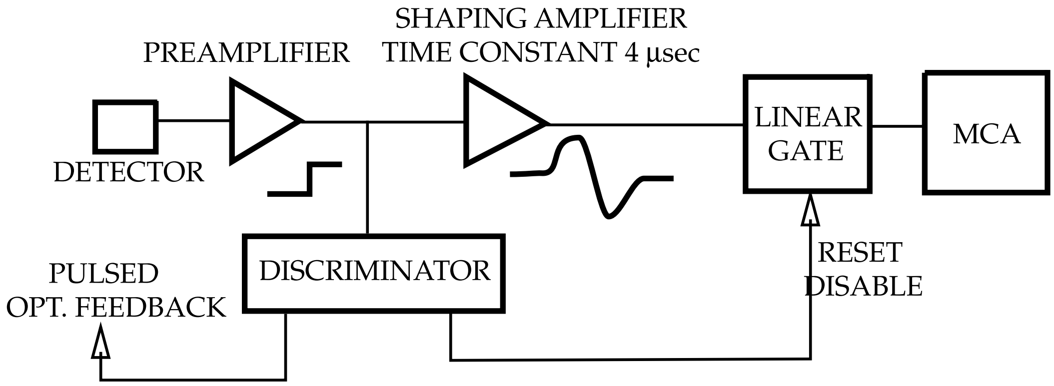

Figure 10.5: Block diagram of the apparatus

it in the fit because it allows us to calculate the χ^2 value for the best fit. An acceptable χ^2 value usually tells you that you have properly identified the 14.41 KeV line (or vice versa).

Energies of K Lines

Record the fluorescence spectra for all known samples and two unknown samples using the experimental arrangement shown in fig. 10.1. Calculate the energies of the observed K transitions from the peak centroids. In the lighter elements you will only observe two peaks. In heavier elements such as lead the spectrum is, however, more complex. Also, notice that some of the peaks, for instance in Pb, are much broader than expected from the experimental line width. These lines are unresolved doublets or multiplets due to spin-orbit splitting[1]. With some care you can extract up to six peak centroids from the spectrum of Pb. The uranium sample emits several γ rays from radioactive decay in the region of interest. These γ rays can easily be distinguished from the x-rays because their intensity is not affected by the presence of the ^{57}Co source.

Consult a published table of x-ray energies (e.g., "Handbook of Physics," American Institute of Physics) and compare your results with the accepted values of K transition energies for all labelled materials. Also, compare the

[1]Spin-orbit splitting occurs in the L-S approximation due to the coupling of the atomic spin angular moment with the orbital angular moment. It is significant for high atomic number atoms.

measurements for the unidentified samples with the table and use the comparison to identify these samples. Use all your data to verify the validity of Moseley's law. Include the K x-ray energies of Fe and Pd from free source spectrum in this comparison.

References

1. *Intrinsic Germanium Instruction Manual*, Princeton Gamma-Tech. (The lab has a copy)

2. *Radiation Detection and Measurement*, G. F. Knoll, John Wiley & Sons 1979. (The lab has a copy)

3. *American Institute of Physics Handbook- Third Edition*, edited by Bruce H. Billings and others, New York, 1972), Math/Phys/Astr QC61 .A5 1972.

4. The following website also lists upto date x-ray energies and the gamma ray energies for each isotope.

   `http://nucleardata.nuclear.lu.se/nucleardata/toi/`

Chapter 11

Mössbauer Effect

Introduction

In this experiment we measure the resonance absorption of 14.41KeV γ-rays ^{57}Fe in two thin absorber foils. One foil consists of stainless steel and has no ferromagnetic properties. The other foil is made from iron isotopically enriched in ^{57}Fe (natural abundance is 2%) and is ferromagnetic.

Many review articles have been written on the Mössbauer effect and some are listed at the end under the references [2-5]. It is suggested that you read some of these papers before you perform the measurements. A good description of the principles of operation for gas proportional counters like the one used in this experiment is given in ref. [6].

Experimental setup

A schematic diagram of the setup is shown in figure 11.1. Source and detector are placed in fixed positions some distance apart. The absorber foil is mounted in the line between source and detector on a movable stage driven by a precision screw drive mechanism. Our source consists of 5 milliCuries of ^{57}Co (at time of manufacture) on a Pd backing. Special care has been taken by the manufacturer to assure that the source atoms are deposited into lattice sites on the Pd surface in order to optimize the recoilless emission of photons. The decay scheme for ^{57}Co is shown in figure 11.2. Only 10% of the decays result in the emission of a 14.41KeV γ-ray because of the strong competition from the internal conversion process.

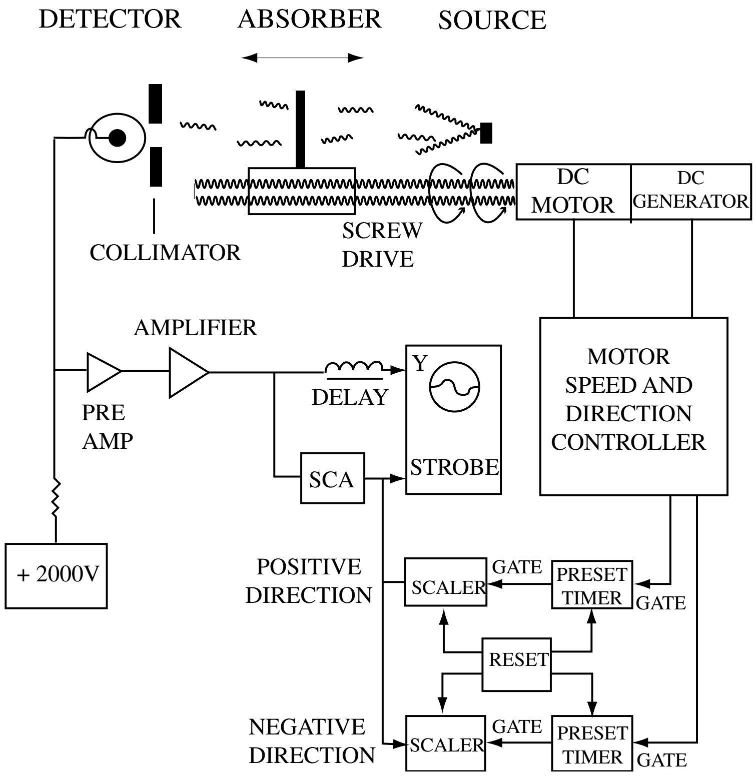

Figure 11.1: Block diagram of the apparatus

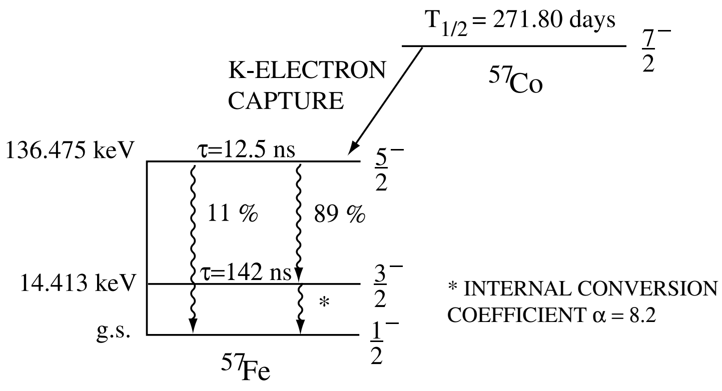

Figure 11.2: Decay scheme for ^{57}Co

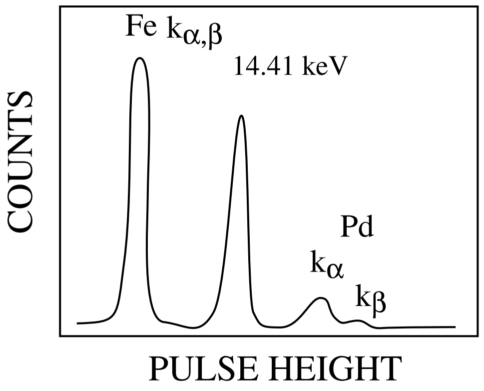

Figure 11.3: Multichannel Analyzer spectrum

The detector is a gas proportional counter [6]. Xenon (Z=54) is chosen as counter gas because of its large photoelectric absorption coefficient. (The atomic photoelectric absorption cross section is proportional to Z^5). The radiation enters the counter through a 0.010" thick Be window. The pulses from the proportional counter are amplified in a charge sensitive preamplifier and a shaping amplifier. A typical spectrum from the ^{57}Co source taken with a multichannel analyzer is shown in figure 11.3. The strongest peak in the spectrum corresponds to K x-ray emission from ^{57}Fe following the K electron capture transition and the internal conversion process. The peak corresponding to the 14.41KeV γ-ray is also strong. Two weaker groups originate from the source backing and are the result of x-ray fluorescence following photoelectric excitation of Pd by the 122KeV or 136KeV γ-rays. For our measurements, we do not require a multichannel analyzer. It is sufficient to set a single channel analyzer on the 14.41KeV peak and to count the number of events in this peak with scalers. Two scalers are provided in our setup, one for each direction of the absorber velocity. The scalers are automatically gated on and off by timers that are preset to a fixed time interval, typically 20s. In addition, both timers and both scalers are controlled by the speed and direction controller to assure that they are only activated while motor speed and direction are correct.

Experimental procedure

1. Apply high voltage (+2000 V) to the proportional counter. Then adjust the gain of the main amplifier and the discriminator levels of the single channel analyzer with the help of an oscilloscope. For this adjustment it is best to remove the absorber because the increased counting rate makes the adjustments easier. Adjust the pulses from the 14.41 keV γ-ray to about 5V in height and set the discriminator levels of the single channel analyzer to exclude all other parts of the spectrum.

2. Mount the 0.0015" thick stainless steel absorber on the movable platform. Preset the electronic timers to 20s and take data for velocities between 0 and 0.9 mm/s in 0.05 mm/s increments.

3. Mount the 0.0015" thick iron absorber (enriched in ^{57}Fe). With this absorber the resonance minimum is split into six fragments which are distributed over a wide range of velocities. Scan the range of velocities from 0 to 6.0 mm/s in 0.1 mm/s steps. Reduce the step size to 0.05 mm/s whenever you scan across a resonance dip. Two minima occur at low velocities and therefore you should use the smaller 0.05 mm/s increments between 0 and 1.2 mm/s.

4. Use a strobe light to obtain an absolute calibration of the rotational velocity of the screw drive mechanism. Fix the strobe frequency around f=700 strobes per minute and then adjust the motor speed until the pattern on the pulley appears to stand still. The full circle on the pulley is divided into a pattern of 12 white and 12 black fields. Therefore a standing pattern can be obtained for rotational frequencies of f/12, 2f/12, 3f/12,etc. A red marker helps to distinguish between the various patterns. The lead screw on the drive mechanism has a pitch of 13 turns per inch. With this procedure you can obtain three calibration points for the speed of the drive mechanism in either direction.

Analysis

Plot your data. Determine the positions, widths, and intensities of all absorption dips. Calculate the isomer shift for both samples. Compare the six

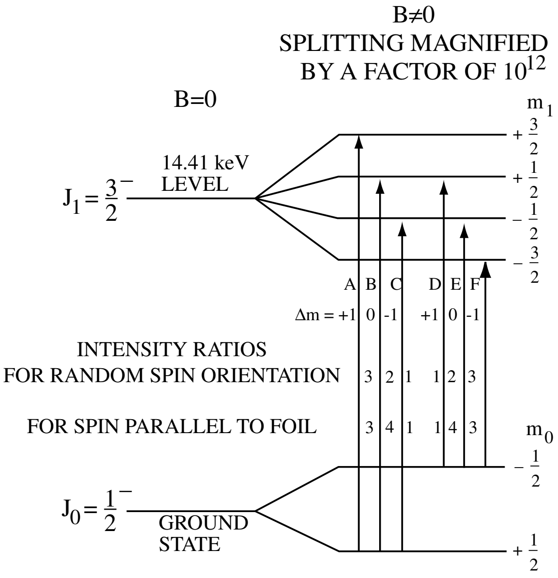

Figure 11.4: Zeeman Splitting and intensity ratios of the ^{57}Fe nuclear levels

minima from the iron absorber with the six transitions shown in figure 11.4. Use the observed strength ratios to obtain an unambiguous identification.

Notice however that several factors can affect these strength ratios. In a absorber that is not magnetized at all, the iron nuclei are randomly oriented. In that case, angular distribution effects may be ignored and the relative strengths of the various transitions are simply given by the square of the ratios of appropriate angular momentum coupling coefficients,

$$< \frac{1}{2} 1 m_0 \Delta m | \frac{3}{2} m_1 >$$

These ratios are shown in fig 11.4. Most iron foils are somewhat magnetized and the resulting alignment of the nuclear spins and magnetic moments in the foil plane along with the $\sin^2\theta$ angular distribution of $\Delta m = 0$ transition enhances these transitions relative to $\Delta m = \pm 1$ transitions. The limits for the intensity ratios for full alignment are also given in fig. 11.4. In most experiments one observes intensity ratios somewhere between the two limits of no magnetization and full magnetization. Any experimental broadening of the absorption minima, e.g., from foil vibrations or drive motor speed fluctuations also reduces their height. Variations in the broadening among the six absorption dips can modify the intensity ratios, so it is important to individually determine the widths of all six minima. Additional deviations from calculated ratios can be observed in thick foils because the absorption as a function of foil thickness is exponential and not linear. From the properly identified pattern, one can extract information about the magnetic field strength B at the nucleus, and the magnetic moments of the ground state (μ_0) and the excited state (μ_1). Two of these three quantities can be determined if one is given. The ground state magnetic moment μ_0 has been determined with other experimental methods [7]. Therefore we can evaluate B and μ_1 (sign and magnitude) from our experiment. The Heisenberg uncertainty principle links the natural width G of the first excited state and its lifetime τ [8].

$$\Gamma\tau = \hbar$$

Verify this relation. Remember that source and absorber contribute to the width of the observed resonances.

References

1. A. C. Melissinos, *Experiments in Modern Physics*, Academic Press, 1966.

2. H. Lustig, *American Journal of Physics* **29**, 1 (1961).

3. H. Frauenfelder, *The Mssbauer Effect*, W.A. Benjamin, 1962.

4. Section 8.8 in E. Segre, *Nuclei and Particles*, 2nd edition, Benjamin/Cummings Publishing, Reading, Massachusetts, 1977.

5. R. L. Mössbauer, *Recoilless nuclear resonance absorption, Beta and Gamma Ray Spectroscopy*, ed. by K. Siegbahn, North-Holland Publishing Company, 1966.

6. V. I. Goldanskii and R. H. Herber, *Chemical Applications of Mssbauer Spectroscopy*, Academic Press, 1968.

7. G. F. Knoll, *Radiation Detection and Measurement*, Wiley and Sons, 1979.

8. *Nuclear Data Tables*, **A5**, 433 (1969).

9. *Nuclear Data Sheets*, **47**, 1, (1986).

Chapter 12

Lifetime of the 14.4 keV level in ^{57}Fe

In this experiment we determine the mean lifetime of the 14.4KeV level in ^{57}Fe. The level is populated in the dominant decay branch of the radioactive isotope ^{57}Co. A decay scheme for ^{57}Co is shown in Fig. 12.1.

In the Mössbauer experiment, the same level is excited through resonance absorption of 14.4KeV γ-rays. One result of the Mössbauer study is the determination of the width of this level. Comparison of the measured width and the lifetime value from the present experiment permits a direct verification of the Heisenberg uncertainty relation.

In our experiment we measure the time that elapses between the emission of the 122KeV γ-ray which signals the formation of the 14.4KeV level and the 14.4KeV γ-ray which is emitted in its decay. A diagram of our apparatus is shown in Fig. 12.1.

Choice of Scintillating material

One of the most critical steps in our experiment is the selection of suitable scintillating materials. For simple energy measurements NaI (Tl) is the preferred scintillator in this energy region because of its high light output and large photoelectric cross section. The value of this cross section is important because for photons at these low energies, the photoelectric process is the only mechanism that deposits sufficient energy in the scintillator to produce a detectable light pulse. This fact is evident from Table 12.1 where the ener-

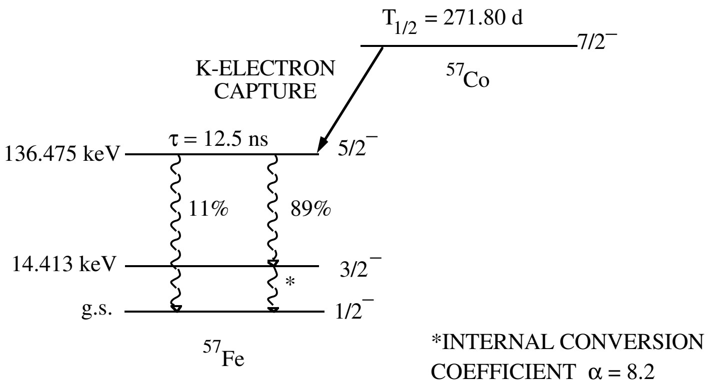

Figure 12.1: Decay scheme for ^{57}Co

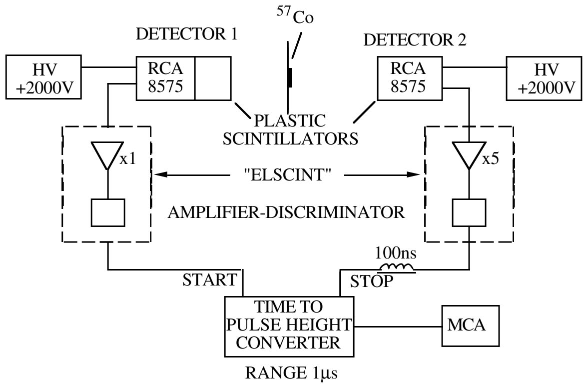

Figure 12.2: Block diagram of the apparatus

Photon energy (KeV)	Compton edge (KeV)
122	40
14.4	12
2^+	0.77
6.4	0.156

Table 12.1: Compton edges at various energies

E_γ (KeV)	Absorption		
(KeV)	Photoelectric	Compton	Total
6.4	75%	7%	82%
14.4	13%	7%	20%
122	0	6%	6%

Table 12.2: Absorption in a 1/8" thick plastic scintillator due to photoelectric and compton processes

gies of the Compton edge (the maximum energies transferred to the Compton electron) are listed for photon energies of interest in this measurement, namely 122KeV and 14.4KeV γ-rays and 6.4 keV X-rays. The importance of detecting the 6.4KeV X-rays is discussed in the next section.

While the Compton effect is still useful in the detection of 122KeV γ-rays, the Compton edges for 14.4 and 6.4 KeV photons are so low in energy that hardly any light is generated by the Compton process inside the scintillator.

NaI (Tl) has however the disadvantage of a slow decay time (230 ns) which makes it unsuitable for timing measurement. Furthermore, about 9% of the light output arrives long after the event (phosphorescence). At high singles rate this delayed light emission produces a lot of baseline noise at the output of the photomultiplier tube. This baseline noise results in many "false" triggers when the discriminator level is set to accept low energy pulses. For that reason we decided to construct our detectors from plastic scintillators. The fractions of photons that interact in a 1/8" thick plastic scintillator are listed in Table 12.2.

For 122KeV γ-rays, we can obtain good counting efficiency simply by choosing a scintillator of sufficient thickness (at least 1 inch). The detection efficiency for 14.4 keV γ-rays can be much improved through addition of small amounts of Pb to the organic scintillator. "Bicron" manufactures plastic scintillator that contains 5% Pb by weight (density 1.1 g/cm^3) The absorption

E_γ (KeV)	Absorption			
(KeV)	Photoelectric Pb	Photoelectric Plastic	Compton	Total
6.4	49%	44%	5	98%
14.4	65%	12%	6%	83%
122	6	0%	6%	12%

Table 12.3: Absorption in a 1/8" thick plastic scintillator with 5% Pb by weight due to photoelectric and compton processes

in an 1/8" slab of this material is shown in Table 12.3.

We can see that such a slab has counting efficiency of 77% at 14.4KeV and 93% at 6.4KeV.

Experimental setup

The radioactive material ^{57}Co is deposited on an Fe substrate and inserted in the space between the two scintillators. To minimize the effects of absorption in the substrate, the source material is directly facing the 1/8" thick Pb doped scintillator that is used to detect the 14.4KeV (Detector 2). The 122KeV γ-rays are detected in a 1" thick plastic scintillator (Detector 1). Both scintillators are attached to RCA 8575 photomultiplier tubes. The anode pulses from these tubes are sent through "ELSCINT" amplifier-discriminator units. The amplifier gain can be varied between 4 (" gain 1") and 20 ("gain 5"). The discriminator levels are fixed around 20 mV. The discriminator threshold in terms of scintillator response (KeV) can be adjusted through changes in the amplifier gain and photo tube high voltage. Ideally, the threshold of detector 1 should be set just above 14.4KeV. This gives it good sensitivity to the 122KeV γ-ray and no sensitivity to the 14.4KeV γ-ray. The optimal threshold setting for detector 2 is somewhat dependent on the source intensity. A strong source generates high count rates in both detectors and leads to substantial contributions from a accidental coincidences to the time spectrum. Therefore, with a strong source a rather high discriminator setting, say 8-10KeV, is advisable. On the other hand, if the source is relatively weak, there are only few accidental coincidences and the discriminator level for detector 2 can be lowered below the ka energy of 6.4KeV. Because of the large coefficient for internal conversion a = 8.2 of the 14.4KeV transition, this lower discriminator setting increases the number of true coincidences by a large factor. Notice, however, that the 14.4KeV transition is not the only source of k X-rays. Every k-capture transition is followed by the emission of a k X-ray. The 122KeV ($\alpha = 0.024$) and the 136KeV ($\alpha = 0.15$) transition can both also proceed by internal conversion and produce prompt true coincidences between the conversion electron and the k X-ray.

The output pulses from the fast discriminators are connected to the inputs of a time to pulse height converter (TAC). A delay cable of 100 ns is inserted at the stop input to enable us to analyze prompt coincidences. The TAC output is analyzed by a multichannel analyzer, preferably the unit incorporated in the PC.

Analysis

The time spectrum from the TAC should have three major contributions. Most visible is an intense and narrow peak from prompt coincidences. In our geometry, the dominant contribution to this peak comes from γ-rays that back scatter in one plastic scintillator and then are detected again in the other scintillator. The presence of this peak in our spectrum is very useful for several reasons. It gives us a good indication how well our timing circuitry is functioning. From the peak width we can extract the resolving times FWHM and FWTM of our system. The insertion of calibrated delay cables in one of the TAC inputs will shift this peak in the spectrum. From such shifts we can obtain a calibration of the time scale of the spectrum. Delayed coincidences from the long-lived 14.4KeV level form a broad exponential tail to the right of the prompt peak. Accidental coincidences contribute a flat background to the entire spectrum. Additional much weaker contributions can sometimes be recognized. For instance, delayed coincidences between a k X-ray following the k capture process and a 122KeV γ-ray can add a narrow exponential tail to the left of the prompt peak. The decay time of this tail corresponds to the lifetime of the 136KeV level in ^{57}Fe. The presence of this tail is a good indication that the discriminator threshold on the "stop" detector is below 6.4KeV.

For the determination of the lifetime of the 14.4KeV level, we use the part of the spectrum to the right of the prompt peak. Data points adjacent to the prompt peak that contain any contribution from the prompt peak should be excluded from this analysis. The data can be fitted with the equation

$$N = Ae^{-t/\tau} + B$$

Use a least square fitting procedure to determine the constants A and B as well as the value of χ^2 for values of τ between 120 and 160 ns in steps of 5 ns. Plot χ^2 as a function of τ. Find the best value of τ and the probable error from this plot. From this result you can calculate the natural width of the 14.4KeV level as well as the width of the absorption dips that should be seen in a Mössbauer velocity plot. Perhaps you have also carried out the Mössbauer experiment that is described in this manual. If so you can compare the estimated width of the structures in the Mössbauer spectrum with the measured widths. Comment on any discrepancies.

Chapter 13

Compton Scattering

Introduction

In 1920 A. H. Compton investigated the scattering of x-rays from various materials. He observed that the intensity of the scattered radiation was smaller than predicted by J. J. Thomson's classical theory. Moreover, the measured intensity distribution had a forward backward asymmetry in contradiction with theory. Subsequent experiments also revealed that the wavelength of the scattered radiation was different from that of the primary x-rays. In 1923 Compton published a paper and explained these results by describing the scattering process as a collision between photons and free electrons. Simple kinematic relations led to the well-known equation for the wavelength shift of the radiation

$$\Delta\lambda = \frac{h}{mc}(1-\cos\theta)$$

where θ is the scattering angle, and the constant h/mc is called the Compton wavelength. Using semi-classical arguments, Compton was also able to reproduce the experimental angular distribution of the radiation. A quantum theoretical description of the scattering process was later provided by Klein and Nishina. The scattering cross section is given by

$$\frac{\partial\sigma}{\partial\Omega} = r_0^2\frac{1+\cos^2\theta}{2}[1+\gamma(1-\cos\theta)]^{-2}[1+\frac{\gamma^2(1-\cos\theta)^2}{(1+\cos^2\theta)[1+\gamma(1-\cos\theta)]}],$$

,

where $r_0 = \frac{1}{4\pi\epsilon_0}\frac{e^2}{mc^2}$ is the classical electron radius, and $\gamma = \frac{h\nu}{mc^2}$.

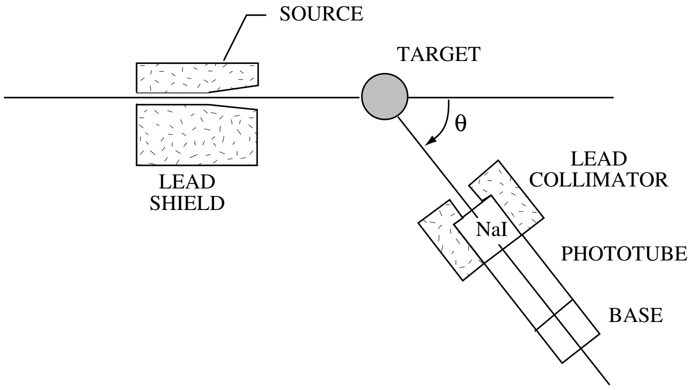

Figure 13.1: Layout of the 'source', 'target' and the 'detector'

In this experiment we measure the energy and differential cross section of Compton scattered γ-rays as a function of angle and compare our results with predictions.

Apparatus

A diagram of the apparatus is shown in Fig. 13.1. A Cu target is bombarded with photons from an intense ^{137}Cs source.

The Compton scattered photons are detected in a scintillation detector. Detector and source are both collimated with Pb shields to prevent photons from the source from reaching the detector directly. The source used in this experiment is ^{137}Cs. The decay scheme of ^{137}Cs is shown in figure 13.2.

In addition to the 662 KeV γ-rays, ^{137}Cs also emits x-rays that are generated after the decay of the $\frac{11}{2}^{-}$ state by internal conversion.

The detector is a 2" diameter x 2" cylindrical NaI (Tl) crystal. (Why would a plastic scintillator not be useful in this experiment?) The crystal is mounted on a 2" diameter 10 stage photomultiplier (Type SRC B50B01). The detector usually contains two light emitting diodes that can be used to monitor the photo tube for gain shifts. A typical response of this detector to a ^{137}Cs source is shown in fig. 13.3

Like all γ-rays detectors, our scintillation crystal is not 100% efficient, i.e., some fraction of the photons within the solid angle of the detector pass through it without interaction. The interaction probability, or total detec-

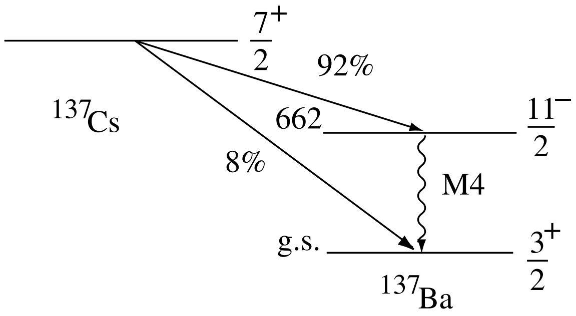

Figure 13.2: Decay scheme for ^{137}Cs

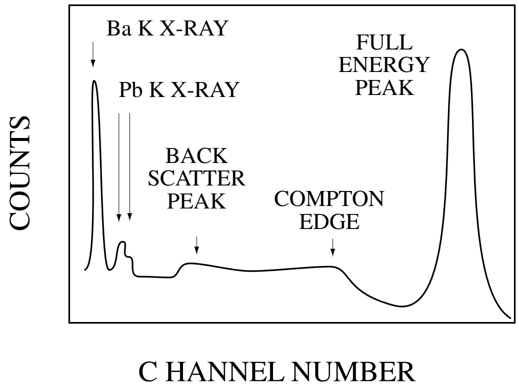

Figure 13.3: Features seen in the energy spectrum

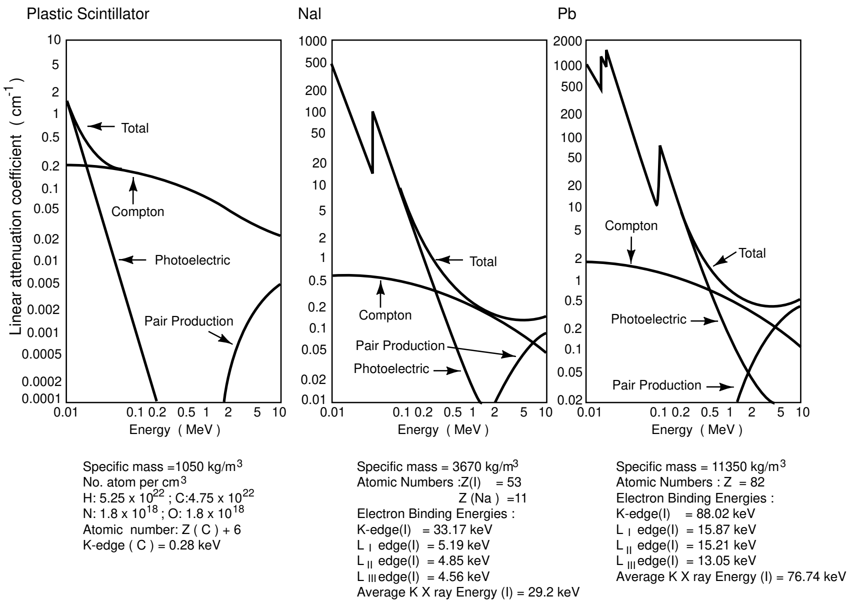

Figure 13.4: Linear attenuation coefficient for the plastic scintillator, NaI and Pb

tion efficiency, ϵ_T is calculated from linear attenuation coefficients which are tabulated in several handbooks as a function of photon energy and absorber material. Fig. 13.4 shows plots of linear attenuation coefficients for plastic scintillator, NaI and Pb. Compton scattering, photoelectric interaction and, at higher energies, pair production are the three major contributions to the attenuation.

In the spectrum in fig 13.3, we can distinguish between the full energy peak that originates mainly from the photoelectric interaction and the broad distribution of pulses below the Compton edge that result from gamma rays which Compton scatter inside the scintillator. Some Pb x-rays are generated through fluorescence in the Pb shield. The strong peak at low energy corresponds to the 32 KeV K x-rays from Ba. An accurate determination of the total number of 662 KeV photons incident on the active area of the crystal can best be made from the number of counts in the photo peak N_P. The calculation requires the knowledge of the total detection efficiency ϵ_T as well

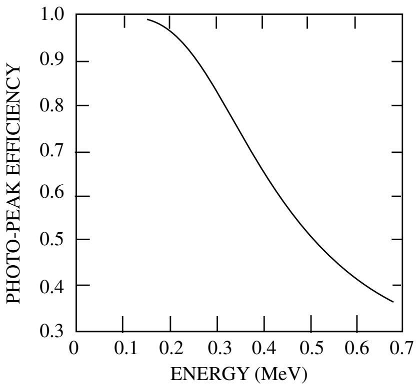

Figure 13.5: $\epsilon_T f_P$ for our detector

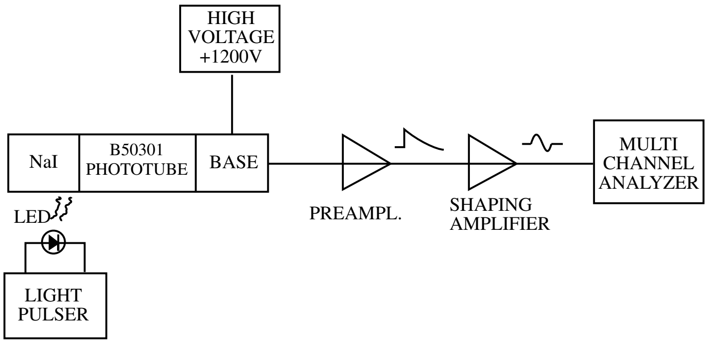

Figure 13.6: Block diagram of the apparatus

as the fraction f_P of all counts that fall under the photopeak. We have

$$n_P = \epsilon_T f_P N_\gamma$$

The product $\epsilon_T f_P$ has been calculated for our detector geometry and is plotted in fig 13.5. The calculation takes the effect of the Pb collimator into account.

An electronics diagram is shown in fig. 13.6.

Despite the large amplification in the photomultiplier tube, the charge pulse at the anode is quite small, of the order of 10^{-10} Coulomb. The preamplifier has the function of converting this charge pulse into a voltage pulse. Because of its high input impedance, it should be placed near the detector. A functional diagram of the circuit is shown in fig. 13.7.

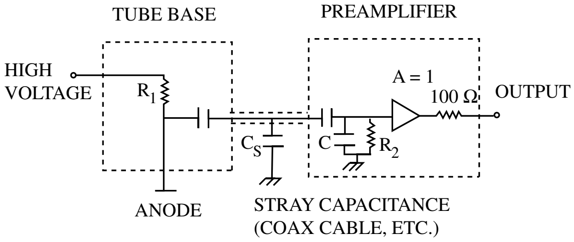

Figure 13.7: Phototube and preamplifier resistances and capacitances (See text)

The charge sensitivity of the preamplifier is the inverse of its input capacitance, which also includes the capacitance of the coaxial cable. The decay constant τ of the exponential decay of the pulse is given by

$$\tau = \frac{R_1 R_2 (C + C_1)}{R_1 R_2}$$

The active circuit has voltage gain A = 1, a very high input impedance ($Z_{in} >> 1M\Omega$) and a low output impedance ($Z_{out} \approx 1\Omega$). Therefore, it is capable of driving long terminated coaxial cables.

The shaping amplifier has the task to produce a signal with the optimum signal to noise ratio. For that purpose, it has a very narrow band width centered around 1 MHz. Our shaping amplifier contains several stages of integration and one stage of differentiation (or two for bipolar pulses) all with equal time constants around 1 μs. It also provides some additional voltage gain to produce a spectrum of output pulse heights that is matched to the dynamic range of the multichannel analyzer (0 - 10 V).

Experimental Procedure

1. Before the actual measurement can be made a good energy calibration has to be obtained for the detector. For this purpose we use three sources: ^{60}Co, ^{137}Cs (not the source used in the scattering measurement but a much weaker source), and a ^{57}Co source. Begin with the ^{60}Co

source and place the photo peak of the 1.333 MeV gamma ray near the top of the ADC range. There are two photo peaks due to 1.333 and 1.173 MeV gamma rays emitted in the decays. For a decay diagram for ^{60}Co see figure 16.1. Take a spectrum with adequate statistics and make sure that you understand all the features in the spectrum. Identify the photo peaks, the Compton edges and Compton distribution in the spectrum. Look for contributions from ambient background. Record the photo peak positions as well as their widths (FWHM and FWTM). Then follow the same procedure with the ^{137}Cs source and the ^{57}Co source. In the spectrum of the ^{57}Co source the 136 KeV gamma rays will only appear as a weak shoulder above the peak from the 122 KeV gamma rays. For a decay diagram for ^{57}Co see figure 12.1.

2. After the calibration has been completed, you have to install the intense ^{137}Cs source. This source had an activity of 1.25 mCuries when it was manufactured in October, 1968. The half-life of ^{137}Cs is 30.17 years, and the source is therefore still quite intense. **Never directly touch the source**. Transfer it between the storage container and the scattering setup as quickly as possible, and always handle it with the stainless steel rod that is provided for that purpose. Using a Geiger counter make sure that the collimated beam has maximum intensity at the target. Acquire spectra of scattered gamma rays for angles between 20^0 and 135^0. Take data in 10^0 intervals up to 90^0 and in 15^0 steps beyond 90^0. Take data for at least 300 sec at forward angles and 500 sec past 90^0. Subtract background with the scatterer removed (but the source still in place) for an equal length of time.

   From the position of the photo peak and from the calibration of the system, determine the energy of the photons at each angle. Construct a suitable plot to verify the Compton expression for the kinematics. What is the mass of the electron from your plot? Determine the yield in the photo peak, corrected for background, at each angle. Also record the intensity of the background in order to estimate the statistical counting error. Calculate the Compton scattering cross section at each angle and compare with the value predicted by the Klein-Nishina relation. Note that you cannot nearly determine the absolute cross section as accurately as the angular dependence of the cross section. Therefore you may wish to scale your cross section in order to compare the angular distribution separately.

References

1. A. H. Compton, Phys. Rev. 21,483 (1953).

2. C. Melissinos, *Experiments in Modern Physics*, Academic Press, 1966.

3. B. Marion and F. C. Young, *Nuclear Reaction Analysis, Graphs and Tables*, North-Holland Publishing Co., 1968.

4. F. Knoll, *Radiation Detections and Measurement*, John Wiley and Sons, 1979.

Chapter 14

Muon Decay

Introduction

Muons are produced in collisions between energetic protons and nuclei (primary cosmic rays) with matter in the upper atmosphere. At sea level the muon flux is roughly 10^{-2} per cm^2-sec-sr (see, e.g., Melissinos, p. 412). When muons reach our laboratory in DRL, they have lost a substantial amount of energy passing through the atmosphere and several floors of the building. Most muons that travel this far are still very energetic and will pass right through our lab and travel on. Only a small fraction stop in our scintillation detector. A detector with an areal density of 30 g/cm^2 can stop muons with a kinetic energy below 100 MeV. Muons stopped inside the scintillator decay into an electron and two neutrinos.

$$
\begin{aligned}
\mu^+ &\rightarrow e^+ + \nu_e + \overline{\nu}_\mu \\
\mu^- &\rightarrow e^- + \overline{\nu}_e + \nu_\mu
\end{aligned}
$$

The kinetic energy of the muons and the decay electrons produce light flashes inside the scintillator. Therefore, we can measure the muon lifetime by inspecting the spectrum of the time interval between all double pulses with a spacing of less than, say, 20μs. In a vacuum both the μ^+ and the μ^- decay with the same lifetime. In a material (scintillator) the μ^- can also be captured by a nucleus reducing its lifetime. Why? For the low atomic number scintillator we use the effect is small. For more information see reference [1].

Experimental Setup

There are two setups to determine the lifetime. In the first setup one just measures the lifetime of energetic particles decaying in the detector. The source of the decaying particles is not determined and are assumed to be muons. The advantage of doing this is that one acquires more data in a given time. In the second method thin scintillators are placed above and below the detector to track the muon. The detector measures the lifetime of only the particles that pass the thin scintillator. This identifies the source of the decaying particle and eliminates effects like two separate muons triggering and stopping the time measurement. The number of events recorded is lower because the tracking scintillators do not cover a large area. One is expected to do the atleast the first part to complete an easy experiment. If you prefer to do a more challenging version you should do the measurement with the second setup or with both setups.

(A) Scintillator

We need a scintillator that has a fast response and is available in large size. NaI is not suitable because of the long response time (light decay time $\tau = 0.25$ s) and high price. Liquid scintillators and plastic scintillators are both inexpensive and fast. We prefer plastic because it is more convenient in this application. We choose a cylinder of "NE 102" with the following properties:

Composition	Polyvinyl toluene ($CH_3C_6H_4C_2H_3$)
Pulse height	60% of anthracene
Decay time	4ns
Max. emission	4500$\AA$
Density	1.035 g/cm^3
Refractive index	1.58
Dimensions	diameter 18 cm
	length 30 cm

Because of the low Z value for the elements in plastic scintillator, the decay branch for negative muons by capture into nuclei is small and we observe the lifetime of free muons.

Consulting a range-energy table we find that 30 g/cm^2 of scintillator will stop approximately 100 MeV muons. The amount of light released in the decay of these muons depends on the kinetic energy of the decay electron. The maximum kinetic energy is 52 MeV and the energy spectrum peaks near

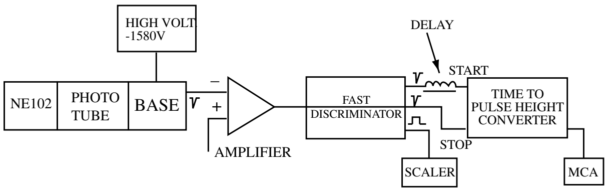

PHOTO TUBE	AMPEREX 2212 B
AMPLIFIER FASTDISCRIMINATOR	ELSCINT STD N-1
DELAY	100 ns COAX CABLE
TPHC	ORTEC 437
SCALER	ORTEC 776

Figure 14.1: Block diagram of the apparatus for setup 1

that value. The two pulses generated by the stopping of the muon and by its decay are therefore of similar amplitude. This simplifies our task because it allows us to send both pulses through the same discriminator circuit.

Muons that pass through the detector are mostly minimum ionizing particles. They lose energy at a rate of 2 MeV g^{-1} cm^2. Their energy loss in the scintillator will be around 60 MeV. Therefore, pulse height alone cannot distinguish between passing and stopping muons, and we have to inspect all pulses for a possible occurrence of a second pulse a few microseconds later.

(B) Electronics Block Diagram Setup 1

We operate the photomultiplier at the lowest practical high voltage setting to minimize the effect of after-pulses.

(C) Discriminator

When adjusting the discriminator level we should keep two points in mind:

1. Because of the broad energy distribution of the pulses from stopping and decaying muons, the rate of observed muon decays increases with decreasing discriminator level down to very low levels. We should keep in mind that the light collection from our large scintillator into the small 2" photocathode is poor and not uniform, so we cannot make

a meaningful energy calibration of the pulse height spectrum. These arguments favor a very low discriminator setting.

2. With the lowering of the discriminator setting, the singles count rate increases rapidly, not only from cosmic rays but also from natural radioactivity. Two of the major contributions are a 2.6l4 MeV gamma ray in ^{208}Pb from the ^{232}Th decay chain and a 1.406 MeV gamma ray in ^{40}Ar from the 10% electron capture decay branch of ^{40}K. Both elements are present in surrounding materials. Too high a singles rate from radioactive decays can lead to significant random double events in the time interval spectrum. We have had good success with discriminator levels that correspond to a singles rate of 10-20 counts per second.

(D) Time to pulse height converter

A pulse from a muon will enter the TPHC start and stop inputs and find the device in a state where it is not busy processing a previous pulse. In this state the start input is ready to accept a pulse while the stop input is blocked. We slightly delay the arrival of the start pulses to be certain that the associated stop pulses will be blocked and not terminate the conversion cycle prematurely. As soon as conversion starts, the start input is blocked and the stop input is enabled. If the muon stops in the scintillator, the decay produces a second pulse that stops the conversion. The TPHC generates an output pulse proportional to the time interval between the two pulses. A suitable range setting is 20μs. These pulses are presented to the multichannel analyzer where they are sorted into a spectrum.

Data Acquisition

1. Record the spectrum from the TPHC in the MCA (use 5l2 channels) for at least 12 hours (overnight).

2. Also, scale the singles rate at the output of the discriminator for several minutes.

3. Calibration of MCA: You have to calibrate the MCA in units of time. For this purpose you have to assemble the following circuit 14.2

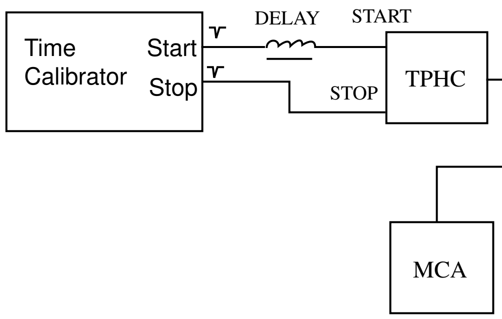

Figure 14.2: Time calibration of the MCA

The 'Time Calibrator' repeatedly puts out pairs of pulses with intervals that are randomly set to be at multiples of the period set upto the range in time.

(B) Electronics Block Diagram Setup 2

The setup is shown in 14.3. The aim is to trigger the TAC when a muon traverses the top scintillator and is stopped in the detector. To minimise acquiring data when a muon does not stop at the detector and passes through the bottom detector, the signal from the bottom scintillator is used as a veto to disable starting the TAC.

The two thin plastic scintillators are 1 ft square, with non-adiabatic light guides attached to their PMT's. These PMT's have been operated at up to 2100 V, and produce good, fast signals of about 20 or 30 mV. The scintillators are attached to the light guide (and the light guide attached to the PMT) with transparent epoxy - although the hold is relatively strong be careful when handling them, as it is possible to break the bond.[1]

[1] The scintillators are wrapped with an inner layer of aluminum foil, followed by several layers of construction paper and tape. Although the detectors were certainly light-tight when they were wrapped it is possible that in the future the detectors will develop light leaks. To test a detector for light leaks connect the detector to a counter. Slowly turn up the high voltage until counts start registering on the counter (this should happen somewhere around 1600 V). Find a voltage with a count rate near 5 or 10 Hz, and then slowly shine a flashlight over the surface of the entire detector. Vary the angle of the light,

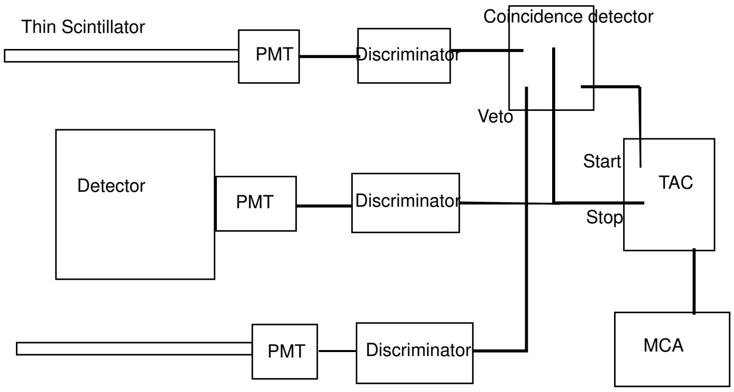

Figure 14.3: Block diagram of the apparatus for setup 2

The coincidence detector takes up to four inputs (negative pulses), and allows for a veto signal. The 'level of coincidence' (ie. number of inputs required for a positive signal) is set by pushing a small pin into the hole next to the desired number. Inputs can be disabled by putting the same pins into the hole next to their name. The coincidence detector is very fast, and to simplify the timing setup it would be best to use discriminators with variable output signal lengths. Difficulties were encountered in the past when very short duration signals were used with the detector (remember that the signal arrival time depends on both cable length and the position of the muon in the scintillator!) If the discriminators do not fire for a long enough time interval it is likely that the system will lose efficiency.

The coincidence detector can be used to choose a discriminator setting for each of the square scintillators, as well as to determine their efficiency of detecting muons.

By placing one of the thin detectors on top of the other, and putting the cylindrical detector above both it is possible to measure detector A's efficiency. The discriminator setting should be chosen at a point where the efficiency does not vary much with changing discriminator setting

---

and be sure to check the top of the detector (where the phototube attaches to the light guide) well. If the flashlight is shone directly into a light leak the counter will register hundreds or even thousands of counts in a fraction of a second. If a leak is discovered it can either be patched over, or the entire detector could be re-covered.

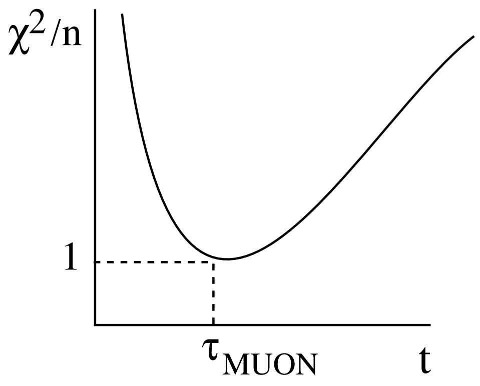

Figure 14.4: Variation of χ^2 with t

Analysis

1. Compress the 512 channel spectrum by a factor of eight into 64 channels. Why would one want to do this?

2. From the measured singles rate you can calculate the number of chance coincidences per channel. The content of the highest channels should equal that number. Subtract these chance events from the spectrum.

3. Generate least squares fits for the remaining spectrum with the function:
$$N = N_0 e^{\frac{-t}{T}}$$

4. Determine χ^2(T). From this function you can extract the best value for the mean lifetime T as well as its probable error.

References

1. Segre, E., Particles and Nuclei, W. A. Benjamin, 1977.

2. C. Melissinos, Experiments in Modern Physics, Academic Press, 1966.

Chapter 15

Electron Spectroscopy

Introduction

In this experiment we investigate the properties of the electron spectrum from a ^{137}Cs source. Some of the data on the ^{137}Cs decay are summarized in the figure 15.1.

The ^{137}Cs source emits electrons in the beta decay to the ground state and second excited state of ^{137}Ba. In addition, there are groups of monoenergetic electrons emitted in the decay of the 662KeV level via internal conversion (Ref. 2). In this experiment we measure a momentum spectrum of the electrons. From the relative strength of the beta decay spectrum and the conversion lines, we determine the internal conversion coefficients. From a Kurie plot we derive the Q value of the decay.

Apparatus

The momentum spectrum of the electrons from the ^{137}Cs source is being analyzed with a single focussing semi-circular spectrometer. For a detailed description see, e.g., Ref. 1. Briefly the source, defining slits and detector are all placed inside a uniform magnetic field.

Electrons of a single energy from an idealized point source pass through the defining slits and meet again after half a revolution. The focussing is however not perfect. There are aberrations that depend in second order on the width of the defining slits. In the direction parallel to the magnetic field, there is no focussing but an additional contribution to the aberration arises

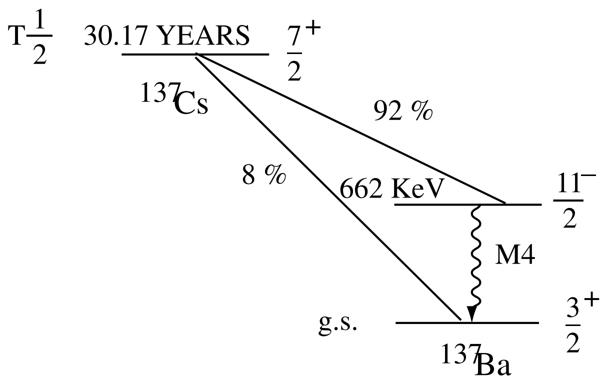

Figure 15.1: Decay scheme for ^{137}Cs

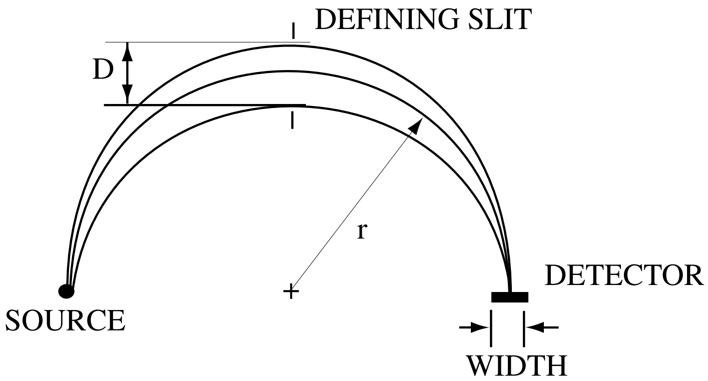

Figure 15.2: Schematic diagram of the electron trajectory

from the finite acceptance angle in that direction (it is also of second order). The momentum resolution of our spectrometer is dominated by the source width W_S and the detector width W_D. Our detector accepts trajectories within a radius interval r and r + Δr where,

$$2\Delta r = W_S + W_D$$

The solid angle of the detector with respect to the source is not constant within this range. It peaks in the center of the range at the value,

$$\Omega \approx \frac{DH}{\pi r^2}$$

where D is the spacing of the defining slits and H is the dimension of the detector parallel to the field. The count rate in the detector is proportional to the number of electrons emitted by the source within the radius interval r and $r + \Delta r$ which can be expressed by the derivative

$$[\frac{\partial N(r,B)}{\partial r}]_{B=const}$$

In our experiment the electron spectrum is scanned by varying B (and not r) in small steps. Therefore the direct integration of peaks is not meaningful and does not allow the determination of peak intensities or branching ratios. For that purpose one converts the plot to a function of a single variable, usually the momentum p of the electrons, $p = erB$. The number of electrons in the momentum interval p, p + dp is then proportional to

$$\frac{dN}{dr}(p) = [\frac{\partial N}{\partial r}]_B[\frac{\partial N}{\partial p}]_B \approx \frac{1}{B}[\frac{\partial N}{\partial r}]_B$$

The effect of this transformation is shown in the figure 15.3 for a hypothetical spectrum.

The electron detector is a Silicon surface barrier detector that depletes to a thickness of $300\mu m$ at a bias of +110 V. Electrons with an energy above 300KeV do not stop in the detector and the spectrum therefore exhibits only a weak full energy peak. For counting purposes we simply accept all pulses above the noise level.

A schematic diagram of the entire setup is shown shown in the figure 15.4.

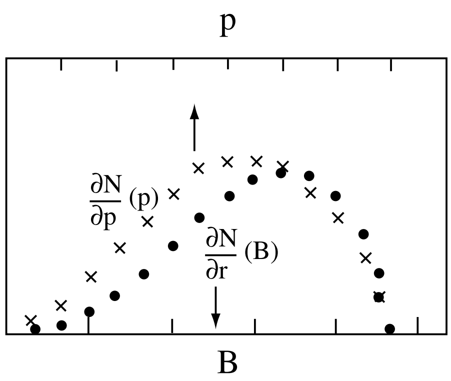

Figure 15.3: $\frac{\delta N}{\delta p}(p)$ and $\frac{\delta N}{\delta r}B$ as a function of p and B

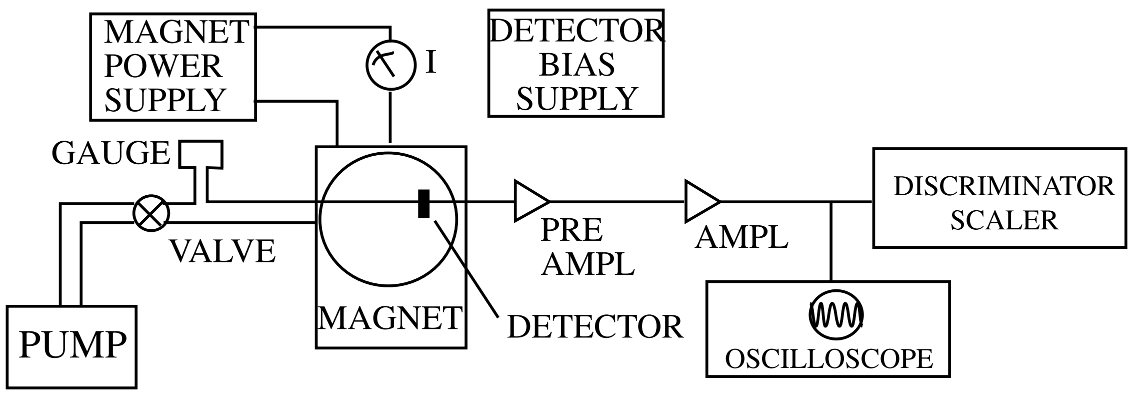

Figure 15.4: Block diagram of the apparatus

Measurement

Cycle the magnet several times around its hysteresis loop between 0 and 1.6 amps so that a reproducible field is obtained. Make sure the same end points are used each time the magent is cycled. Using the thermocouple gauge to measure the pressure, evacuate the chamber with the mechanical pump to a pressure lower than 1 mm. **Carefully** apply bias to the solid state detector while monitoring the amplifier output for possible breakdown. Measure the counting rate as a function of magnet current around the hysteresis loop in steps of 0.05 A up to the conversion line. Scan the conversion line in finer steps of 0.005 A and the spectrum above in 0.15 A steps up to 1.6 A.

Then remove the detector bias, shut down the pump and vent the vacuum chamber. Remove the defining slits, insert the Hall probe and measure the field as a function of current, always remaining on the same hysteresis loop.

Generate a momentum spectrum. The source detector distance is 76.2 mm. Compute the energy of the conversion electrons, if possible for K and L conversion separately. Calculate the conversion coefficients. Compare your values with theoretical predictions (Ref. 2,3). Construct a Kurie plot to find the end point of the continuous beta spectrum for the decay branch to the excited state. Discuss the shape of the beta spectrum.

References

1. Segre, *Particles and Nuclei*, Benjamin, 1977.

2. Siegbahn, *Alpha-, Beta-, and Gamma-Ray Spectroscopy*, North Holland Publishing Company, 1966.

3. Conversion coefficients are tabulated in *Nuclear Data, Section A*, Vol. 4, 1 (1968).

4. X-ray absorption edges can be found, e.g. in the *American Institute of Physics Handbook*, Third Edition, 1972.

Chapter 16

γ Correlation Measurement in ^{60}Ni

The β decay of the ground state of ^{60}Co populates almost exclusively a level in ^{60}Ni at 2506KeV excitation. In this experiment we are investigating the γ decay of this level in order to determine its spin.

First we look at the shell model configurations of low lying levels in ^{60}Ni to obtain some guidance about the spins that are likely for a level at 2506KeV. 60Ni has four neutrons outside the doubly closed shell nucleus ^{56}Ni. In ^{56}Ni 28 neutrons and 28 protons fill the 1s, 1p, 2s1d and 1f7/2 shells. The four additional neutrons in 60Ni can be distributed over the 2p3/2, 2p1/2 and 1f5/2 subshells.

If we place them all into the p3/2 shell, that shell is also filled and the only state that can be formed is a I = 0 state. However, if we consider all possible states with the neutrons in the three subshells, a large number of states can be formed.

I	Number of States
0^+	9
1^+	12
2^+	21
3^+	15
4^+	15
5^+	4
6^+	3

Shell model calculations with reasonable parameters predict I = 0^+ for the ground state and I = 2^+ for the first excited state. Between 2 and 3 MeV

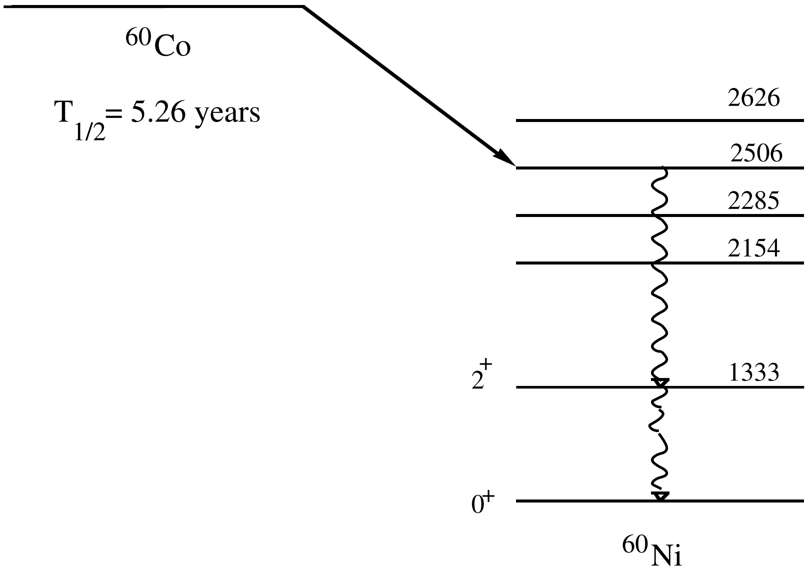

Figure 16.1: Shell Model Picture of ^{60}Ni

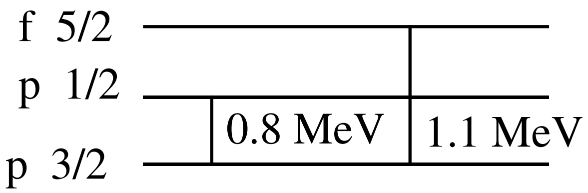

Figure 16.2:

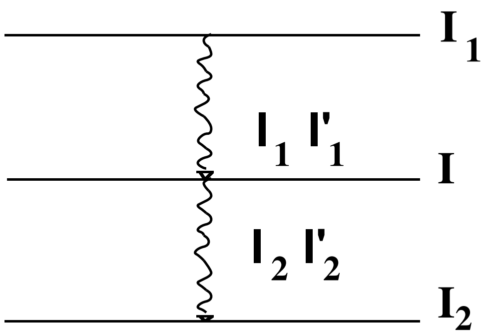

Figure 16.3: Cascade of γ-rays

excitation, they predict additional levels with spins 0^+, 1^+, 2^+ (2 levels), 3^+, and 4^+. Therefore we restrict our considerations to these spins and parities.

Calculation of the Angular Correlation Function

We consider a cascade of two γ-rays and a spin sequence $\mathrm{I}_1 \to I \to I_2$. In transitions of states of the same parity, the allowed multipolarities are magnetic dipole (l=1), electric quadrupole (l=2), magnetic octupole (l=3), etc. M1 and E2 transitions are generally of comparable speed but all higher multipolarities proceed much more slowly and they can therefore be neglected in all cases where angular selection rules, allow M1 or E2 transitions or both. The most general case that we consider here is therefore a cascade where both γ-rays are mixtures of M1 and E2 strength. (In our particular application, the second transition has to be pure E2 because I = 2 and $\mathrm{I}_2 = 0$). The angular correlation functions can be calculated from the known dipole and quadrupole radiation patterns shown in Fig 16.4.

For our calculations we find it most convenient to choose the z axis of our coordinate system along the direction of the first γ-ray.

In this coordinate frame we will only observe $\mathrm{m}_1 = 1$ transitions because of the longitudinal polarization of photons. To illustrate the calculation we choose a very simple example, the spin sequence $0^+ \to 2^+ \to 0^+$.

In this case both transitions are pure E2. The only M states that are populated in the 2^+ level are M = 1 and the correlation function therefore

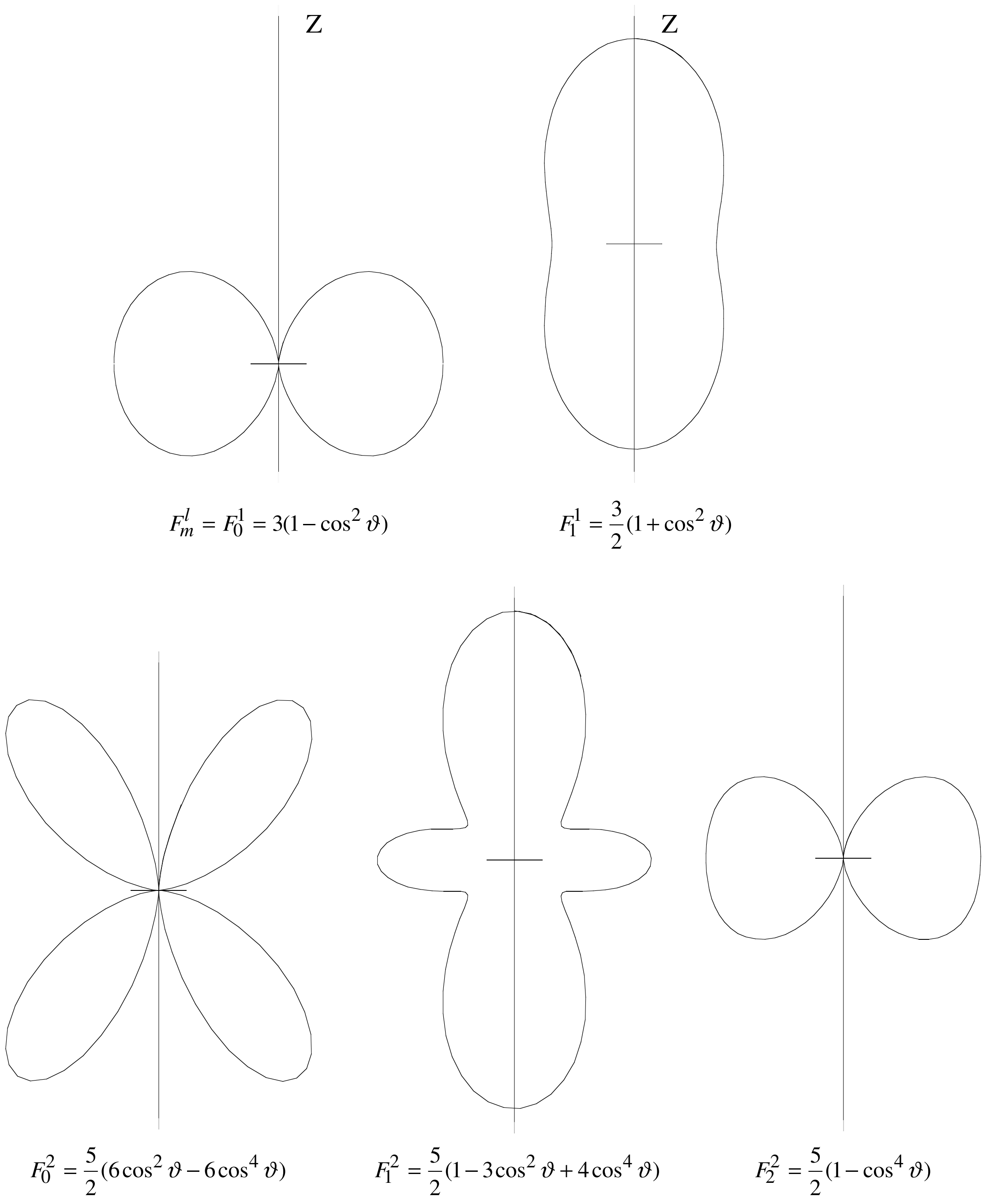

Figure 16.4: Dipole and Quadrapole Radiation Patterns

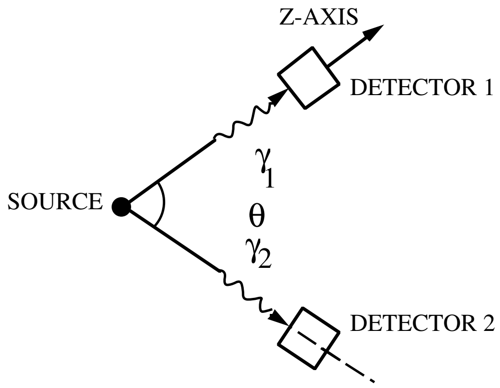

Figure 16.5: Coordinate System for Calculation

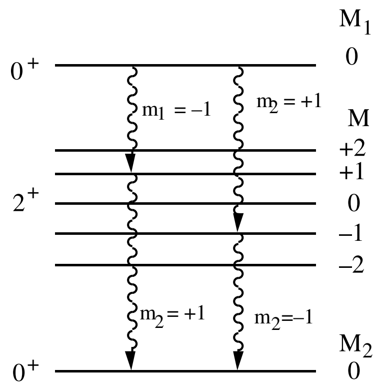

Figure 16.6: M states in the γ cascade $0^+ \to 2^+ \to 0^+$

consists of a single term.

$$W(\vartheta) \approx F_1^2 = \frac{5}{2}(1 - 3\cos^2\theta + 4\cos^4\theta)$$

The calculations for other spin sequences are in principle very similar but computationally they are much more complicated because the summation has to extend over many substates of the initial and intermediate state and more than one multipolarity may contribute. It is therefore much more convenient to expand the correlation in terms of Legendre Polynomials

$$W(\theta) = \sum_{\nu} A_{\nu}^{(1)} A_{\nu}^{(2)} P_{\nu}(\cos\theta)$$

and to compute the expansion coefficients from tabulated values of angular correlation coefficients $F_{\nu}(II'll'$. For multipolarities not higher than quadrupole, this sum has only three terms.

$$\begin{aligned} W(\theta) &= 1 + A_2^{(1)} A_2^{(2)} P_2(\cos\theta) + A_4^{(1)} A_4^{(2)} P_4(\cos\theta) \\ &= 1 + A_{22} P_2(\cos\theta) + A_{44} P_4(\cos\theta) \end{aligned}$$

with,

$$A_{\nu}^{(k)} = (1 + \delta_k^2)^{-1}[F_{\nu}(II_k l_k l_k) + 2\delta_k F_{\nu}(II_k l_k l_{k'}) + \delta_k^2 F_{\nu}(II_k l_{k'} l_{k'})]$$

where k = 1,2 for first and second transitions, respectively, and δ_k is the multipole mixing ratio. The spins I, I_k, and the multipolarities I_k, $I_{k'}$ are defined in figure 16.3. In ^{60}Ni the second transition is a pure E2 transition ($l_2 = 2$, $l_{2'} = 3$, and $\delta_2 = 0$) between spins 2 and 0. Therefore,

$$\begin{aligned} A_{\nu}^{(2)} &= F_{\nu}(2022) \\ A_2^{(2)} &= F_{\nu}(2022) = -0.5976 \\ A_4^{(2)} &= F_4(2022) = -1.0690 \end{aligned}$$

Now we can compute the theoretical correlation functions for all possible spins I1 of the 2506 KeV level.

$$I_1 = 4$$

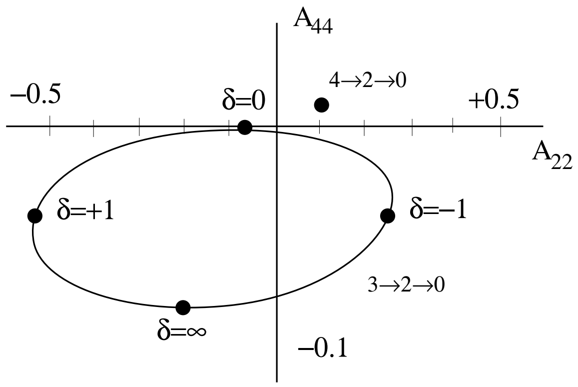

Figure 16.7: Parametric plot of allowed coefficients in the angular correlation

In this case the first transition is also pure quadrupole.

$$
\begin{aligned}
A_4^{(1)} &= F_4(2422) = -0.0085 \\
W(\theta) &= 1 + 0.102 P_2(\cos\theta) + 0.0091 P_4(\cos\theta) \\
&= 1 + 0.1248\cos^2\theta + 0.0418\cos^4\theta
\end{aligned}
$$

This correlation is nearly isotropic and differs very strongly from that of a $0 \to 2 \to 0$ spin sequence.

$3 \to 2 \to 0$

$$
\begin{aligned}
A_\nu^{(1)} &= (1+\delta^2)^{-1}[F_\nu(2311) + 2\delta F_\nu(2312) + \delta^2 F_\nu(2322)] \\
W(\theta) &= 1 - (1+\delta^2)^{-1}[(0.0714 + 0.7825\delta + 0.2041\delta^2)P_2(\cos\theta) + 0.01817\delta^2 P_4(\cos\theta)]
\end{aligned}
$$

In the absence of any knowledge of the actual M2 - E2 mixing ratio δ, the range of possible correlation functions describes an ellipse in A_{22}/A_{44} space.

Note that the ellipse passes very close to the point which describes the correlation of the $4 \to 2 \to 0$ spin sequence. It is therefore quite impossible to distinguish between these two cases from an angular correlation measurement alone. The same is also true about the spin sequences $2 \to 2 \to 0$ and $1 \to 2 \to 0$. In fact the ellipse that describes the $2 \to 2 \to 0$ sequence passes almost exactly through the point which corresponds to a $4 \to 2 \to 0$ decay. For that reason we have to turn to additional information before we

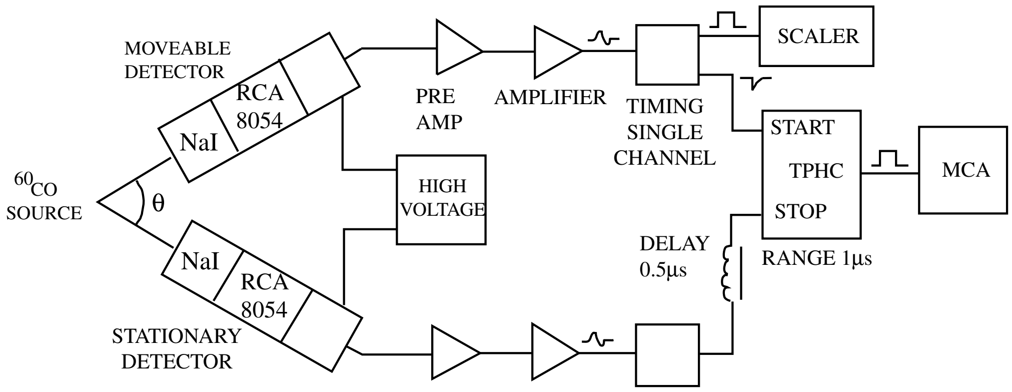

Figure 16.8: Experimental Setup

can determine the spin of the 2506KeV level. What additional information is available from the electromagnetic decay of this level?

(1) Absence of a direct ground state decay. No direct ground state decay is expected for spins 0^+, 3^+, and 4^+. Levels of spin 1^+ and 2^+ , on the other hand, should show a direct decay branch to the ground state via M1 or E2 radiation respectively. For that reason these spins are unlikely and we therefore no longer consider them.

(2) The 2506KeV level also decays via internal conversion to the 1333KeV level. The relative strength of this decay mode (called the internal conversion coefficient) can be very precisely calculated from electromagnetic theory. It is different for M1 and E2 decays. The experimental value of the internal conversion coefficient (ref. 3) favors a transition that is either pure E2 or predominantly E2. In combination with this additional information, the correlation measurement can distinguish between spins 3 and 4.

Experimental setup

The experimental setup used in this measurement is shown in Fig. 16.8. The γ-rays are detected in two 2" dia. x 2" long NaI (Tl) scintillators. The scintillators are bonded to 2" dia. photomultiplier tubes (RCA 8053) and hermetically and optically sealed inside an aluminum container. The charge pulses from the anodes of the phototubes are sent through preamplifiers and shaping amplifiers and then presented to timing single channel analyzers.

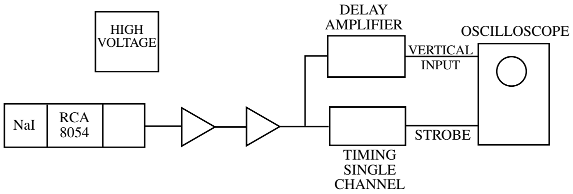

Figure 16.9:

The timing single channels generate an output pulse whenever the pulse height of the linear input pulse lies between the lower and upper discriminator level. The timing of the output pulse is precisely related to the arrival time of the input pulse and is quite independent of the pulse height. When two γ-rays emerging from one nucleus are observed in our two detectors, the outputs at the two single channels occur at exactly the same time. We call such an event a true coincidence. The time to pulse height converter measures the time difference between these two output pulses (shifted by the stop delay) and converts it into a pulse height. The pulse height spectrum for true coincidences consists of a single narrow peak. This peak rides on a background generated by accidental coincidences between γ-rays originating from independent decays (See Fig. 16.10).

Experimental procedure and analysis

(1) Adjust the gains of the shaping amplifiers and discriminator levels of both timing single channels such that only the photo peaks of the two γ-rays from the ^{60}Co source are accepted. This adjustment can most quickly be done with an oscilloscope as shown in Fig. 16.9.

(2) Acquire coincidence spectra with adequate statistics (at least 1000 true events) for the angle settings 90^0, 105^0, 120^0, 135^0, 150^0, 165^0 and 180^0. For each angle setting you have to record the number of coincidence events in the region of the true peak. The contribution from random coincidences to the events in this region can be estimated from an adjacent region of equal width.

In order to be able to detect and correct for a small mis-centering of the source, the singles counts from the timing single channel of the movable detector should be scaled while coincidences are acquired (See Fig. 16.8).

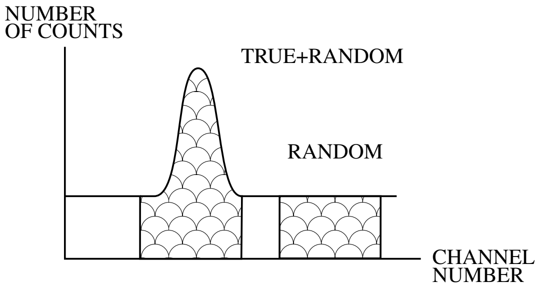

Figure 16.10:

(3) Calculate the coefficients A_{22} and A_{44} from your data using the method of least squares. It is very poor practice to give the measured data points unequal weight by forcing the theoretical fit through the data point at 90^0 (This is however frequently done, see e.g. ref. 2 page 423). Instead we prefer to fit our data with the function.

$$W(\theta) = a_0 + a_2 P_2(\cos\theta) + a_4 P_4(\cos\theta)$$

and derive the values of A_{22} and A_{44} from that fit.

$$A_{22} = \frac{a_2}{a_0}, A_{44} = \frac{a_4}{a_0}$$

Find the standard deviations for A_{22} and A_{44}. Discuss the implications of your results regarding the spin of the 2506KeV level.

Legendre Polynomials

$$\begin{aligned} P_0(\cos\theta) &= 1 \\ P_2(\cos\theta) &= \frac{1}{2}(3\cos^2\theta - 1) \\ P_4(\cos\theta) &= \frac{1}{8}(35\cos^4\theta - 30\cos^2\theta + 3) \end{aligned}$$

I$'$	L	L$'$	$\nu = 2$	$\nu = 4$
0	2	2	-0.598	-1.069
1	1	1	0.418	0
1	1	2	-0.935	0
1	2	2	-0.299	0.713
2	1	1	-0.418	0
2	1	2	-0.612	0
2	2	2	-0.128	-0.305
3	1	1	0.120	0
3	1	2	0.655	0
3	2	2	0.341	0.076
4	2	2	-0.171	0.008

Table 16.1: Table of $F_\nu(II'LL')$ for $I = 2$. These coefficients are symmetric in L, L'

References

1. K. Siegbahn, *Alpha-, Beta-, and Gamma-Ray Spectroscopy*, North Holland Publishing Company, 1966.

2. A. C. Melissinos, *Experiments in Modern Physics*, Academic Press, 1966.

3. M. A. Waggoner, M. L. Moon and A. Roberts, Phys. Rev. **80**, 420 (1950).

4. H.W. Taylor, B. Singh and F. S. Prato, $\gamma - \gamma$ *Angular Correlation Coefficients, Nuclear Data Tables*, **A9**, 1 (1971).

Chapter 17

Velocity Dependence of the Electron Mass

One of the most significant results of the theory of relativity is the deduction that the mass of a body varies with its velocity.

$$m = m_0[1 - (\frac{v}{c})^2]^{-\frac{1}{2}}$$

In this experiment we verify this relationship.

Apparatus

A schematic diagram of our setup is shown in Fig. 17.1. Briefly, electrons from a ^{90}Sr source pass through a momentum analyzer and a velocity filter. A plastic scintillator counts the electrons that pass through both analyzers.

A decay scheme for ^{90}Sr is shown in Fig. 17.2.

$$\begin{aligned} {}^{90}Sr &\Rightarrow \beta^- + \overline{\nu} + {}^{90}Y \\ {}^{90}Y &\Rightarrow \beta^- + \overline{\nu} + {}^{90}Zr \end{aligned}$$

The ^{90}Sr source decays to ^{90}Y by emitting an electron (β^- particle) and an antineutrino ($\overline{\nu}$) with a smooth energy distribution for the electrons up to the 546KeV endpoint of the beta decay of ^{90}Sr[1]. The half life for this

[1] The antineutrino is emitted because from many experiments it is known that lepton number is conserved for particle decay. The electron has lepton number of +1 and the antineutrino a lepton number of -1.

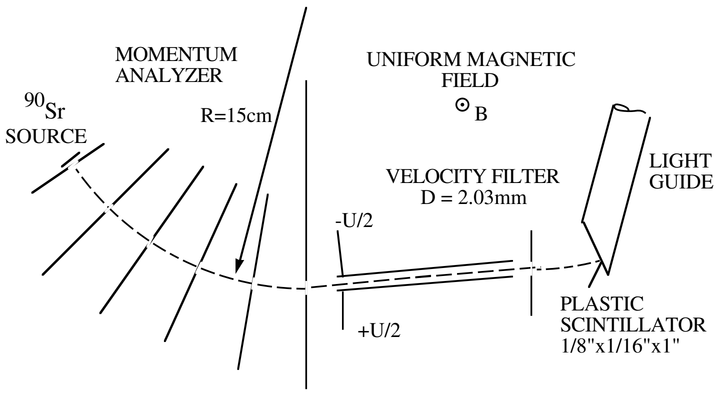

Figure 17.1: Path traversed by an electron

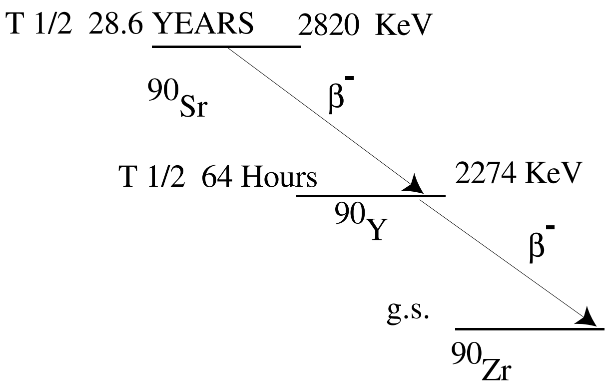

Figure 17.2: Decay scheme for ^{90}Sr

decay is 28.6 years. Why is there a smooth energy distribution of electrons? Similarly the ^{90}Y decays to ^{90}Zr with a half life of 64 hours. The endpoint energy of this beta decay is 2274 KeV.

The entire setup shown in Fig. 17.1 is placed inside an evacuated chamber between the pole pieces of a large magnet. The magnet maintains a uniform field that can be varied between 0 and 200 Gauss. The momentum analyzer consists of six 1.6 mm wide apertures, that only pass electrons on an orbit with a radius in a narrow range centered around R = 15.00 0.01 cm. The momentum of the electrons that exit from this device is given by

$$p = mv = eRB$$

In the velocity analyzer two 10 cm long parallel plates with a spacing of D =2.03 0.01 mm maintain an intense electric field perpendicular to the magnetic field. The polarity of the applied voltage U is chosen such that the electric force counteracts the magnetic force from the large magnet. For any charged particle with a velocity,

$$v = \frac{E}{B} = \frac{U}{DB}$$

the two forces are equal in magnitude and electrons with that velocity can therefore pass unperturbed through the narrow gap between the plates and through the 1.6 mm wide exit slit.

Caution: The electric field between the parallel plates reaches extremely high values, up to 5 x 10^6 Volt/m. For that reason, the high voltage should only be operated at pressures below 5 x 10^{-4} Torr. At higher pressures, including atmospheric pressure, a glow discharge can develop between the two plates which might permanently damage the ceramic spacers of the plate assembly.

Electrons that successfully pass through both analyzers are detected by a plastic scintillator with a sensitive area of 25 mm x 3 mm and at a thickness of 1.6 mm. The scintillator is viewed through a long light guide by a photomultiplier tube (PMT) which is situated outside the magnetic field. The multiplier is wrapped in magnetic shielding material to eliminate the adverse effects of the stray field of the magnet. A block diagram of the electronics is shown in Fig. 17.3. The signal from the anode of the PMT is amplified in a charge sensitive preamplifier and in a voltage amplifier before it is presented to a multi-channel analyzer. The light output from the scintillator is quite

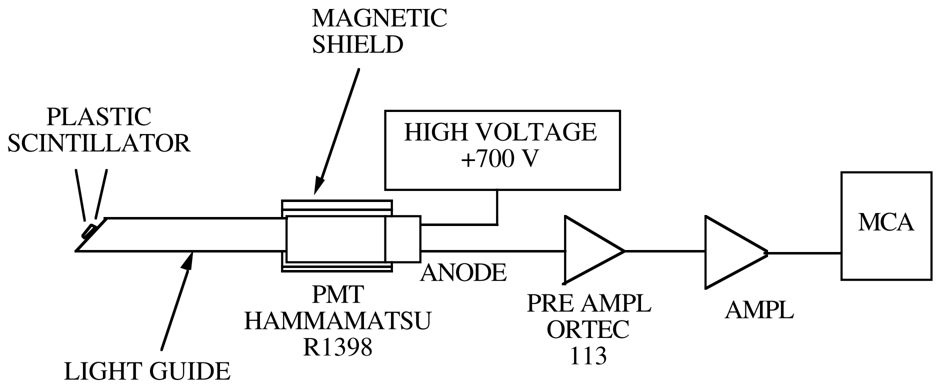

Figure 17.3: Block diagram of the electronics

low and not far above the noise generated by the dark current in the PMT. Best results are therefore obtained with the amplifier set to a maximum gain and the PMT operated at the lowest possible high voltage (about 700 V). Typical spectra from the detector for two different field settings are shown in Fig. 17.4. Several 12.7 cm thick lead plates are inserted in different locations between source and detector. These shielding plates substantially reduce the background count rate in the detector. Even though only beta particles are emitted in all directions by the radioactive source, gamma rays are produced when the electrons are stopped (decelerated) in a material. The shielding reduces the counts due these gamma rays.

Experimental Procedure

Consult with your instructor about the state of the vacuum system before you start the experiment. The vacuum ionization gauge should read a pressure below 5 x 10^{-4} Torr before the experiment can begin[2]. Slide the vacuum chamber from the magnet and insert a Hall probe into the pole gap. Cycle the magnet at least two times around its hysteresis loop between 0 and 1.99 amps. This is done to get a reproducible field for a given current[3]. Now

[2]It takes about 15 minutes to reach the desired pressure once the turbo pump is turned on. Once the turbo pump is turned on do not accidently bump into it.

[3]Make sure the end points of the hysteresis loop are always the same. The rate of cycling is not important.

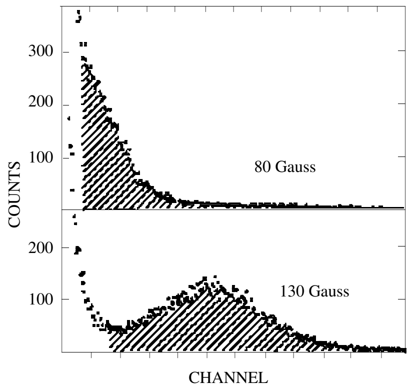

Figure 17.4: Output form the multichannel analyzer

determine the current settings that correspond to magnetic field values of 80, 100, 120, 140, 160, 180 and 190 Gauss[4].Then remove the Hall probe and slide the vacuum chamber back into the magnet gap.

Now power up all the electronics. Choose one of the magnetic field values listed above (120 and 140 Gauss give nice results and are good values to start with). Calculate the expected voltages from the dimensions given using the relativistic equations. Scan the voltage of the velocity filter in 50 V steps about the expected voltage until you have located the transmission peak. To be able to determine the peak well it is good to scan at least about 11 points around the peak. Count for at least 100 seconds for each voltage setting. Obviously a good guess for the starting value of the plate voltage will expedite your measurements.

Repeat the same procedure for all the other magnetic field settings listed above.

Analysis

Plot your data. For each magnetic field setting B determine the peak value U of the deflection voltage. Calculate the measured electron mass

$$m = \frac{p}{v} = \frac{eRDB^2}{U}$$

[4]While changing the current be very careful and *do not* backtrack. If you overshoot a setting cycle the magnet and return to the desired setting

and velocity parameter β

$$\beta = \frac{v}{c} = \frac{U}{DBc}$$

Plot m versus β . Also plot the curve that corresponds to the relativistic relation,

$$m = \frac{m_0}{\sqrt{1-\beta^2}}$$

Determine the best value for e/m0 from your data.

$$\frac{e}{m_0} = \frac{e}{m\sqrt{1-\beta^2}} = \frac{U}{RB[D^2B^2 - (\frac{U}{c})^2]^{\frac{1}{2}}}$$

Pay attention to proper error propagation.

Appendix A

Some Notes on Statistics, Errors, and Fluctuations

Experimenters usually have or are searching for a simple, mathematical model (i.e. a "theory") that predicts how a system will behave under certain conditions. They soon discover that even if they exercise all possible care to make the conditions of an experiment identical from one trial to the next, they find different values for the quantity measured (let's call this A). These fluctuations may be intrinsic to the measurement (determined by quantum or thermal effects), or, more likely unless you are quite careful, they result from random fluctuations in the measurement apparatus. One thing to keep mind is that in some experiments, the fluctuations themselves are very interesting!

Suppose we have an ideal apparatus for measuring a physical quantity whose true value is A_T (we won't worry about intrinsic fluctuations in A_T). Just before we record the outcome, a "demon" enters the picture and adds a random value, positive or negative, to the result. The experiment produces $A_T = 1.41$, but after the demon jumps in, we measure $A = 1.41 + \epsilon$. The next trial the value of ϵ is different, and we measure a different value for A. After many measurements, we make a table of the probability that A fell in a given range (e.g., $1.43 \leq A \leq 1.44$. We have chosen the "bin" size to be 0.01). The probability is simply the number of times we measured A between 1.43 and 1.44, divided by the total (hopefully large) number of measurements. Since we know that each measurement produces SOME value for A, we can say, $\sum p_i = 1$, where the sum is over all the bins. The table and a histogram might be as shown in Fig 1 (200 measurements total).

We can extend this idea to the case of an infinitesimally small bin of size

Range	Frequency	Probability
1.37-1.379	2	0.01
1.38-1.389	0	0
1.39-1.399	20	0.1
1.40-1.409	72	0.36
1.41-1.419	82	0.41
1.42-1.429	16	0.08
1.43-1.439	4	0.02
1.44-1.449	4	0.02

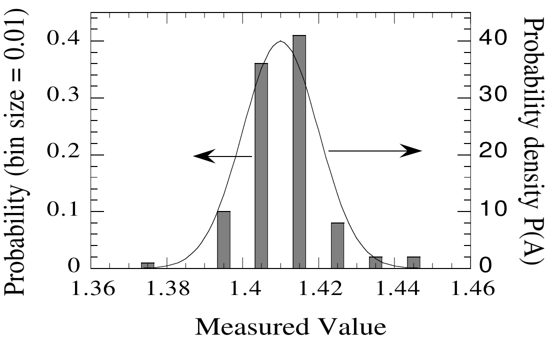

Figure A.1: Table, probability histogram and best fit Gaussian probability density for a possible experiment

dA. We define a function P(A), the "probability density distribution", such that the probability of measuring a value between A and A+dA is P(A)dA. That is, the total number of times we measured a value between A and A+dA is NP(A)dA, where N is the total number of measurements we performed. Fig 1 shows a plot of a reasonable fit for P(A) in the case described above (the fit is to a Gaussian function - see below). Notice that P(A) is peaked at a central value, and falls off roughly symmetrically and rather rapidly as one moves away from the central value. This is typical of most (but NOT all!) experiments, and is often assumed to be the case for all experiments. Since the total probability is one, we know the normalization of P(A):

$$\int_{\infty}^{-\infty} P(A)dA = 1 \tag{A.1}$$

Let's model the error-producing demon and see where it takes us. Suppose the demon chooses a random number g between 0 and 1 (all values equally likely), picks a value for $\epsilon(g)$ depending on the value of the random number (all values of ϵ are NOT equally likely), and then adds ϵ(g) to the correct value A_T. We can imagine that there is a probability density distribution for the demon, p(ϵ). That is, the probability that the demon chooses an error between ϵ and $\epsilon + d\epsilon$ is just $p(\epsilon)d\epsilon$. One possibility for $p(\epsilon)$ is shown in Fig. 2. Note that $P(\epsilon)$ is not necessarily a Gaussian, but its integral is normalized to one, as it must be.

Suppose that the measured value "before" the demon gets to it is always

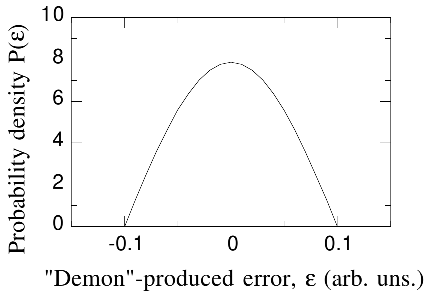

Figure A.2: A possible probability density function for a single error-producing process

A_T. We say that the probability density distribution for the ideal measurement is $P_0(A) = \delta(A - A_T)$. [Remember that we are ignoring intrinsic (e.g. quantum) fluctuations in the measurement. See the end of this section for a brief discussion of the $\delta(x)$, the Dirac delta function] After the demon affects the measurement once, there is a new probability density function, we'll call $P_1(A)$.

$P_1(A)$ can be determined as follows. One way that we could measure the value A is for the "demon" to choose the value e and the "perfect" measurement to produce the value $A - \epsilon$. The probability of this happening is simply $P_{\epsilon_1} P_0(A - \epsilon)$ (we make the key assumption that the error and the measurement are **independent** of each other). Add up the chance for all possible values of e, and you have the total probability form measuring the value A. Note that in the integral below, as for all integrals in the rest of this write-up, the limits of integration are assumed to be $[-\infty, \infty]$, unless otherwise noted.

$$P_1(A) = \int_{\infty}^{-\infty} P_0(A - \epsilon) p(\epsilon) d\epsilon \tag{A.2}$$

This very useful sort of integral is called the convolution of the functions P_0 and p. Notice that for the case when P_0 is a Dirac delta function, the result is particularly simple, namely $P_1(A) = p(A_T - A)$. If we knew the proper value of A_T ahead of time, and we had the patience to do an infinite number of measurements, we could determine the physics of the demon simply by graphing P_1! Unfortunately, nature is not so kind. We rarely know A_T before we begin, and even worse, there are many "demons" lurking in any experiment, and they each get a chance to disturb the ideal result. There are a whole sequence of probability distribution functions, P_1, P_2, P_3, ..., and we only get to see the last one, P_∞. So, there is an infinite sequence of convolution integrals, with each individual error being rather small, but the total error being what we see in the experiment. It turns out that there is a fundamental theorem of mathematics (the "Central Limit Theorem") that states that if many convolutions of the sort in Eq. A.2 take place, the resulting distribution function has a simple form, as long as the individual error functions $p(\epsilon)$ have an average value of zero and are not too pathological. In this special, idealized case, the resulting probability distribution function is a **Gaussian** or **Normal** distribution:

$$P(A) = \frac{1}{\sigma\sqrt{2\pi}} e^{-\frac{(A-A_T)^2}{2\sigma^2}} \tag{A.3}$$

A plot of this distribution is shown in Fig. A.1 (the fit to the probability histogram). The distribution has an integral of 1 (check this), is peaked at the "ideal" value A_T, and has a width proportional to σ, the "standard deviation" or the "typical" error introduced by the infinite sequence of demons. More mathematically, the "mean" of the distribution (the average value of A) is:

$$< A >= \frac{\int A' P(A') dA'}{\int P(A') dA'} = A_T \tag{A.4}$$

while the "mean square deviation" or "variance" is:

$$< (A - A_T)^2 >= \frac{\int (A - A^*)^2 P(A) dA}{\int P(A) dA} = \sigma^2 \tag{A.5}$$

It is worth knowing that about 2/3 of the probability lies between $A_T - \sigma$ and $A_T + \sigma$, and roughly 95% of the probability is between $A_T - 2\sigma$ and $A_T + 2\sigma$. Physicists usually say that the "error of the measurement" is σ, while engineers (by nature more cautious?) often say that the error is 2σ.

The normal distribution is what you might expect to find if you repeated a measurement an infinite number of times. You can easily construct a normal distribution that **approximates** the result of a finite data set, as we did in Fig. A.1. Take your N measured values A_i, and find the average and mean square deviation:

$$A_{T,exp} = \frac{1}{N}\sum_{i=1}^{N} A_i$$

and

$$\sigma^2_{T,exp} = \frac{1}{N-1}\sum_{i=1}^{N}(A_i - A_{T,exp})^2$$

Use A_{Texp} and σ_{exp} to construct an **empirical** probability distribution, $P_{exp}(A)$.

You might wonder about the $N-1$ in the definition of the variance, instead of N (some people call the quantity "s" instead of σ when the $N-1$ is in the denominator). Basically, it is there to remind you that one measurement doesn't give you enough information to estimate both the mean and the variance of the "true" distribution. You might be interested to know that if for some reason you know the mean of the distribution *a priori*, you can change the $N-1$ back to N. You should also keep in mind that if the difference between N and $N-1$ has a big impact on the results of your experiment, you're definitely pushing your luck!

What can you say about the **real** probability distribution (which you would measure if you made an infinite number of trials)? We'll discuss that after a brief digression into how errors propagate.

Error propagation

Suppose you have done several measurements of two different quantities, leading to average values $A_{T,exp}$ and $B_{T,exp}$, and standard deviations σ_A^{exp} and σ_B^{exp}. We *assume that both A and B are normally distributed, and that errors in A and B are independent of each other.* We would like to know the error associated with various functions of A and B, for example Z = A+B. The probability distribution for Z can be calculated exactly. To find it, we integrate over all possible values of A and B, subject to the constraint that $A + B = Z$:

$$\begin{aligned} P(Z) &= \int\int dA^{'}dB^{'}\delta(Z-(A^{'}+B^{'}))P_A(A^{'})P_B(B^{'}) \\ &= \int\int dA^{'}dB^{'}\delta(Z-(A^{'}+B^{'}))\frac{1}{\sigma_A\sqrt{2\pi}}e^{-\frac{(A^{'}-A^*)^2}{2\sigma_A^2}}\frac{1}{\sigma_B\sqrt{2\pi}}e^{-\frac{(B^{'}-B^*)^2}{2\sigma_B^2}} \end{aligned}$$

If you insert normal distributions for P_A and P_B and integrate carefully (a good piece of work) you will find that Z also has a normal distribution, with average value $Z_T = A_T + B_T$, and standard deviation $\sigma_Z^2 = \sigma_A^2 + \sigma_B^2$. We say that the errors for A and B "add in quadrature." If you consider the function Z = A B, the results will be similar: $Z_T = A_T - B_T$, and the error is $\sigma_Z^2 = \sigma_A^2 + \sigma_B^2$. If you consider the product $Z = AB$, you will find mean value $Z_T = A_T B_T$, and

$$(\frac{\sigma_Z}{Z_T})^2 \approx (\frac{\sigma_A}{A_T})^2 + (\frac{\sigma_B}{B_T})^2$$

This last relation is only approximate, and has a correction that is of order $(\frac{\sigma_A}{A})(\frac{\sigma_A}{A})$. The general function G(A,B) has mean value $Z_T = G(A_T, B_T)$, and standard deviation:

$$\sigma_Z^2 \approx (\frac{\partial G}{\partial A})^2_{A=A_T}\sigma_A^2 + (\frac{\partial G}{\partial B})^2_{B=B_T}\sigma_B^2$$

This is the fundamental equation that describes error propagation. All the "rules" you followed during your introductory physics lab come from this source.

Connecting the experiment to reality

Let's continue with our model that a real experiment consists of an ideal measurement, convolved with a normally distributed error source. If we did an infinite number of measurements, we expect to approach the ideal probability density distribution, P(A), so that the probability of a measurement between A and A+dA is P(A)dA. If, in contrast, we perform N trials, we only know that the expected number of measurements between A and A+dA is NP(A)dA; the actual number of times we find a value between A and A+dA could be greater or fewer than this (see Fig. A.3). How much deviation is to be expected, and when should we worry that something is wrong with our experiment?

We can phrase the problem as follows. Suppose the probability of the outcome we are interested in is p =P(A)dA, and we repeat the experiment N times. What is the likelihood that the desired outcome will occur M times? Call the desired outcome "A" (that is, a measured value between A and A+dA), and label all other outcomes "B". One way to have A occur M times is to have the following sequence of results:

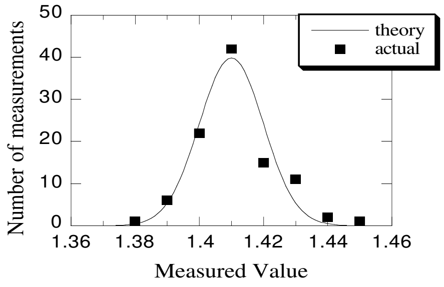

Figure A.3: A possible measured histogram compared with theory

$$\underbrace{AAAA\cdots AAA}_{Mtimes}\underbrace{BBB\cdots BBBB}_{N-Mtimes}$$

The probability of this happening is simply $p^M(1-p)^{N-M}$. However, any other sequence containing the same number of desired outcomes is also acceptable, since we are not concerned with the order of occurrences of the outcome A. The number of such sequences is the number of different ways to choose M objects from a total population of N, or

$$\frac{N!}{M!(N-M)!}$$

So, the total probability of having M occurrences of the outcome A in N trials is:

$$p(M) = \frac{N!}{M!(N-M)!}p^M(1-p)^{N-M} \tag{A.6}$$

This probability distribution function is called the **binomial distribution**. Notice that the total probability of measuring A some number of times between 0 and N is:

$$\sum_{i=0,N} p(i) = \sum_{i=0,N} \frac{N!}{i!(N-i)!}p^i(1-p)^{N-i} = [p+(1-p)]^N = 1$$

, as it should be. You can verify that the average number of successful trials is simply pN.

The distribution function has an important form if we let the number of trials N approach infinity, while the chance p of the desired result approaches zero, so the expected number of successful trials, $\overline{n} = pN$, remains constant. We use that fact that for large N, $\frac{N!}{(N-M)!} \approx N^M$, and that $(1-p)^{N-M} \approx (1-p)^N$. The limiting distribution function is:

$$P(M) = \lim_{\substack{n\to\infty, p\to 0\\ pN=const}} p(M) = \lim_{\substack{n\to\infty, p\to 0\\ pN=const}} \frac{(Np)^M}{M!}(1-\frac{Np}{N})^N \tag{A.7}$$

$$P(M) = \frac{\overline{n}^M}{m!}e^{-\overline{n}} \tag{A.8}$$

This is the famous *Poisson* distribution function. It tells us the probability of having M successful outcomes of a process which on average has $\overline{n}$ successful outcomes, when the experiment obeys the assumptions made above. Some key facts:

1. The Poisson distribution is normalized: $\sum P(i) = 1$.
2. The mean value of M is ¡M¿ $= \sum iP(i) = \overline{n}$.
3. The mean square deviation of M is $< (M- < M >)^2 >= \sum (i-\overline{n})^2 P(i) = \overline{n}$.

The standard deviation of M is just $\sqrt{\overline{n}}$.

As is clear from Figure A.4, the Poisson distribution approaches the Normal distribution for large $\overline{n}$, and $M \approx \overline{n}$. You can show this by using Stirling's approximation, $x! \approx x^x\sqrt{2\pi x}$ for large x.

For large $\overline{n}$, you will find that

$$p(M) \to \frac{1}{\sqrt{2\pi\overline{n}}}e^{-\frac{(M-\overline{n})^2}{2\overline{n}}}$$

Let's apply these tools to an experiment to find some physical quantity A. We assume A has an (unknown) ideal value A_T, and an experimental demon introduces a normally distributed error, with average value 0 and (unknown) standard deviation σ_A (later we will discuss how this assumption can break down). We make a series of N *identical* measurements, with the resulting data set $\{A_i\}$. We are interested in three parameters:

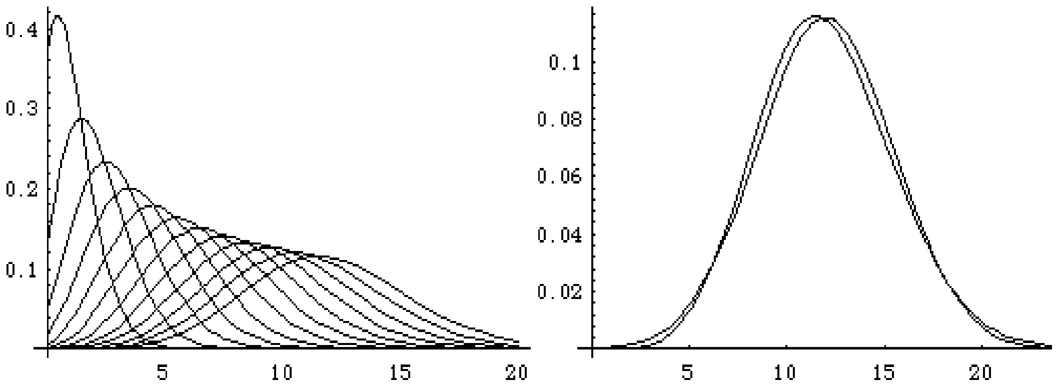

Figure A.4: The Poisson distribution for = 1 to 12 (left) and a comparison between the Poisson distribution for = 12 and a Gaussian distribution (right).

1. Our best estimate A_{est} of A_T, the peak of the experimental distribution.
2. Our best estimate σ_{est} of the measurement random error or width of the distribution σ_A.
3. The uncertainty ϵ in the estimate of A_T, given the N measurements.

One's first idea is that the "best guess" for A_T is simply the average of all the measurements.

$$A_{est} = \frac{1}{N} \sum_{i=1}^{N} A_i \tag{A.9}$$

This is correct, but it is instructive to think about the problem in another way. Consider the probability of measuring the data set $\{A_i\}$, for various values of A_{est}. The value of A_{est} that **maximizes the probability** of measuring $\{A_i\}$ is the best estimate for A_T. The probability of measuring the set $\{A_i\}$ is the product of the probabilities of measuring each A_i individually:

$$P(\{A_i\}) = \prod_i \frac{1}{\sigma_A \sqrt{2\pi}} \exp[-\frac{(A_i - A_{est})^2}{2\sigma_A^2}]$$

The probability$P(\{A_i\})$ is a maximum when A_{est} is such that the sum of the arguments of the exponential is a minimum, that is **when the mean square deviation is minimized**.

Our best estimate A_{est}, then, minimizes the function:

$$\sum(A_{est}) = \frac{1}{N}\sum_{i=1}^{N}(A_i - A_{est})^2$$

This approach is called the "method of least squares". By considering $d\Sigma/dA_{est}$, you can show in about 3 lines that the desired value of A_{est} is exactly the mean of the data set, Eq. A.9.

The best estimate for the typical error of the "demon" is the standard deviation of the data set:

$$\sigma_{est} = [\frac{1}{N-1}\sum_{i=1}^{N}(A_i - A_{est})^2]^{\frac{1}{2}}$$

(I'll say a bit about the $[N-1]$ below).

We assign an error of σ_{est} to each member of $\{A_i\}$. The rule for error propagation gives the uncertainty in our best guess for the "real" value A_T. Since $A_{est} = (\frac{1}{N})\sum A_i$, and errors add in quadrature, we have,

$$\epsilon = \frac{\sigma_{est}}{N^{\frac{1}{2}}} \tag{A.10}$$

If the errors that affect the data are normally distributed, you can generate an extremely accurate estimate for A_T by spending time and money to conduct a large number of measurements.

An interesting issue arises if we combine measurements of A with different uncertainties: $\{A_1 \pm \sigma_1, A_2 \pm \sigma_2, \cdots\}$. Each data point could result from reducing a large data set using the approach of the last paragraph. We wish to combine the data to generate our best guess A_{est}. In this case, it makes no sense to average the measurements; we have to give more weight to the more certain data points. We should maximize the probability of the data set, which leads to minimizing the function:

$$\chi^2(A_{est}) = \sum_{i=1}^{N}\frac{(A_i - A_{est})^2}{\sigma_i^2}$$

each value is weighted by its error.

A little algebra shows that the best guess α is now:

$$A_{est} = \frac{\sum(A_i/\sigma_i^2)}{\sum 1/\sigma_i^2} \tag{A.11}$$

Notice that if the data points are statistically "compatible", α should lie within the error bars for each point, so $\chi^2(\alpha)$ should be of order N. The error associated with this estimate is,

$$\epsilon^2 = (\sum_{i=1}^{N} \frac{1}{\sigma_i^2})^{-1} \tag{A.12}$$

We can gain intuition about these results by considering the data set $A_1 \pm 1, A_1 \pm 2$. Since the uncertainty drops as the square root of the number of measurements, we can replace this data set by the "equivalent" set $\{A_1 \pm 2, A_1 \pm 2, A_1 \pm 2, A_1 \pm 2, A_1 \pm 2\}$. The usual rules for collapsing data give the same results as Eq A.11 and A.11.

You might why there is the $(N-1)$ in the denominator of the equation for σ_{est}. There is an in-depth statistical analysis that you will find in many texts on error analysis, but one can use the mnemonic that a single measurement gives you no idea of the uncertainty in the measurement, which is consistent with the equation for σ_{est} which is indeterminate. Finally, if you're doing an experiment where the difference between N and $(N-1)$ in that formula is crucial to your results, you're probably pushing your data too hard.

Random and systematic errors

It is absolutely critical that you assign an uncertainty to each measurement you make. Consider a measurement of the local acceleration due to gravity at the earth's surface. In any textbook you will find the quoted value 9.8 m/s^2. Suppose you do a measurement and find a value of 9.5 m/s^2. What can you conclude? Three possibilities come to mind, depending on the error quoted:

1. You measure 9.5 0.5 m/s^2. Your result is consistent with the book value.

2. You measure 9.5 0.003 m/s^2. You have an amazing discovery on your hands. Publish!

3. You measure 9.5 5 m/s^2. You definitely need to learn how to do a better experiment.

Two types of errors dominate in real experiments. Random errors, which change in an unpredictable fashion from trial to trial, cause a spread in the measurement distribution, but no change in its average value. Systematic errors, in contrast, are the *same* from run to run, but cause the measured value to shift from the "true" value. For example: when you measure a resistor with a meter, you will certainly see fluctuations in the last digit of the display (random error). If you have the setting on kΩ, but believe it is set on ohms, this leads to a (very large!) systematic error.

The hallmark of a good experimenter is to minimize and *realistically* estimate random errors, and work hard to reduce the systematic error to a lower level. Note that multiple measurements lead to a reduction in the uncertainty in the estimate of the central value of a physical quantity (see Eq. A.10) due to random errors, but not if the error is systematic. Do you see why?

Fitting and modelling data – χ^2 analysis and goodness of fit

Most of the ideas in this section are found in more detail in Chapter 14 of the book Numerical Recipes cited in the Reference List.

In many experiments you will fit a graph of the data to a theoretically predicted form, e.g. a straight line or exponential decay. From the best fit to the data, you extract values for interesting physical parameters (e.g. the line slope and intercept, or the lifetime of the decay). A standard procedure to do this is based on the χ^2 quantity defined above (I'll say more about it in a while).

Whenever you perform a fit of this type, you MUST do 3 things:

1. Find the best fit values of the parameters.

2. **Estimate the errors of the parameters** (To quote the eminent Steve Myers, "Getting the error bar right is more important than finding the central value.")

3. Give a quantitative measure of the goodness of your fit. **If this measure is poor, all the information you found in parts 1 and 2 is suspect!!!**

Avoid the common temptation to stop after step 1 and simply say the fit "looks good". Don't get into the habit of "chi-by-eye"!

Suppose we are fitting N data points (x_i, y_i) to a model with M adjustable parameters a_j, j = 1, 2, ..., M. The model we are using predicts a relation between x and y:

$$y(x) = y(x; a_1, a_2, \cdots, a_M)$$

. How can we quantify our intuition that some sets of fit parameters $\{a_i\}$ give a good fit to the data, while others are totally unreasonable? How can we choose the set $\{a_i\}$ that gives the *best* fit? How do we decide whether the fit is "really good" or if we should distrust the model itself?

One way to look at the problem of judging the fit quality is to ask the question, "Given a particular set of parameters, what is the probability that our data set would be produced?" If the variable y is continuous, we need to add the words "plus or minus a fixed Δy for each data point". to make this probability non-zero. Now we proceed to find the parameter set $\{a_i\}$ that maximizes the likelihood of our measured data set.

Suppose each data point yi has a Gaussian distributed measurement error with standard deviation s around the "true" value y(x). Then the probability of measuring the data set is simply the product of the probabilities for measuring each point:

$$probability = \prod_{i=1}^{N} \{exp[-\frac{1}{2}(\frac{y_i - y(x_i)}{\sigma})^2]\Delta y\}$$

Maximizing this probability is the same as minimizing the negative of its logarithm:

$$[\sum_{i=1}^{N} \frac{[y_i - y(x_i)]^2}{2\sigma^2}] - N \log \Delta y$$

Since Δy is arbitrary, and the "2" is not crucial, this is equivalent to minimizing

$$\sum_{i=1}^{N} \frac{[y_i - y(x_i)]^2}{2\sigma^2} \tag{A.13}$$

This shows that *least-squares fitting* is a maximum likelihood estimation of the parameters $\{a_i\}$, if the measurement errors are normally distributed with the same standard deviation and independent. If the standard deviation is different for different data points, we seek to minimize a variant of Eq A.13, the "chi-square" given by

$$\chi^2 = \sum_{i=1}^{N} \frac{[y_i - y(x_i)]^2}{\sigma_i^2} \tag{A.14}$$

If the model produces a good fit, each y_i should be within σ_i of the "real" value $y(x_i)$, so the value of χ^2 you find should be roughly N. Sometimes people define a "normalized chi-square" by dividing Eq. A.14 by N, so a good fit has a normalized chi-square near 1.

It turns out one can show that for large values of $\nu = N - M$ (when we have a large number of data points, this is just N), the quantity χ^2 defined above becomes normally distributed with a mean of ν and a standard deviation of $(2\nu)^{0.5}$. A value of χ^2 much greater than N indicates that the fit is suspect, **even if it looks good to the naked eye**. This could occur for several reasons: the model may be faulty, the actual value of the error could be underestimated, or the errors may NOT normally distributed. In contrast, a value of χ^2 much less than N often indicates that you have been too conservative and overestimated the experimental error.

Many good data analysis packages are available for the PC, Macs, and Unix machines. **You should find such a package, and learn how to use it well**. You need to be able to do least-squares fits to non-linear models, **taking into account that each data point may have a different error bar**. You will get practice in the Data Analysis exercise assignment.

Now you have determined your best estimate of the unknown parameters, i.e. the set $\{a_i\}$ that minimizes χ^2. We will call this best fit set $\mathbf{a_0}$ (a "vector" consisting of the fit parameters), and we now turn to determining the uncertainty associated with each of the parameters. Unknown to us is the actual parameter set $\mathbf{a_{TRUE}}$. Our data set is but one member of the set of all possible data sets, each of which would give a slightly different set of fit parameters, $\mathbf{a_1}, \mathbf{a_2}, \mathbf{a_3}, \cdots$. The parameter sets $\mathbf{a_i}$ occur with some probability distribution, clustered (one hopes) around $\mathbf{a_{TRUE}}$.

The best way to find out how all possible experimental fit parameters a_i cluster around the true set $\mathbf{a_{TRUE}}$ is to assume the set $\mathbf{a_0}$ is the "true" value and *simulate* multiple trials of the experiment, using your best understanding of how the measurement apparatus works (which may take into account the fact that the errors are **not** Gaussian distributed). Such Monte Carlo simulations are much more feasible than only a decade ago because of the dramatic decrease in the cost of computing power. Such techniques are often more valuable than a host of "exact" analytic results.

Despite this, there are several analytic results that can be easily applied to generate uncertainties in the fit parameters $\mathbf{a_0}$. We usually express our results in terms of "confidence limits", that is compact regions of the M-dimensional space of parameters a that contain large fractions of the probability distribution. One might indicate a region such that the chance that $\mathbf{a_{TRUE}}$ falls within this region around the measured value $\mathbf{a_0}$ is 68%, or 95%, or 99%, etc.

A common situation is more simple than this. We might want to know what range in a single parameter, say $\mathbf{a_1}$, contains 68% of the probability distribution. It turns out that this can be expressed in terms of the value of χ^2 defined above, and the analytical results remain rather accurate even when the errors are not normally distributed. The procedure is:

1. Find the best estimate fit parameters by minimizing χ^2 (including the parameter of interest, a_1).

2. Vary a_1 above and below the optimum value, and run the fit again, now with M 1 parameters. The best value of χ^2 will be greater than what you found in step 1.

3. Construct a table of test values of a1 versus variation $\Delta\chi^2$ from the minimum value. You may assume that $\Delta\chi^2 < 1$ occurs 68% of the time (1σ for a normal distribution), $\Delta\chi^2 < 4$ occurs 95% of the time (2σ for a normal distribution), and $\Delta\chi^2 < 9$ occurs 99.7% of the time (3σ for a normal distribution). Use these values to quote a confidence interval on a_1.

A few notes on the breakdown of the Gaussian ensemble

The ideas presented above rely on the idea that the error demon can be represented by a Gaussian probability distribution with a mean error of zero, and that various demons in the world produced **uncorrelated** errors. When these assumptions break down (and they do!), the results of experiments deviate from the ideal. Unfortunately, sniffing out the existence of such a breakdown and eliminating the cause is a difficult art. Keep an eye on your

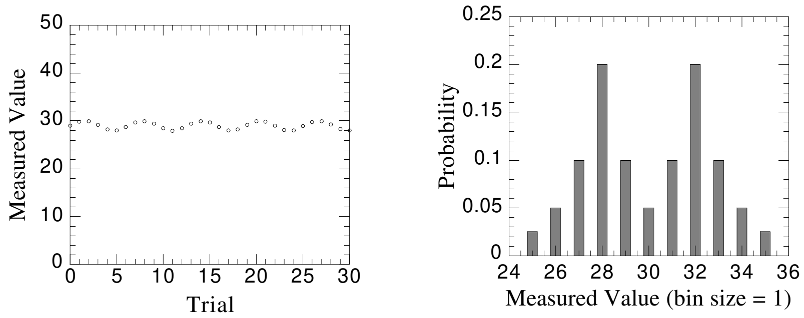

Figure A.5: Data with errors which do not obey a random Gaussian distribution.

data, plotting it as you go along, and you might get a hint of trouble before you spend a lot of time and effort taking bad data. A key rule of experimental physics: don't confuse lots of data with convincing data!

Figure A.5 show two different experiments whose errors are NOT randomly distributed:

When errors are not randomly distributed, the usual rules for error propagation do not hold. Consider the following proof that errors add in quadrature for the sum of two randomly distributed variables, $z = x + y$. We use the notation $\delta z = z - \overline{z}$ for the deviation of an individual measurement from the mean, $\overline{z}$. The standard deviation is then $< \delta z^2 >= (z - \overline{z})^2 = \int (z - \overline{z})^2 P(z) dz$, where $< \cdots >$ indicates the expectation value.

$$
\begin{aligned}
< \delta z^2 > &= [(x + y) - (\overline{x} + \overline{y}]^2 >= [(x - \overline{x} + (y - \overline{y})]^2 >= (\delta x + \delta y)^2 > \\
&= < \delta x^2 > + < \delta y^2 > +2 < \delta x \delta y > \\
&= < \delta x^2 > + < \delta y^2 > +2 < \delta x >< \delta y > \\
&= < \delta x^2 > + < \delta y^2 >
\end{aligned}
$$

We explicitly used the fact that the errors in x and y are **uncorrelated**, that is that $< \delta x \delta y >=< \delta x >< \delta y >= 0 * 0$. If this is not true, the usual formula does not hold, and the error in z is almost certainly **greater** than that found by adding errors in quadrature. Finally, this proof shows that the addition of errors in quadrature works even if x and y are not Gaussian distributed. As long as the distributions have well defined standard deviations, and the errors are uncorrelated, the usual formula holds. A question: you have a meter stick marked every millimeter. You think that with care you can read off a measurement to 0.25mm (250μm). Your lab partner suggests you measure a length in an experiment to an accuracy of 2.5 microns by repeating the measurement 10,000 times, taking advantage of the fact that the error drops as $1/N^{0.5}$. Will this work?

Closing Notes

The Dirac Delta Function, $delta(x)$, is a function that is infinitely peaked at the value x = 0, but whose area is exactly 1, that is:

$$\int_{-\infty}^{\infty} \delta(x)dx = 1$$

The function $\delta(x - x')$ is the same, but peaked at the value $x = x'$. The Dirac Delta Function has a sort of "filtering" property when convolved with another function g(x), as long as the latter is not too pathological:

Appendix B

A Brief Review of Radiation Safety

This Appendix reviews only the most basic concepts in radiation safety. You should most definitely read the appropriate section in one or more reference books.

Radiation is harmful because it can destroy cells by ionization, and it may also induce genetic changes. It seems established that low level radiation does not cause any permanent injury, but we assume that the effect of exposure to radiation is cumulative (this will lead to very conservative estimates of risk). It is possible (but not likely) that (permanent) genetic changes may be induced by low level radioactivity, but humans are continually exposed to cosmic rays and other natural sources of radioactivity.

There are 4 types of radiation that you will be concerned with in the advanced lab:

1. An **alpha ray** is simply a bare helium nucleus, ${}_2He^4$. Alpha rays have a very short range in dense matter because of their large mass and charge. The greatest hazard is posed by an alpha emitter that has been ingested, because the alphas then deposit their energy in a small amount of tissue. However, alphas represent a negligible hazard when the emitter is outside the body. Only the most energetic alpha particles are able to penetrate the outer layer of (already dead) skin. A single piece of paper is an effective shield against alphas.

2. **Beta particles** are energetic electrons or positrons emitted by nuclei. Because of their low mass and charge, betas penetrate further than

alphas, but much less than neutrons or gamma rays (photons). A good shield against beta rays is a thin sheet of aluminum or 1/4in of glass. Betas are unlikely to penetrate the skin, but pose a threat to unprotected eyes.

3. **Gamma rays** are photons emitted by an excited nucleus or produced by a meson decay. An x-ray is a photon produced by an electronic transitions in an atom. Other than their energy levels (x-rays are typically in the keV range, gammas have higher energy, up to 10^{12} eV for gammas of galactic origin), these particles are identical (i.e., photons). Since gamma rays have no charge or rest mass, they penetrate deeply into matter. Effective shielding is provided by lead and other high Z (atomic number) metals.

4. **Neutrons**, along with gamma rays, represent the greatest hazard for external exposure. Since they have no charge, they travel long distances in air and other materials. Fast neutrons (energy ¿ 10KeV) lose energy via elastic collisions with protons in tissue, and the recoil protons (with energies of order the neutron energy) deposit their kinetic energy rapidly in tissue via ionization. These processes make fast neutrons more hazardous than slow neutrons or other particles of similar energy.

A radioactive source can be described by the number of quanta emitted, without regard to the type of particle or the danger to humans. One common unit is the **Curie**, which corresponds to $3.7 * 10^{10}$ quanta emitted/sec. The official SI unit is the **Becquerel**, which is 1 decay/sec. We may also speak of the particle **flux**, that is the number of quanta incident on a given area per unit time.

Another type of unit attempts to quantify the damage the radiation causes to biological systems. This is, in fact, extremely difficult to do with high accuracy. A common unit is the **rad**, which is the amount of radiation that deposits 100 erg of energy in each gram of tissue traversed. However, radiation due to two types of particles may cause different amounts of damage to tissue, even if both are rated at 1 rad. To account for this, another unit, the **rem** ("radiation equivalent man") is defined to be the product of the dose in rad and a "relative biological effectiveness" (RBE) factor.

$$\text{(number of rem)} = \text{(number of rad)} * \text{RBE}$$

Not all types of radiation are equally hazardous when they interact with tissue. Since alphas and neutrons (along with protons, which we will not encounter in this lab) deposit their energy in a small tissue volume, they are more damaging than betas or gammas. This is reflected in the RBE, which is 20 for alphas, ranges from 2.5-20 for neutrons, and is 1 for betas and gammas. The most hazardous situation is when a source is ingested, exposing the body to 4π radiation. Since we use sealed sources, the risk of this occurring is low.

The integrated radiation dose due to natural radioactivity is between 0.5 and 1 rem for most parts of the country (it is significantly higher in mountain states, where high altitude leads to higher cosmic ray flux). A dose of 10^{-3} rem/hr (= 1 mrem/hr) is considered to present no danger. If you measure a level above 5 mrem/hr at your work position, you should contact the instructor for help in building a shield or moving the work position further away from the source. Note that neutrons are not detected by conventional radiation detectors such as Geiger counters, so you should be particularly careful when working with a neutron source.